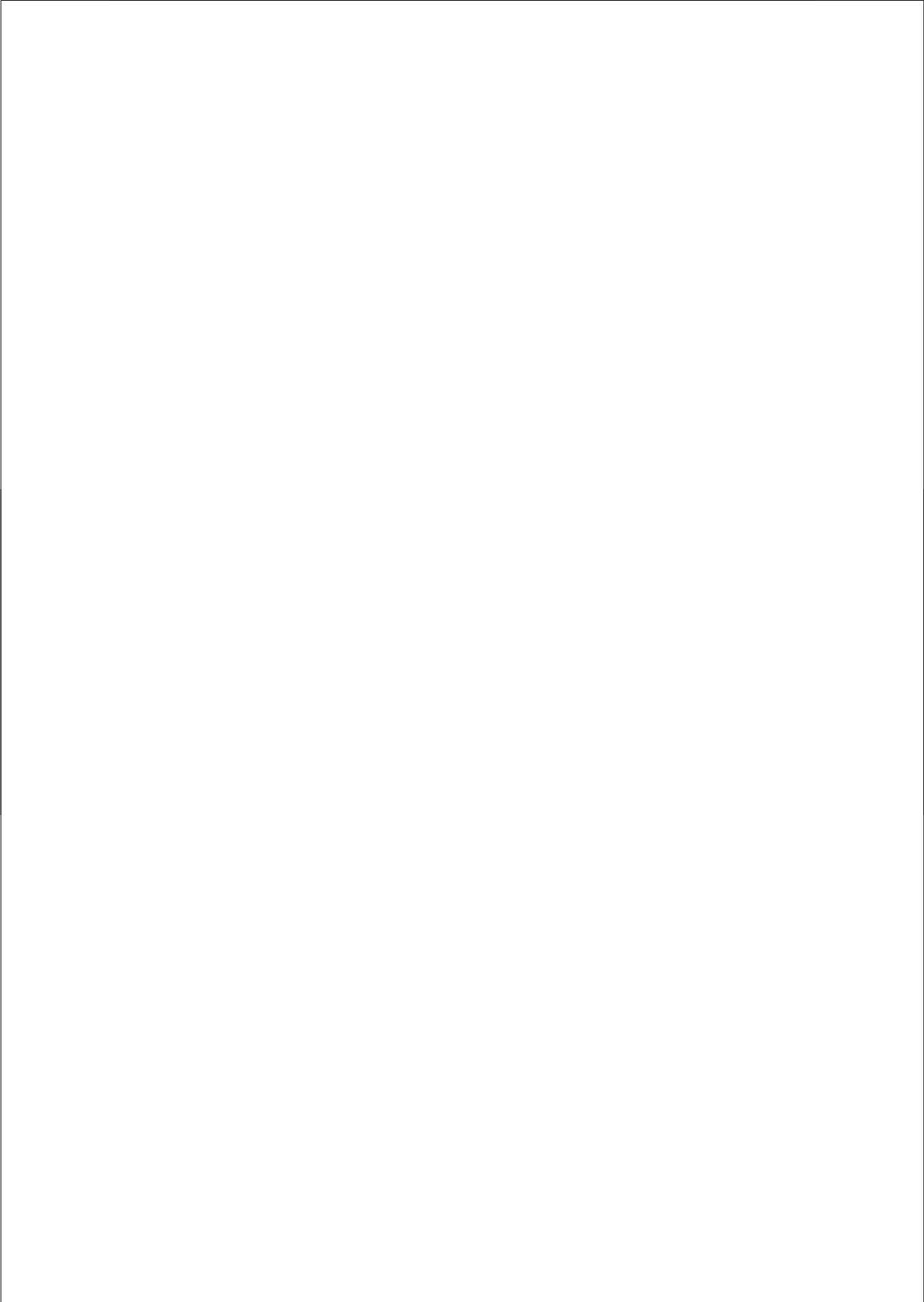


Long liquid slugs

in stratified gas/liquid flow
in horizontal and slightly inclined pipes



Long liquid slugs

in stratified gas/liquid flow in horizontal and slightly inclined pipes

PROEFSCHRIFT

ter verkrijging van de graad van doctor
aan de Technische Universiteit Delft,
op gezag van de Rector Magnificus prof. dr. ir. J. T. Fokkema,
voorzitter van het College voor Promoties,
in het openbaar te verdedigen op
Vrijdag 28 September 2009 om 10:00

door

Usama Kadri

M.Sc. Aerospace Engineer, Technion – Israel Institute of Technology
geboren te Kfar Saba, Israel

Dit proefschrift is goedgekeurd door de promotor:

Prof. dr. R.V.A. Oliemans

Prof. dr. R.F. Mudde

Samenstelling promotiecommissie:

Rector Magnificus,	voorzitter
Prof. dr. R.V.A. Oliemans,	Technische Universiteit Delft, promotor
Prof. dr. R.F. Mudde,	Technische Universiteit Delft, promotor
Prof. dr. ir. R.A.W.M Henkes,	Technische Universiteit Delft
Prof. dr. ir. G. Ooms,	Technische Universiteit Delft
Prof. dr. ir. H.W.M. Hoeijmakers,	Universiteit Twente
Prof. dr. P. Andreussi,	University of Pisa
Prof. dr. O.J. Nydal,	Norwegian University of Science and Technology

This project was supported by the Dutch Foundation for Technological Research (STW)

Keywords: two-phase flow, gas-liquid, long slugs

Cover design by: Arch. Lidia Badarnah-Kadri

The cover of the thesis is based on M.C. Eschers "Sky and Water I" ©2009 The M.C. Escher Company – The Netherlands. All rights reserved. www.mcescher.com

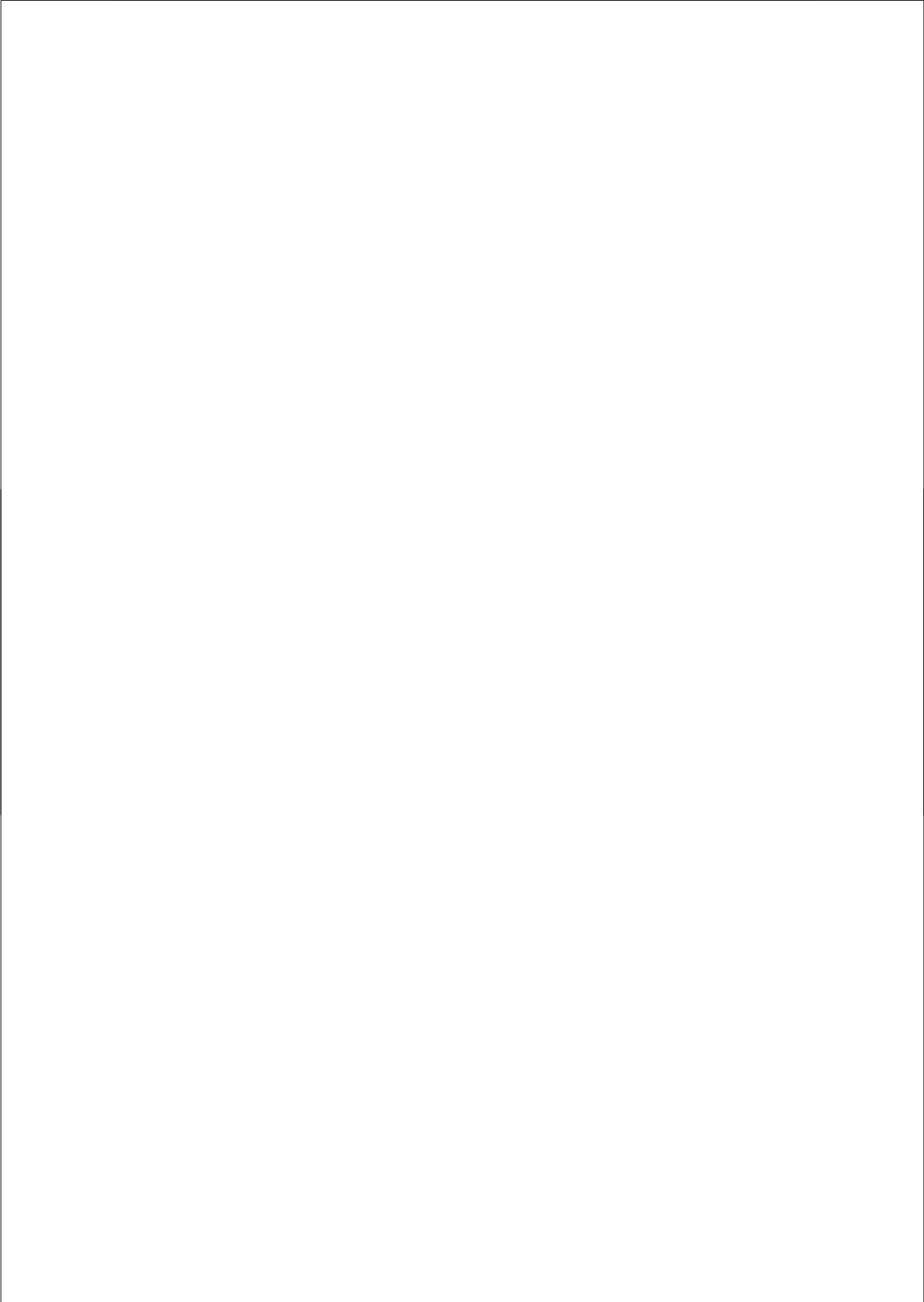
Printed in The Netherlands. PrintPartners Ipskamp. www.ppi.nl

ISBN 978-90-9024536-2

© 2009 Usama Kadri.

All rights reserved. No part of the material protected by this copyright notice may be reproduced or utilized in any form or by any means, electronic or mechanical, including photocopying, recording, or by any information storage and retrieval system without written permission from the publisher.

For the ultimate victory of blood over sword



Contents

Nomenclature	xi
Summary	xiii
Samenvatting	xv
1 Introduction	1
1.1 Motivation	1
1.2 Scope	2
1.3 Outline	3
2 Dynamic slugs	5
2.1 Introduction	6
2.2 Theoretical background	8
2.2.1 Stratified flow pattern	8
2.2.2 Viscous long wavelength theory	8
2.2.3 Slug stability analysis	10
2.3 Experiments on the occurrence of long slugs	11
2.3.1 Experiments	11
2.3.2 Sub-regimes in the slug flow map	11
2.4 Dynamic slug model	14
2.4.1 Properties of forming slugs	14
2.4.1.1 Wave velocity	14
2.4.1.2 Slug at initiation	15
2.4.1.3 Slug tail extension	15
2.4.1.4 Initial slug length	16
2.4.2 Slug growth and final length	17
2.4.2.1 The liquid area downstream of the slug, $A_{L_{max}}$	17
2.4.2.2 The liquid area upstream of the slug, $A_{L5}(t)$	17
2.4.2.3 Slug length, $L_S(t)$	18

2.4.3	End of slug growth	19
2.5	Results	20
2.5.1	Predictions for horizontal air–water flow	22
2.5.2	Predictions for declined air–water flow	22
2.5.3	Predictions for SF_6 gas– <i>ExxsolD80</i> oil flow under varying pressure	22
2.5.4	Predictions at large mixture velocities	25
2.6	Conclusions	27
3	Transition to slug flow and roll–waves	29
3.1	Introduction	30
3.1.1	Waves	30
3.1.2	Transition to roll–waves	30
3.1.3	Transition to slug flow	31
3.2	Theoretical background	32
3.2.1	Stratified flow pattern	32
3.2.2	Slug stability theory	34
3.2.3	The liquid level downstream of the growing wave	34
3.3	A roll–wave/slug formation time model	35
3.3.1	The vertical growth time	36
3.3.2	The axial growth time	37
3.4	Experiments	38
3.4.1	The KLFT flow loop	38
3.4.2	The NTNU flow loop	39
3.5	Numerical tests	41
3.6	Results	43
3.6.1	Crest growth near the pipe top	43
3.6.2	Prediction of roll–wave/slug formation time	44
3.6.3	Formation time predictions for different pipe diameters	45
3.6.4	Critical Froude number for the transition	46
3.7	Conclusions	48
4	Operation pressure and slug length	51
4.1	Introduction	52
4.2	Background	53
4.2.1	Stratified flow pattern	53
4.2.2	Average liquid area	53
4.2.3	Slug stability model	54
4.3	Experiments	55
4.4	Definition of slug types by liquid excess	57
4.4.1	Discrimination between slug types in measurements	57
4.4.2	Measurements of the liquid excess, Δh_L	58
4.4.3	Theoretical predictions of the liquid excess, Δh_L	59
4.4.3.1	Slugs type I	59
4.4.3.2	Slugs type II	59

4.4.3.3	Slugs type III	59
4.5	Results	59
4.5.1	Slug types and the normalized liquid excess, $\Delta h_L/D$	60
4.5.2	The length of the different slug types at atmospheric pressure	61
4.5.3	The length of the different slug types at $P = 1.5 \text{ barA}$ ($\rho_G = 9 \text{ kg/m}^3$)	62
4.5.4	The length of the different slug types at $P = 3 \text{ barA}$ ($\rho_G = 18.5 \text{ kg/m}^3$)	63
4.5.5	Effect of pressure on the long slugs – summary	64
4.6	Conclusions	65
5	A probabilistic slug frequency model	67
5.1	Introduction	68
5.2	Background	69
5.2.1	Stratified flow pattern	69
5.2.2	Average liquid area	71
5.2.3	Slug stability model	71
5.3	Slug frequency model	72
5.3.1	Frequency of turbulent eddies in gas and liquid	72
5.3.2	Interfacial frequency of turbulent eddies, $f_{r,i}$	73
5.3.3	Triggering of slug precursors	74
5.3.4	Conditional probability of slug formation	74
5.4	Results	76
5.5	Conclusions	80
6	Conclusions and final remarks	81
6.1	Slug growth and the long slug region	82
6.2	Evolution of waves and transition to slug flow or roll-waves.	82
6.3	The effect of operation pressure	83
6.4	Slug flow and turbulence	83
6.5	Final remarks	84
A	Calculation of the wave growth coefficient, C_2	91
	Publications	93
	Acknowledgements	95
	About the author	97

Nomenclature

Greek letters

δ	boundary layer thickness	m
ε	gas void fraction	-
η	wave amplitude	m
θ	angle to horizontal	deg
λ	wavelength	m
ν	kinematic viscosity	$\text{m}^2.\text{s}^{-1}$
ρ	density	$\text{kg}.\text{m}^{-3}$
$\Delta\rho$	fluids density difference	$\text{kg}.\text{m}^{-3}$
τ	wall shear stress	$\text{kg}.\text{m}.\text{s}^{-2}$
ω	frequency of rotation	s^{-1}

Roman symbols

A	cross-sectional area	m^2
C, C_R	wave velocity	$\text{m}.\text{s}^{-1}$
C_F	slug front velocity	$\text{m}.\text{s}^{-1}$
C_B	slug tail (bubble) velocity	$\text{m}.\text{s}^{-1}$
C_1, C_2	wave growth constants	-
c_w	a constant equal to 2 for air-water system	-
D	pipe diameter	m
D_H	hydraulic diameter	m
Fr	Froude number	-
f	frequency	s^{-1}
f	friction factor	-
g	gravity constant	$\text{m}.\text{s}^{-2}$
h	height of the fluid layer	m
K	nonlinear wave growth rate	$\text{m}.\text{s}^{-1}$
k_1, k_2	boundary layer constants	-
L	length	m
l_T	turbulence length scale	m

m	defined in Eq. (5.30)	-
n	number of slug precursor locations	-
\mathbb{P}	conditional probability for slug formation	-
P, p	pressure	Pa
Q	volume flux	$\text{m}^3 \cdot \text{s}^{-1}$
Re	Reynolds number	-
S	cross-sectional length	m
St	Strouhal number	-
t	superficial velocity of phase .	$\text{m} \cdot \text{s}^{-1}$
U	actual gas velocity	$\text{m} \cdot \text{s}^{-1}$
U_{Mix}	mixture velocity	$\text{m} \cdot \text{s}^{-1}$
u	actual liquid velocity	$\text{m} \cdot \text{s}^{-1}$
\mathbf{u}	fluid velocity	$\text{m} \cdot \text{s}^{-1}$
V	volume	m^3
v	velocity	$\text{m} \cdot \text{s}^{-1}$
x	axial coordinate	-
y	distance from the wall	m

Subscripts

a, b, c, O	points along the slug tail
avg	average
B	bubble
G	gas
L	liquid
F	front
f	final
i	interfacial, index
k	index
o	initial value
r	rotation
S	slug
SG	superficial gas
SL	superficial liquid
s	smooth surface
W	wall
w	wave
x, y	Cartesian coordinates
∞	steady-state
1, 3, 5	stations along the slug unit defined in Fig. 2.2

Summary

Long liquid slugs

Usama Kadri, Delft University of Technology

Long liquid slugs reaching several hundreds pipe diameter may appear when transporting gas and liquid in horizontal and near horizontal pipes. The long slugs cause system vibration and separation difficulties that may lead to operational failures. Identifying and predicting the time and length scales of slugging is important for gas and oil production technologies (e.g. for the design of offshore gas and oil pipelines and process facilities). Although mainly short hydrodynamic slugs (40 pipe diameters) have been observed in offshore production fields, the appearance of the long slugs becomes more likely as the field becomes older the operation pressure drops. Therefore, predicting the transition between the different slug types and the flow conditions at which the long slugs appear may be crucial preventing or reducing the negative effects of slugging.

The approach adopted in this study is the construction of simplified theoretical models that successively approximate the flow conditions and the corresponding time and length scales of slugging. Experiments and numerical modelling have been performed for validation and comparison matters.

The first part of the research deals with identifying the long slug region and sub-regions. Experiments carried out by Zoetewij (2007) present a detailed flow map for the long slug region and the transition to hydrodynamic slugs or stratified wavy flow. For the prediction of the long slug region a simplified predictive model was constructed. The model calculates the average slug length based on the volumetric liquid rates adjoining the slug, and derives the change in the liquid level, at the tail of the slug, by linear kinematic relation between the tail and the following upstream wave. The model predicts the transition from hydrodynamic to long slugs with a satisfactory agreement.

In the second part of the research the emphasis is put on predicting the transition from stratified flow to slug flow or roll-waves. Slugs formed by coalescence between roll-waves are hydrodynamic. Hence, only the flow conditions that lead to a direct transition from strat-

ified flow to slug flow (i.e. not via roll-waves) may lead to long slugs. For the prediction of the transition to slug flow or roll-waves a theoretical model was developed. The model tracks the displacements of the crest of a long wavelength wave in axial and radial directions. If the wave crest reaches the top of the pipe a slug is formed, whereas if it approaches the downstream end of the wave a roll-wave is produced. Besides to the predictive tool provided, the model sheds some light on the stage prior to forming a slug.

The third part of the research considers the effect of the operation pressure on the slug length, and the effect of the liquid excess between the slug front and tail at the formation time. Measurements by Kristiansen (2004) for two-phase air-oil and SF_6 gas-oil were investigated. The measurements were carried out at $P = 1-8 \text{ barA}$ with high density SF_6 gas simulating a pressure up to 65 bar . Three different types of slugs were categorized based on the liquid excess. Slugs with larger liquid excess at formation can grow to become longer. Even a small difference in the liquid excess may lead to a large difference in the slug length. However, at high operating pressures there is no liquid excess and only hydrodynamic slugs are observed.

In the final part of the research we investigated and derived the slug frequency by the frequency of vortices due to turbulence in the gas and liquid. We found that the slug frequency and the frequency of oscillation at the interface behave similarly to the frequency of oscillations in the gas phase. However, the intensity of the oscillation at the interface is dominated by the liquid phase. The proposed mechanism for the formation of slugs covers a large range of pipe diameters and flow conditions. Moreover, it reveals the significance of the small-scale initial turbulence on the final development of the large-scale slug flow.

Samenvatting

Lange vloeistof slugs

Usama Kadri, Technische Universiteit Delft

Lange vloeistof slugs (vloeistof slokken) met lengtes van wel honderden buisdiameters, kunnen voorkomen bij transport van gas en vloeistof in horizontale en nagenoeg-horizontale pijpleidingen. Dergelijke lange slugs kunnen door drukfluctuaties en vloeistof/gas scheiding problemen operationele verstoringen geven. Het identificeren en voorspellen van de tijd- en lengteschalen van de slugs is van belang voor de gas/olie productietechnologie (regels voor een betrouwbaar ontwerp van de pijpleiding en process apparatuur). Hoewel tot nu toe hoofdzakelijk korte, hydrodynamische, slugs van hooguit $40D$ in productieleidingen van buitengaatsse olie/gas velden zijn waargenomen, zijn er aanwijzingen, dat bij oudere velden met lagere operatiedrukken de kans op lange slugs zal toenemen. Het is daarom zaak om door een verdieping van de kennis over lange slugs te pogen de negatieve effecten van hun aanwezigheid te reduceren.

De in deze studie gekozen aanpak is om eenvoudige, theoretische modellen te ontwikkelen, waarmee bij benadering de condities waaronder lange slugs ontstaan en hun tijd en lengteschalen berekend kunnen worden. Bestaande experimenten en computer simulaties zijn vervolgens gebruikt om de modellen te valideren.

Het eerste deel van het proefschrift betreft het identificeren van het lange slug gebied en sub-gebieden in het stromingspatroondiagram. Experimenten, uitgevoerd door Zoetewij (2007), geven een uitstekend beeld van het gebied met lange slugs en de overgangen naar hydrodynamische slugs en gelaagde tweefasenstroming. Om het lange slug gebied te kunnen vaststellen is een eenvoudig theoretisch model ontwikkeld. Het model bepaalt de gemiddelde sluggrootte op basis van het vloeistofdebiet naar de slug en de verandering van het vloeistofniveau achter de slug via een lineaire, kinematische, relatie tussen de slug-staart en de golf stroomopwaarts. Met het model kan de overgang van hydrodynamisch naar lange slugs redelijk goed voorspeld worden.

In het tweede deel van het onderzoek ligt het accent op het voorspellen van de overgang

van gelaagde gas/vloeistofstroming naar slug stroming of gelaagde stroming met rol-golven. Vloeistof slugs, die ontstaan door coalescentie van rol-golven hebben een hydrodynamisch karakter. Dit betekent, dat alleen slugs, die rechtstreeks ontstaan uit de gelaagde stroming, en niet via coalescerende rol-golven, lange slugs zijn. Ook voor deze genoemde overgangen is een theoretisch model ontwikkeld. Het model beschrijft de verplaatsing van de top van een lange golf in axiale en opwaartse richting. Als de top van de golf de top van de pijp raakt vormt zich een slug. Als de axiale snelheid zo hoog is dat de top het eind van de golf stroomafwaarts bereikt worden rol-golven gevormd. Het model geeft ook inzicht in de stromingssituatie vlak voor de vorming van een slug.

Het derde deel van het onderzoek betreft het effect van de operatiedruk op het optreden van lange slugs en de rol van het verschil in vloeistof hoogte aan voor en achterkant van de opbouwende slug. Metingen van Kristiansen (2004) met tweefasen lucht/olie en SF_6 -gas/olie zijn geanalyseerd. De metingen bij laboratoriumdrukken van 1–8 barA met het hoge dichtheid SF_6 -gas simuleren operatiedrukken tot 65 bar. Op basis van de overmaat vloeistof kunnen drie verschillende typen slugs worden onderscheiden. Slugs met zelfs maar een geringe vloeistof-overmaat kunnen in lange leidingen heel lang worden. Bij hoge druk is er echter geen vloeistofovermaat meer en ontstaan alleen hydrodynamische slugs.

In het laatste deel van het project hebben we onderzocht in hoeverre de slugfrequentie gerelateerd kan worden aan de frequenties van vortices in the turbulente gas en vloeistof gedeeltes van gelaagde gas/vloeistof stroming. De slug frequentie en de frequentie van oscillaties aan het vloeistof/gas scheidingsvlak blijken te correleren met de oscillaties in de gasfase. De intensiteit van de oscillaties aan het scheidingsvlak wordt echter bepaald door de vloeistoffase. Het voorgestelde mechanisme voor de vorming van de slugs geeft goede resultaten voor bestaande waarnemingen voor een reeks van diameters en stromingscondities. Ook wordt duidelijk dat turbulente fluctuaties op kleine schaal grote gevolgen kunnen hebben voor de grote schaal aspecten van de slugs.

1

Introduction

1.1 Motivation

Gas–liquid flows are present in various engineering applications including aerospace, atmospheric, biological, biomedical, chemical, civil, mechanical, and nuclear systems. Conducting a multiphase flow system is clearly not a simple task. It involves serious multiphase production technology challenges, that require various levels of understanding the processes involved. Unfortunately, our understanding of multiphase flows is quite immature compared to single–phase flows. The need to improve the scientific understanding of the fundamentals of multiphase flows is the main motivation in the current study.

Here, we focus on two–phase gas–liquid flows in a pipe. “*The study of flow in a pipe is a starting point for a scientific treatment of gas–liquid flows, as was Poiseuille’s law and measurements of fully–developed flows, a starting point for the analysis of single phase flows*” (Hanratty (2004)). Moreover, application of the results by gas and oil production technologies is rather direct, e.g. the design of offshore gas and oil pipelines.

The main challenges in gas–liquid flows are caused by the interfacial interactions leading to different flow configurations evolving through a complex flow. The simultaneous transportation of gas and liquid in a pipeline may result in a number of flow patterns, characterised by different time and length scales. In long pipelines, multiple flow regimes may exist simultaneously in different parts of the pipe (Oliemans (1987)). Sketches of the different flow patterns and flow regime maps in horizontal gas–liquid pipe flow are presented in Figures 1.1 and 1.2. At relatively low gas and liquid flow rates, a *stratified flow* patterns occurs with a

continuous gas phase flowing on the top of the liquid phase. At larger gas and liquid flow rates, a *stratified-wavy flow* is formed, whereby waves appear at the interface. These waves can grow to reach the top of the pipe forming liquid plugs travelling in the pipeline, separated by large gas bubbles. At relatively low gas flow rates, this intermittent flow regime is known as *plug flow*, whereby the gas flows along the top of the pipe as steady elongated bubbles. However, at higher gas flow rates slugs of liquid move downstream approximately at the gas velocity with highly aerated unsteady fronts. This type of flow pattern is known as *slug flow*. Slug flow produces large pressure transients and system vibrations that may lead to operational failures. Slug flow is frequently observed in production pipelines, where slugs are

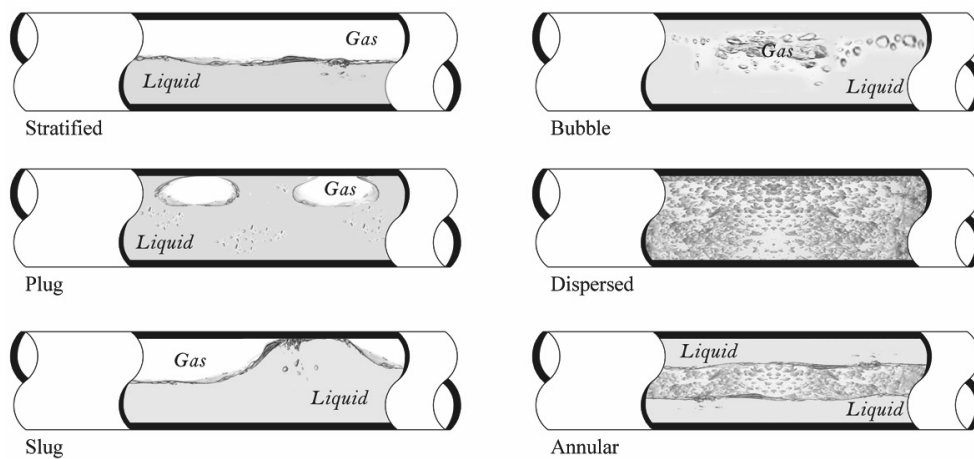


Figure 1.1: Sketches of flow regimes for gas-liquid in a horizontal pipe.

relatively short (less than 40 pipe diameter). These slugs are formed due to instabilities in the stratified flow, often referred to as *hydrodynamic slugs*. However, operating at relatively low pressures and at relatively low gas and liquid flow rates, very *long slugs* with sizes reaching several hundreds pipe diameters may form. Such long slugs cause severe operational failures due to the strong fluctuations in flow supply and pressure. The particular focus of this study is put on this type of slugs, and the physical mechanisms responsible for its generation and development.

1.2 Scope

The aim of this research is to investigate the formation of the long slugs in the stratified flow regime, and to construct scientific tools that helps in understanding and predicting the behaviour of slug flow pattern. The focus is given on the formation and growth of the long slugs, and the effect of flow conditions and pipe sizes on slug length and frequency.

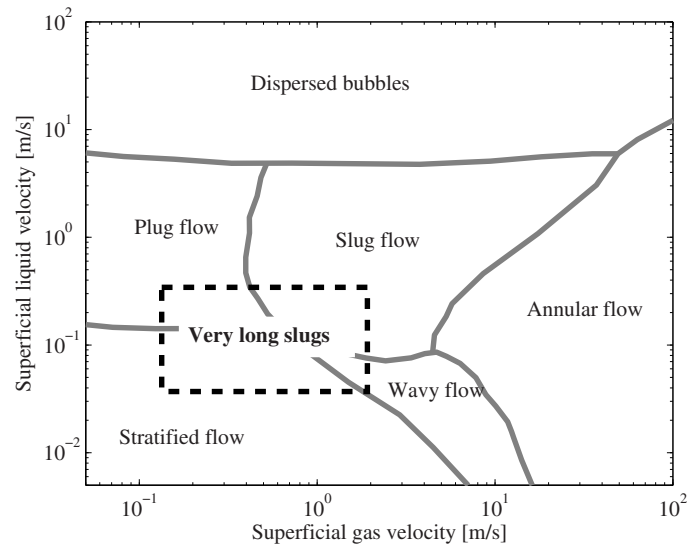


Figure 1.2: A flow regime map for gas-liquid in a horizontal pipe.

1.3 Outline

Properties of the long slugs, as well as the long slug regime and sub-regimes are presented in chapter 2. The long slug regime appears at relatively low gas and liquid flow rates, at which slugs can reach a length of several hundred pipe diameters. The long slugs are found to be either fully developed (steady length) or growing. A growth model for calculating the average slug length in horizontal and slightly inclined pipes is introduced. The model is validated by measurements in a 137 m length air-water horizontal pipe flow with an internal diameter of 0.052 m performed by Zoetewij (2007). The measurements provide a detailed flow map of the long slug regime and sub-regimes. Furthermore, predictions by the model are compared with other available data for different pipe sizes, various operation pressures, different inlet conditions, different fluid properties, and slight pipe inclinations. The model enables prediction of the transition from hydrodynamic to long slugs, as well as the average slug length in the long slug sub-regimes.

The model presented in chapter 2 considers the development of existing slugs with initial lengths associated with long wavelength waves. However evolution of waves can lead to a transition to either slug flow or roll-waves. In chapter 3 the evolution of waves is investigated. Slugs form by regular growing gravity waves may become long at certain flow conditions, whereas slugs evolving by coalescence roll-waves are identified as short hydrodynamic. A wave transition model from stratified to slug flow or roll-wave regimes is developed in order to identify the mechanism of possible forming slugs. The model is validated by measurements in a 137 and 16 m long air-water horizontal pipe flows with diameters of 0.052 and 0.06 m,

respectively. Moreover, predictions by the model are compared with numerical calculations using a multiphase flow simulator, MAST, in order to investigate the pipe scaling effect where no experimental data are found.

In chapter 4, gas–liquid pipe an analysis of flow measurements is presented in order to investigate the dominant factors responsible for the formation of different slug lengths. Three types of slugs are defined based on the liquid excess between the slug front and tail immediately after formation: (1) large liquid excess; (2) intermediate liquid excess; and (3) no liquid excess. The first two types are associated with the long growing and stable slugs, respectively. The third type is found to be always a short hydrodynamic slug. The conclusion is that small changes in the initial conditions of the liquid excess may lead to a large difference in the slug length and frequency. Moreover, the effect of practical field operation pressure on the long slugs is investigated. The long slug region shrinks with increasing pressure, however, long stable slugs may still form at operation pressure below 65 *bar*.

Chapter 5 discusses the source of slug formation with stratified flow as a starting point. The frequency of oscillations generated by turbulent eddies in gas and liquid are found to be responsible for the periodic formation of slugs. However, a moving slug destroys the memory of the turbulent eddies downstream, preventing the formation of new slugs. The two–scale physics of turbulent eddies and slug flow are coupled. Therefore, a probabilistic model, that defines sub–spaces at which each scale is dominant, is developed. The slug frequency is derived from the frequency of oscillations and probabilistic effect, then compared with measurements for different pipe sizes and flow conditions.

Finally, the conclusions and final remarks are presented in chapter 6.

2.1 Introduction

Slug flow is commonly observed in horizontal and slightly inclined pipe flows. It is characterized by the appearance of plugs of liquids, moving downstream, separated by elongated bubbles, moving along the top of the pipe. Although mostly short hydrodynamic slugs are observed, at relatively low gas flow rates very long slugs with sizes reaching 500 pipe diameters or more may form. Such long slugs cause severe operational failures due to the strong fluctuations in flow supply and pressure. A frequent appearance of the long slugs is likely to occur in older gas production offshore fields, where the operation pressure is low. Therefore, predicting the transition from regular hydrodynamic to long slug regimes plays a prominent role in preventing or reducing future operational failures.

Two theoretical concepts are used to predict the flow conditions at which, both hydrodynamic and long, slugs are observed: stability of stratified flow and stability of slugs. The stability of stratified flow describes waves on thin films over which gas is blowing (Hanratty and Hershman (1961)). Whereas slug stability analysis considers a volumetric liquid balance between the front and the tail of a slug. For a fully developed slug moving at the bubble velocity, this balance results in the minimum liquid height, $h_{L_{min}}$, at the front required for the slug to be stable (Ruder et al. (1989); Bendiksen (1984)). Measurements and photographs done by Woods and Hanratty (1996) support the idea that the back of a slug can be modelled as a bubble (Benjamin (1968)). Hurlburt and Hanratty (2002) compared predictions by slug stability for the critical superficial liquid velocity, $U_{SL_{crit}}$, needed for transition to slug flow, with transition measurements by Andritsos et al. (1989). The comparisons show that the theoretical predictions of $U_{SL_{crit}}$ overpredict the measurements with a factor of two. The overprediction reflects inaccuracies in estimating the interfacial shear stresses (Hurlburt and Hanratty (2002)).

Wallis and Dobbins (1973), Lin and Hanratty (1986) and Wu et al. (1987) followed the analysis by Hanratty and Hershman (1961) to examine the growth of a viscous long wavelength instability (VLW). The VLW theory correctly predicts that the critical gas velocity needed for the transition from stratified to slug flow for air–water flows will increase with increasing pipe diameter (Hurlburt and Hanratty (2002)). On the other hand, Kristiansen (2004) made an experimental investigation based on slug and stratified inlet conditions and found different critical liquid height, $h_{L_{crit}}$, and $U_{SL_{crit}}$ for the two different flow inlet cases. He found that $h_{L_{crit}}$ and $U_{SL_{crit}}$ are successfully predicted by the slug stability model for slug flow inlet conditions, whereas $h_{L_{crit}}$ is well predicted by VLW for stratified flow inlet conditions only at low gas flow rates. On the basis of these findings, Kadri et al. (2008b) presented a new model for predicting the average slug length as a function of time. The model applies a volumetric balance between the front and tail of a slug in order to calculate the slug growth rate and length. At the front, VLW was used to calculate the liquid height, $h_{LV_{LW}}$; and at the tail linear kinematic relations and geometric considerations were used to describe the dynamic behaviour of the liquid at the slug tail. Kadri et al. (2008b) postulated that the slug tail extends due to the fact that the back of the slug travels faster (at the bubble velocity) than the tail upstream, which they assumed to travel at the wave velocity. In their model, the slug reaches its final length when the ratio between the length of the extended slug tail to the calculated slug length equals the ratio between the bubble to the slug average lengths. The

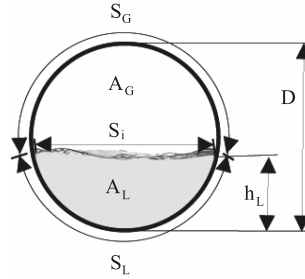


Figure 2.1: Cross-section of the pipe, stratified flow representation.

ratio of the latter is based on conservation of mass were the average liquid height in bubbles of the fully developed slug flow is calculated from slug stability (h_{Lmin}). Their model is only valid at low U_{SG} when $h_{LV LW} > h_{Lmin}$.

In this chapter we extend the work by Kadri et al. (2008b) such that larger ranges of flow rates can be applied. Here, we consider the average maximum liquid height, h_{Lmax} , that can appear at the slug front instead of $h_{LV LW}$ (when $h_{LV LW} < h_{Lmin}$). The parameter h_{Lmax} is, therefore, the equilibrium level of the liquid phase for the given flow conditions assuming stratified flow. Special attention was given for predicting the transition from hydrodynamic to long liquid slugs. For the validation of the model we performed slug length measurements in a 137 m long air–water horizontal pipe flow of an internal diameter (i.d.) of 0.052 m. The measurements are original and unique in the sense that they provide a clear and detailed presentation of the long slug regime which is, unlike the hydrodynamic slug regime, not well reported in literature. Moreover, we compare theoretical predictions of the model with measurements done by Kristiansen (2004) for 0.06 and 0.069 m i.d. pipes at different, flow rates, operation pressures, fluids properties, and slight inclinations. We also compare theoretical predictions with slug length calculations based on frequency measurements by Gregory and Scott (1969), Hubbard (1965), Woods and Hanratty (1999) and Fan et al. (1993a) for 0.019, 0.0351, 0.0763 and 0.095 m i.d. pipes, respectively. The predictions show a satisfactory agreement with the slug length measurements, and a qualitative agreement with the slug length calculations (from slug frequency measurements).

Theoretical background including stability of stratified flow, VLW and slug stability is presented in section 2.2. The experimental setup and the methods used for performing the measurements are given in section 2.3. In section 2.3 we further present an overview of the regimes in the flow map and sub-regimes in the slug flow regime, as found in the experiments. Section 2.4 provides a detailed analysis of the proposed model for calculating the final average slug length. Comparisons between theory and measurements are given in section 2.5. Finally, a discussion and the conclusions are presented in section 2.6.

2.2 Theoretical background

2.2.1 Stratified flow pattern

An idealized model of the stratified flow pattern is represented by a simplified geometry as given in Figure 2.1. The diameter of the pipe is D . The height of the liquid layer along the centerline is h_L . The length of the segments of the pipe circumference in contact with the gas and liquid are S_G and S_L , respectively. The length of the gas–water interface is represented by S_i . The areas occupied by the gas and the liquid are A_G and A_L , respectively. Given the pipe diameter and the liquid height (or area), these parameters can be calculated using the geometric formulae by Govier and Aziz (1972). Now we can write the momentum balances for the gas and the liquid flows as follows,

$$-A_G \left(\frac{dp}{dx} \right) - \tau_{WG} S_G - \tau_i S_i + \rho_G A_G g \sin \theta = 0, \quad (2.1)$$

$$-A_L \left[\left(\frac{dp}{dx} \right) - \rho_L g \cos \theta \left(\frac{dh_L}{dx} \right) \right] - \tau_{WL} S_L + \tau_i S_i + \rho_L A_L g \sin \theta = 0 \quad (2.2)$$

where ρ_G and ρ_L are the gas and the liquid densities, θ is the inclination angle of the pipe from the horizontal, dp/dx is the pressure gradient, dh_L/dx is the liquid hydraulic gradient, and g is the acceleration due to gravitational forces. The time-averaged resisting stress of the gas and the liquid at the wall are τ_{WG} and τ_{WL} , respectively. Term τ_i represents the resisting stress at the interface. The stresses τ_{WG} , τ_{WL} and τ_i are defined in terms of friction factors, which are calculated using the Blasius equation if $Re < 10^5$ and the wall roughness effect can be ignored, otherwise the Churchill equation is used (see Churchill (1977)). For given flow rates of the gas and the liquid, Eqs. (2.1) and (2.2) are used to find the pressure gradient and the height of the liquid layer. However, these equations do not determine the stability of the stratified flow. The flow is assumed to be varying slowly enough that pseudo–steady–state assumptions can be made (e.g. $dh_L/dx = 0$ and τ_{WG} , τ_{WL} and τ_i can be related to flow variables).

2.2.2 Viscous long wavelength theory

The transportation of gas and liquid in horizontal pipes results in a wide range of wavelength waves and wave frequencies along the pipe. At low gas and liquid flow rates, high frequency waves are formed close to the inlet (Woods and Hanratty (1999)). Among those, waves with frequencies 10–12 Hz grow and bifurcate further downstream due to energy accumulations (Fan et al. (1993a)). The bifurcation results, among other, in long wavelength waves that can grow, roll or decay, depending on the height of the liquid layer (Fan et al. (1993a)). For the “right” flow conditions, they grow to become slugs. If the pipe is long enough and the long wavelength waves form far downstream the inlet such that the evolving slugs are independent from the flow disturbances at the inlet, the slugs can grow to become extremely large.

The viscous long wavelength (VLW) stability theory describes such long waves on thin films over which gas is blowing. The waves are assumed to be long enough so that a change in pressure can be described by a hydrostatic approximation and the stresses vary so slowly

in time that a pseudo steady-state approximation describes the change in stresses. The equations of conservation of mass and momentum for the liquid phase in the horizontal pipe are, respectively,

$$\frac{\partial A_L}{\partial t} + \frac{\partial (uA_L)}{\partial x} = 0, \quad (2.3)$$

and

$$\begin{aligned} \frac{\partial (uA_L)}{\partial t} + \frac{\partial (u^2 A_L)}{\partial x} = & -\frac{A_L}{\rho_L} \left[\left(\frac{\partial p}{\partial x} \right) + \rho_L g \cos \theta \left(\frac{\partial h_L}{\partial x} \right) \right] + \\ & + \frac{1}{\rho_L} (\tau_i S_i - \tau_{wL} S_L) + A_L g \sin \theta, \end{aligned} \quad (2.4)$$

A disturbance is assumed to occur at the interface,

$$A_L = \bar{A}_L + \hat{A}_L \exp[ik(x - Ct)], \quad (2.5)$$

where \bar{A}_L is the average area occupied by the liquid, \hat{A}_L is the amplitude of the disturbance, C is the complex wave velocity and k is the wave number. Introducing complex amplitudes of the wave-induced variations of the pressure and of the resisting stresses and substituting equations of the form of Eq. (2.5), Lin and Hanratty (1986) obtained a relation for the critical velocities for the initiation of a long wavelength disturbance,

$$0 = \rho_L (C_R - \bar{u})^2 + \frac{\bar{A}_L}{A_G} \rho_G (\bar{U} - C_R)^2 - g \bar{A}_L \rho_L \cos \theta \frac{\hat{h}}{\bar{A}_L}. \quad (2.6)$$

Terms \bar{U} and \bar{u} are the time average gas and liquid velocities. Term C_R is the real part of C , for given superficial gas and liquid velocities at neutral stability, where C_I , the imaginary part of C , is zero. Substituting the critical velocities in Eq. (2.4) results in the liquid area, A_{LVLW} (or h_{LVLW}), required for the initiation of instabilities at the surface (e.g. waves or slugs). A detailed analysis of the VLW theory can be found in Lin and Hanratty (1986) and in Hurlburt and Hanratty (2002).

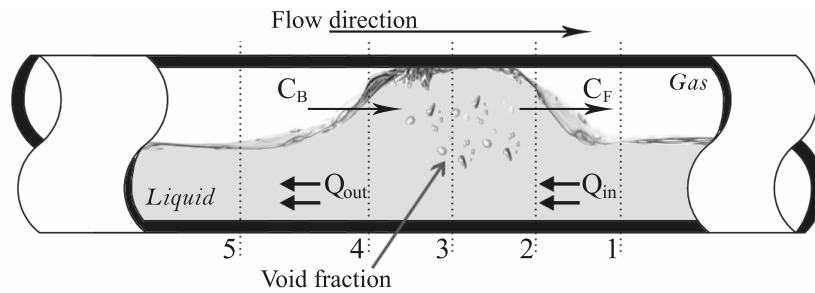


Figure 2.2: Sketch of a slug.

2.2.3 Slug stability analysis

The slug stability analysis considers the rates of liquid adjoining and detaching from a slug at its front and rear. Slugs are defined here as stable when the rates of liquid adjoining are not less than the rates at which liquid detaches, and they are addressed as “neutrally stable” when their length is neither growing nor decaying. Figure 2.2 gives an illustration of a slug moving with a front velocity C_F over a stratified liquid layer, at station 1, of area A_{L1} and velocity u_1 . The volumetric flow rate of liquid adjoining the slug is

$$Q_{in} = (C_F - u_1)A_{L1}. \quad (2.7)$$

The rear of the slug is assumed to behave as a bubble moving with a velocity C_B . Following Bendiksen (1984), Woods and Hanratty (1996), Hurlburt and Hanratty (2002) and Soleimani and Hanratty (2003) the velocity at the back of a slug can be modelled as a Benjamin bubble (Benjamin (1968)) where three main regimes are defined:

$$C_B = U_{Mix} + 0.542\sqrt{gD} \quad U_{Mix} < 2\sqrt{gD}, \quad (2.8)$$

$$C_B = 1.1U_{Mix} + 0.542\sqrt{gD} \quad 2\sqrt{gD} < U_{Mix} < 3.5\sqrt{gD}, \quad (2.9)$$

$$C_B = 1.2U_{Mix} \quad U_{Mix} > 3.5\sqrt{gD}. \quad (2.10)$$

The velocity of the liquid in the slug is u_3 (the liquid velocity at station 3). The volume fraction of the gas in the slug is ϵ . The volumetric flow rate of the liquid detaching from the slug is

$$Q_{out} = (C_B - u_3)(1 - \epsilon)A, \quad \text{at station 3.} \quad (2.11)$$

Assuming neutral stability, $Q_{in} = Q_{out}$ and $C_F = C_B$, and making use of Eqs. (2.7)–(2.11), the following relation is obtained,

$$\left(\frac{A_{L1}}{A}\right)_{crit} = \frac{(C_B - u_3)(1 - \epsilon)}{(C_B - u_1)}, \quad (2.12)$$

for the area of the stratified flow. For incompressible flow, the term u_3 is calculated from a volumetric balance between the inlet of the pipe and station 3 as follows,

$$U_{Mix} = \epsilon U_3 + (1 - \epsilon)u_3, \quad (2.13)$$

where U_3 is the gas velocity at station 3. At low mixture velocities aeration is negligible ($\epsilon = 0$) so that Eq. (2.13) gives $u_3 = U_{Mix}$. Eq. (2.12) is used later to calculate the average liquid level below the elongated bubbles in the “fully developed” slug flow. The detailed analysis of the slug stability model is well documented by Hurlburt and Hanratty (2002); Soleimani and Hanratty (2003).

2.3 Experiments on the occurrence of long slugs

2.3.1 Experiments

Experiments have been carried out in order to investigate the long slug regime (Zoetewij (2007)). Not many researchers are aware of this regime and its properties due to a number of conditions required for such slugs to appear, e.g. long pipe and low flow rates and operation pressure. The flow facility used for this aim consists of a 137 m long horizontal pipeline with a diameter of 0.052 m (see Figure 2.3). The pipe is made of Perspex (Plexiglass) to allow visual observations of the flow conditions. At the inlet, the two phases are combined in a Y-shaped section with the gas phase always entering from the top in a horizontal direction in order to prevent the impact of the gas-jet coming from above. The pressure is atmospheric and the gas and liquid phases used are air and water, respectively.

Two different measurement techniques, based on liquid conductance, were installed. The first technique consists of a set of sensors that measure the presence of passing slugs. It consists of point detector sections positioned at 8 locations along the pipe at: 29, 43, 62, 74, 93, 107, 120, and 132 m from the inlet. A schematic drawing of these positions is given in Figure 2.4. Each measurement section contains 2 pairs of sensors separated by 0.7 m. Each pair of sensors consists of two electrodes one at the bottom of the pipe and the second on top. Due to the fact that the electrodes at the bottom are circular plates of 0.01 m diameter the electrical conductance between the liquid phase and these electrodes are always good. On the other hand, the top electrodes consist of a metal pin with a diameter of 1 mm. The slug length and velocity are calculated from the time difference of the slug passing two different sensors of the same section: (1) the velocity is calculated from the distance between the two sensors divided by the time difference; and (2) the slug length is calculated from the velocity and the time difference between the front and tail passing the same sensor. The second measurement technique is based on wire-mesh sensors. Unlike the point probe sensors, this technique provides a more detailed flow imaging in stratified and slug flows. The technique is based on the difference in electrical conductivity of both phases. A set of 4 sensors is used at different positions: 38, 56, 105 and 125 m from the inlet (see Figure 2.4). Each sensor consists of two planes with 16 parallel 0.12 mm wires each. The wires in different planes are perpendicular to each other. Measuring the signal of all vertical receiver wires crossing a horizontal sending one results in the local conductivity around the crossing points in the mesh. The conductivity signals indicate the local phase composition in the grid cell. Further details on the wire-mesh can be found in Zoetewij (2007).

The experiments were performed at atmospheric pressure and constant flow rates with superficial gas and liquid velocities being 0.5–2.5 and 0.05–0.30 m/s, respectively. The different combinations of flow rates used in the experiments resulted in a detailed overview of the slug flow development in different regimes, and sub-regimes within the long slug flow regime.

2.3.2 Sub-regimes in the slug flow map

The different flow regimes and a number of different sub-regimes within the long slug flow regime observed in the experiments are shown in Figure 2.5. The dashed-dotted line is the

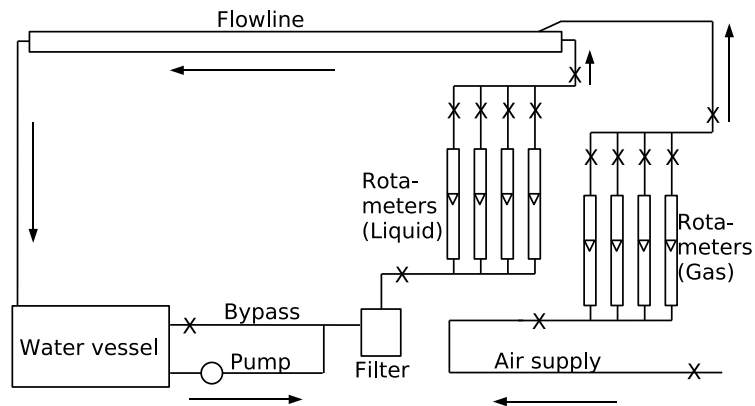


Figure 2.3: Sketch of the experimental setup (after Zoetewij (2007)). The valves are indicated by \times .

observed transition from stratified (\times) or stratified-wavy flow ($*$) to slug flow; the solid-line is the observed transition from hydrodynamic slug flow (\circ) to the long slug flow regime. Within the long slug flow regime, two sub-regimes were observed: (1) above the dashed-line long but neutrally stable slugs (\blacktriangle); and (2) below the dashed line, long and positively growing slugs were found (\bullet).

The hydrodynamic slugs are characterized by a relatively short length, less than $40D$. Whereas the long slugs have at least a length of $40D$ and can reach lengths up to several hundred pipe diameters. Note that the long slug region shrinks for increasing gas velocity – the long slugs are found to exist only at low gas and liquid flow rates, as shown in Figure 2.5. Therefore, the transition from stratified flow to hydrodynamic slugs, at low superficial gas velocities, passes through the long slug regime. For higher superficial gas velocities, $U_{SG} > 2.5 \text{ m/s}$, the transition from the stratified-wavy to hydrodynamic slug flow is direct. The absence of the long slugs at higher U_{SG} is related to the higher slug frequency and lower amount of liquid adjoining the passing slug due to a decrease of the liquid level (conservation of mass and momentum) which results in a neutral stability ($Q_{in} = Q_{out}$ and $C_F = C_B$) earlier

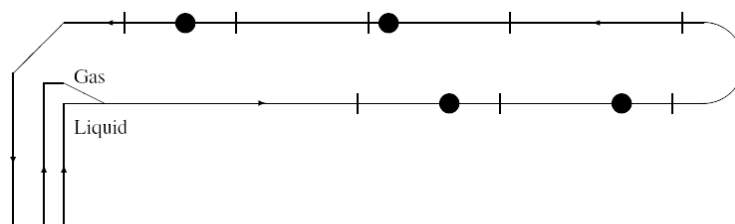


Figure 2.4: Schematic drawing of the position of the point probe (|) and wire-mesh (\bullet) sensors (after Zoetewij (2007)).

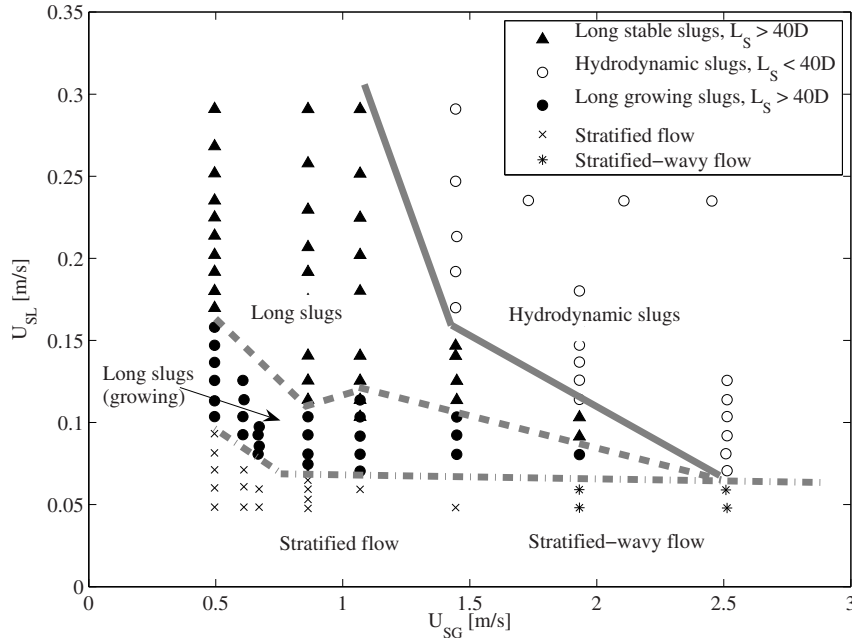


Figure 2.5: Air–water measurements of the slug flow regime and sub–regimes for different U_{SG} and U_{SL} , $D = 0.052 \text{ m}$, $\theta = 0^\circ$, $P = 1 \text{ barA}$.

in the pipe. Consequently, in the long slug regime, the slug length and growth time decrease at larger flow rates, as observed in the experiments.

Figure 2.6 is a flow regime map by Woods and Hanratty (1999) for air–water flow in a horizontal 0.0763 m pipe. In the figure, curve *A* indicates the transition from stratified to slug flow; the region between curves *A* and *B* (areas *I* and *II*) covers slugs that form about $40D$ downstream of the entrance; area *III* represents slugs that form within $40D$ from the entrance; and along curve *C* the Froude number, $Fr = u / \sqrt{gh_{Lmax}}$, is unity at the inlet. Comparing Figures 2.5 and 2.6, and noting the difference in the diameters, we find the following: (1) The long growing slugs correspond to the slugs evolving from long wavelength waves downstream (at $Fr < 1$). (2) The long stable slugs evolve from the same type of waves but further upstream. Their frequency is higher and they travel over a thinner liquid layer, that is why they reach neutral stability earlier in the pipe. (3) The hydrodynamic slugs correspond to slugs that form upstream (close to the inlet) at $Fr > 1$. These slugs are no longer formed by the long wavelengths but close to the entrance by disturbances that are created there (Woods and Hanratty (1999)). The high frequency of such slugs and the thin liquid layer downstream result in their short length. These findings are in agreement with our above mentioned experimental observations.

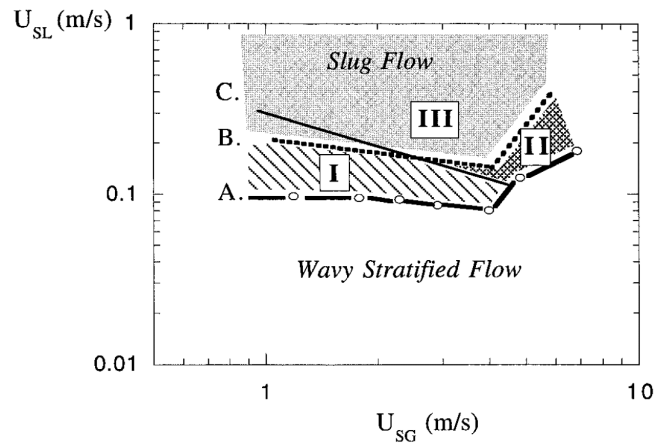


Figure 2.6: Flow regime map for air–water flow in a horizontal 0.0763 m pipe. Curve A indicates the transition to slug flow; between curves A and B, slugs from downstream ca. 40D; along curve C, Froude number $Fr = 1$ at the inlet (Woods and Hanratty (1999))¹.

2.4 Dynamic slug model

In the model presented here, the average length of a fully developed slug is determined from volumetric liquid considerations between the front and the tail of a slug. The liquid level at the front is assumed to be constant, whereas at the back, the liquid level drops during the initiation of the slug and then rebuilds during its growth. The liquid level at the back is obtained from linear kinematic relations between the slug and the wave behind it. The properties of slugs at formation time are presented in section 2.4.1. In section 2.4.2, the calculation method of the dynamic slug is introduced. A stopping criterion for the calculation of the slug growth, based on conservation of mass of the gas and liquid phases, is addressed in section 2.4.3.

2.4.1 Properties of forming slugs

2.4.1.1 Wave velocity

We address the formation of slugs from growing waves. The growing waves are assumed to be sinusoidal with an initial wavelength, λ , large compared to the average maximum liquid height, $h_{L_{max}}$. A characteristic property of such waves is the dependency of the wave velocity, C , on the liquid level alone,

$$C = \sqrt{gh_{L_{max}}}. \quad (2.14)$$

¹Reprinted from International Journal of Multiphase Flow, Vol 25, Bennett D. Woods, Thomas J. Hanratty, Influence of Froude number on physical processes determining frequency of slugging in horizontal gas–liquid flows, 1195–1223, Copyright (1999), with permission from Elsevier.

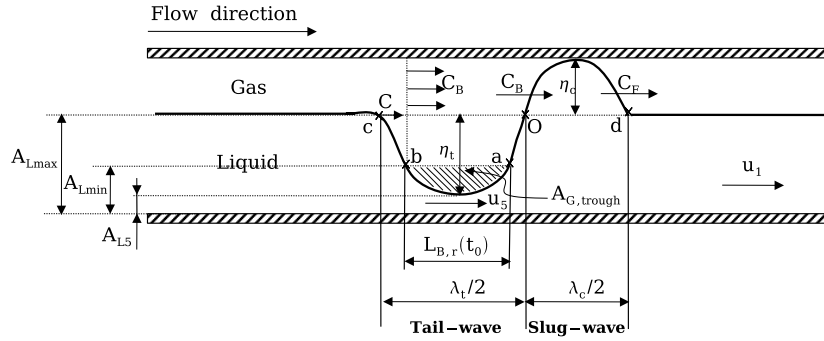


Figure 2.7: A slug at initiation time expressed as two sinusoidal waves.

2.4.1.2 Slug at initiation

When a wave keeps on growing, its amplitude will eventually be so large that the top of the wave hits the top of the pipe. This is the initiation of a slug. As the initiated slug is the result of a growing wave, its initial shape will be sinusoidal (note that after the initiation the slug grows and changes shape and it is no longer sinusoidal). Here, the front of the wave is addressed as *slug-wave*, and the back as *tail-wave* (Figure 2.7). These two parts of the wave are coupled via a mass balance; the liquid required to create the slug is shed from the tail-wave. The amplitude of the front of the wave (*slug-wave*) is

$$\eta_c = D - h_{L_{max}} \quad 0 < h_{L_{max}} < D, \quad (2.15)$$

as the wave started from the stratified layer of height $h_{L_{max}}$. At the back of the wave (*tail-wave*), the amplitude η_t will be the same, provided that $\eta_c \leq h_{L_{max}}$. Otherwise, the amplitude of the tail-wave is

$$\eta_t = h_{L_{max}} \quad h_{L_{max}} \leq D/2. \quad (2.16)$$

In this case, the length of the tail-wave, $\lambda_t/2$, is no longer equal to the length of the slug-tail $\lambda_c/2$ (which is $\lambda/2$). The actual length of the tail-wave in this case is computed from a simple mass balance (i.e. all extra liquid in the slug-wave comes from liquid originally filling up the tail-wave) and the pipe geometry at the location of the tail-wave. The length of the tail-wave is then calculated using the geometric formulae by Govier and Aziz (1972). A schematic drawing of a slug at initiation is given in Figure 2.7. In the figure, the parameters A_{L5} and u_5 are the liquid area and velocity at the trough (station 5). The term $A_{L_{min}}$ is the critical liquid area calculated by the slug stability model (Eq. (2.12)). The hatched area, $A_{G,trough}$ is the gas area between $A_{L_{min}}$ and A_{L5} .

2.4.1.3 Slug tail extension

At slug formation time, t_0 , the slug front and the back of the tail-wave, at point c , propagate at the actual velocities C_F and C , respectively. On the other hand, the back of the slug propagates

at the bubble velocity C_B . The front of the tail-wave (point O) is obviously the back of the slug. Therefore, it propagates together with the back of the slug. The $A_{L_{min}}$ line in Figure 2.7 is the slug stability line representing the average liquid level below the bubbles in the fully developed slug flow. Points a and b refer to two points on the tail-wave (at time t_0) being at the height of the final liquid level, $h_{L_{min}}$ (calculated from $A_{L_{min}}$).

Due to the relative velocity between the two sides of the tail-wave (points O and c) the wave volume in between is expanded in time. While point a propagates with the slug back at velocity C_B , from a linear expansion point b propagates at a velocity,

$$v_b = C + r(C_B - C), \quad (2.17)$$

where r is the ratio between the horizontal displacements of points b , calculated from the wave equation, and a relative to c . The ratio r has a value $0 \leq r \leq 1$. Due to the relative velocity between points a and b the relative distance between them, $L_{B,r}$, grows linearly as

$$L_{B,r}(t) = L_{B,r}(t_0) + (v_b - C)t. \quad (2.18)$$

Eq. (2.18) describes the extension of the tail in time. It plays a major role in a stopping criterion for the calculations of the average slug length, as will be seen in section 2.4.3.

2.4.1.4 Initial slug length

The initial slug length, L_0 , is calculated from the wavelength, λ ,

$$L_0 = \frac{\lambda}{2}. \quad (2.19)$$

Term λ is calculated from the wave velocity ($\lambda = C/f_w$) and the relation $f_w = c_w f_S$ by Tronconi (1990) for the slug and the wave frequencies, f_S and f_w , as follows,

$$\lambda = \frac{C}{c_w f_S}, \quad (2.20)$$

where c_w is a constant equal to 2 for air–water systems (Tronconi (1990)). In this chapter the same value of c_w was used for the different fluids. Kadri et al. (2008b) suggested to use a correlation by Nydal (1991) for the slug frequency,

$$f_S = 0.088 \frac{(U_{SL} + 1.5)^2}{gD}. \quad (2.21)$$

Quantities in Eq. (2.21) are in meters and seconds. The application condition of Eq. (2.21) is that the frequency of slugs is dominated by U_{SL} . Note that the slug frequency correlation is used here only in order to obtain a “realistic” initial length of the long waves (which are in agreement with experiments). Other methods can be implemented to obtain an initial wavelength. Alternatively, L_0 can be calculated from the minimum stable slug length by Dukler et al. (1985).

2.4.2 Slug growth and final length

The calculations of the slug growth are not sensitive to small changes in the initial wavelengths especially for long slugs where the final length of slugs $L_{S,f} \gg \lambda$. Therefore, the main contribution to the final slug length is the additional slug growth due to the volumetric differences between liquid adjoining the slug at the front and detaching from the slug at the trough. The volume of the liquid in front of the slug is the product of the cross-sectional area, $A_{L_{max}}$, occupied by the liquid times the length of this liquid part. Similarly, for the liquid volume at the back of the slug, we need to calculate the cross-sectional area of the liquid layer at the trough. Hence, we need to calculate the two liquid areas, at the trough and downstream of the slug.

2.4.2.1 The liquid area downstream of the slug, $A_{L_{max}}$

The liquid area downstream is calculated from the momentum balances for the stratified flow pattern, Eqs. (2.1)–(2.2). Substituting $A_L = A_{L_{max}}$ and $A_G = A - A_{L_{max}}$, Eq. (2.1) is written in the following form,

$$\left(\frac{dp}{dx} \right) = \frac{\tau_{WG}S_G + \tau_i S_i}{A - A_{L_{max}}} - \rho_G g \sin \theta. \quad (2.22)$$

Plain stratified flow is reached when the pressure gradients of the two phases on the interface cancel each other. Therefore, substituting Eq. (2.22) in Eq. (2.2) and after basic algebra we obtain,

$$A_{L_{max}} = A \frac{\tau_{WL}S_L - \tau_i S_i}{\tau_{WL}S_L + \tau_{WG}S_G} + g A_{L_{max}} (A - A_{L_{max}}) \left[\rho_L \cos \theta \left(\frac{dh_L}{dx} \right) - \sin \theta (\rho_L - \rho_G) \right]. \quad (2.23)$$

For a fully developed horizontal flow Eq. (2.23) reduces to the simple form,

$$A_{L_{max}} = A \frac{\tau_{WL}S_L - \tau_i S_i}{\tau_{WL}S_L + \tau_{WG}S_G}. \quad (2.24)$$

Eq. (2.24) successfully predicts that increasing the gas flow rates or decreasing the liquid flow rates results in a lower $A_{L_{max}}$.

At low flow rates slugs evolve downstream from long wavelength waves as mentioned above. In that case, the liquid level of the stratified flow at t_0 is calculated by VLW theory. If the liquid flow rates are larger than those predicted by VLW theory, we use Eq. (2.24) for the calculation of the stratified liquid level. On the other hand, the minimum liquid area, $A_{L_{min}}$, at the front of a fully developed slug is calculated by the slug stability model, Eq. (2.12), as mentioned earlier.

2.4.2.2 The liquid area upstream of the slug, $A_{L5}(t)$

Making use of the neutral stability assumptions ($Q_{in} = Q_{out}$ and $C_F = C_B$), the liquid velocity at the trough u_5 is obtained from a volumetric flow balance between the liquid entering at station 1 (front) and detaching at station 5 (see Figure 2.2) for the fully developed case, thus

$$u_5 = u_1 \frac{A_{L_{min}}}{A_{L5}(t)}, \quad (2.25)$$

where u_1 is the liquid velocity downstream of the slug (station 1) and $A_{L5}(t)$ is the cross-sectional area of the liquid at the trough.

The average velocity of the gas above $A_{G,trough}$ is assumed to be the bubble velocity C_B and therefore the gas volume is conserved there. This also implies that the initial gas volume above the trough and below A_{Lmin} is constant (see the hatched area in Figure 2.7). Since $h \ll \lambda$ the area $A_{G,trough}$ was considered instead of the volume. The parameter $A_{G,trough}$ is calculated by integrating the wave function between points a and b at any time t as follows,

$$A_{G,trough} = [h_{Lmin} - h_{L5}(t)] \int_b^a \sin \left[\frac{2\pi}{\lambda_c + 2(C_B - C)t} x \right] dx. \quad (2.26)$$

The left hand side of Eq. (2.26) is a constant. Therefore, substituting two cases in Eq. (2.26), the first $t = 0$ and the other $t = t$, and equating between them results in the liquid level at the trough, $h_{L5}(t)$, as follows,

$$h_{L5}(t) = h_{Lmin} \left[1 - \frac{\lambda_c}{\lambda_c + 2(C_B - C)t} \right] + h_{L5}(0) \frac{\lambda_c}{\lambda_c + 2(C_B - C)t}, \quad (2.27)$$

where $h_{L5}(0) = D - \eta_c - \eta_t$. For the pipe diameter and flow conditions used in this chapter $h_{L5}(0) \ll (D - h)$ and therefore was neglected. The liquid area $A_{L5}(t)$ is calculated from $h_{L5}(t)$ in Eq. (2.27) and the geometric formulae presented by Govier and Aziz (1972).

Eq. (2.27) provides an explanation for the behaviour of the slug length at different flow rates, which decreases when increasing the flow rates (as shown in Figure 2.9). In the equation, increasing the flow rates results in larger values of, h_{L5} . This means that the rebuild rate of the liquid behind a slug increases with the flow rates, and thus the growth time of the slug decreases which results in a shorter slug.

2.4.2.3 Slug length, $L_S(t)$

The change in the additional liquid volume entering the slug describes the rate of change of the slug volume,

$$\frac{dV}{dt} = [C_F(t) - u_1] A_{Lmax} - (C_B - u_5) A_{L5}(t), \quad (2.28)$$

and the front velocity is

$$C_F(t) = \frac{dV}{d(At)} + C_B. \quad (2.29)$$

To simplify the problem we assumed that C_B is constant in time.

The total slug volume is calculated from the sum of Eqs. (2.19) and (2.28),

$$V_{slug}(t) = L_0 A + \int_0^t ((C_F(t) - u_1) A_{Lmax} - (C_B - u_5) A_{L5}(t)) dt. \quad (2.30)$$

Once Eq. (2.30) is solved, the slug length follows as

$$L_S(t) = \frac{V_{slug}(t)}{A}. \quad (2.31)$$

2.4.3 End of slug growth

If only one slug would have been initiated in the pipe, it would keep growing until it finally exits the pipe. However, in general more slugs are present at the same time. A slug will stop growing as soon as its front approaches the back of the tail of the next slug downstream. Thus, we need to estimate when this happens. We do so by inspecting what happens when all slugs are formed at regular distances. This means that we will find the average slug length and ignore that actually a distribution of slug lengths develops as slugs are initiated in an irregular way. However, with this approach we can estimate the average slug length and by that predict where the long slug regime is located in the flow map. As a consequence, all slugs and bubbles reach their final lengths simultaneously, say at time t_∞ . This conclusion leads to a stopping criterion for the calculation of the average slug length: the final average slug length is reached when the extension of the tail (the distance between points a and b) becomes equal to the bubble final length,

$$L_{B,r}(t) = L_{B,f}, \quad (2.32)$$

as shown in Figure 2.8. In the figure, the fully developed average slug problem is presented for a pipe cross-sectional area A . The cross-sectional liquid area of the stratified flow is A_{Lmax} and for the fully developed slug flow is A_{Lmin} along the bubble. Choosing a control volume with the unit length, $L_U = L_{B,f} + L_{S,f}$, and making a volumetric balance between the stratified flow and the fully developed slug flow cases, a relation between the bubble and slug lengths is obtained as follows,

$$L_{B,f} = L_{S,f} \frac{A - A_{Lmax}}{A_{Lmax} - A_{Lmin}}. \quad (2.33)$$

At the limit of Eq. (2.33) when $A_{Lmax} \rightarrow A_{Lmin}$, term $L_{B,f} \rightarrow \infty$, which means that there are no slugs in the pipe, as expected.

Since $L_{S,f}$, $L_{B,f}$, L_U and t_∞ are unknowns, t_∞ is calculated recursively by substituting Eqs. (2.18) and (2.32), and $L_S(t)$ instead of $L_{S,f}$, in Eq. (2.33) as follows,

$$t_\infty = \frac{1}{v_b} \left[L_S(t_\infty) \frac{A - A_{Lmax}}{A_{Lmax} - A_{Lmin}} - L_{B,r}(t_0) \right]. \quad (2.34)$$

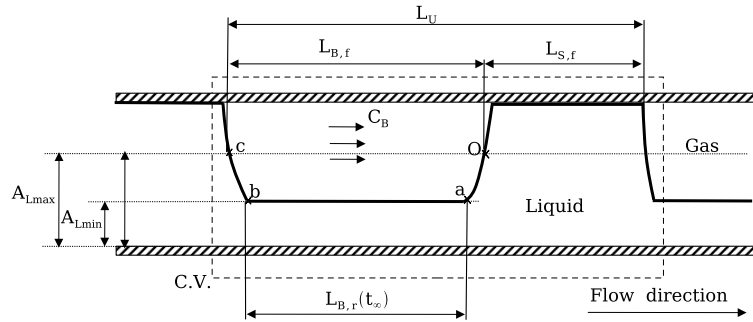


Figure 2.8: A presentation of the average fully developed slug flow.

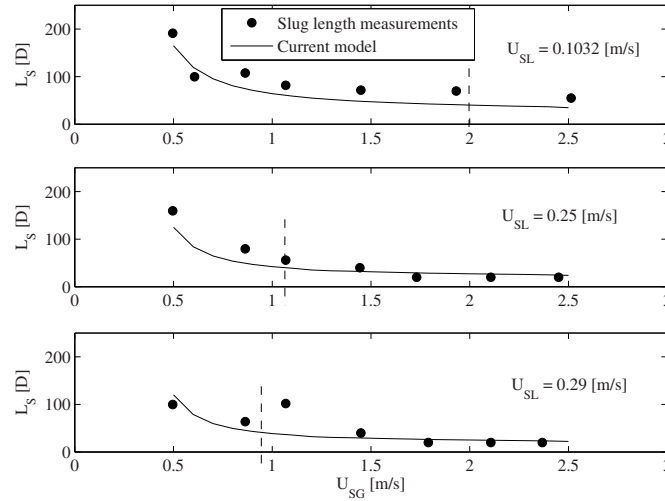


Figure 2.9: Air–water theoretical predictions and measurements of slug length as a function of gas superficial velocity, $D = 0.052 \text{ m}$, $\theta = 0^\circ$, $P = 1 \text{ barA}$.

It is known from experiments (e.g. Kristiansen (2004)) that increasing the gas flow rates results in faster development of the slug flow. This is well observed in Eq. (2.34), at higher gas flow rates v_b increases and t_∞ decreases.

2.5 Results

The measurements presented in this section were performed by a number of researchers at different flow conditions and pipe sizes. A summary of the properties of the different systems is found in Table 2.1.

Table 2.1: Summary of system properties

	Air–water	Air–water	SF_6 –Oil	CO_2 –water
Pipe diameter [cm]	9.5, 7.63, 6, 5.2, 3.51	6	6.9	1.9
Pressure [Pa]	1×10^5	1×10^5	$1\text{--}3 \times 10^5$	1×10^5
Pipe inclination [deg]	0	–0.5	–0.1	0
Interfacial tension [N/m]	0.07	0.07	0.022	0.07
Gas density [kg/m^3]	1.2	1.2	1.2, 9, 19	1.8
Gas viscosity [kg/ms]	1.8×10^{-5}	1.8×10^{-5}	1.37×10^{-5}	1.5×10^{-5}
Liquid density [kg/m^3]	1000	1000	800	1000
Liquid viscosity [kg/ms]	0.001	0.001	0.0018	0.001

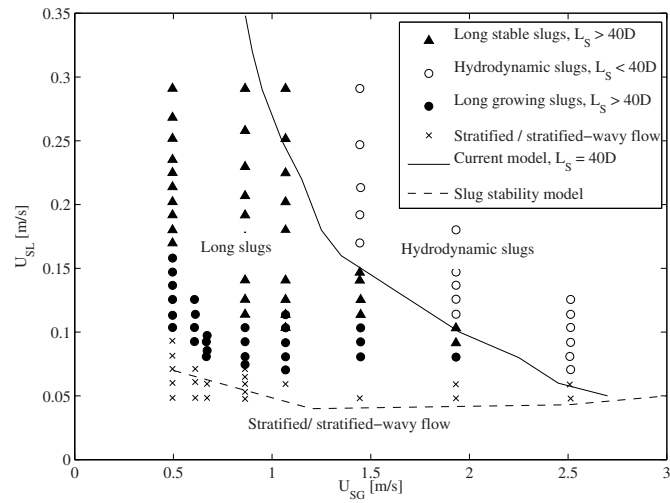


Figure 2.10: Air–water theoretical predictions and measurements of the flow regime transition for different U_{SG} and U_{SL} . $D = 0.052\text{ m}$, $\theta = 0^\circ$, $P = 1\text{ barA}$.

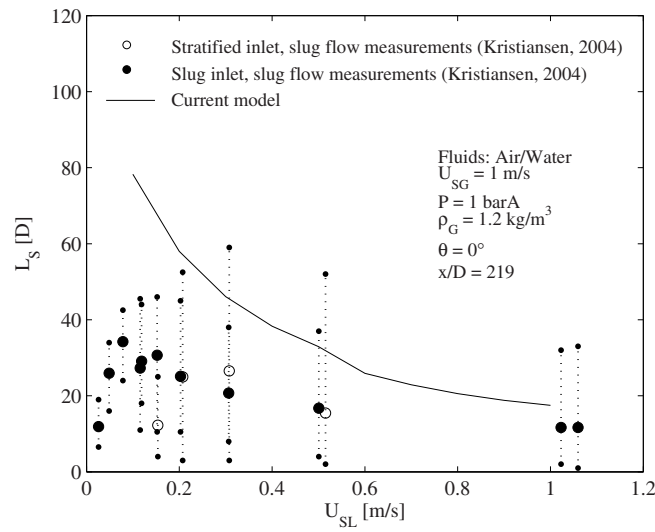


Figure 2.11: Air–water theoretical predictions and measurements of slug length as a function of liquid superficial velocity, $D = 0.06\text{ m}$, $\theta = 0^\circ$, $P = 1\text{ barA}$, $U_{SG} = 1\text{ m/s}$.

2.5.1 Predictions for horizontal air–water flow

Theoretical calculations of slug final lengths, $L_{S,f}$, are compared with measurements for air–water horizontal flow in Figures 2.9, 2.10 and 2.11. The measurements in Figures 2.9 and 2.10 were carried out in a 137 m long pipe with 0.052 m i.d. at the TU Delft facility (Zoetewij (2007)). The subplots in Figure 2.9 show $L_{S,f}$ as a function of U_{SG} for three different U_{SL} : 0.1032, 0.25 and 0.29 m/s. The figure shows a satisfactory agreement between predictions and measurements for the given flow rates. The vertical dashed lines indicate the critical U_{SG} for the transition from hydrodynamic to long slugs (i.e. slugs larger than $40D$). The transition is further presented in Figure 2.10, a flow map for different slug flow regimes and sub–regimes. Here, the dashed line represents the transition from stratified to slug flow by the slug stability model, and the solid line is the prediction by the current model for $L_{S,f} = 40D$, which represents the transition from hydrodynamic to long slug regimes. The current model for the transition from hydrodynamic to long slugs underpredicts the measurement at low U_{SG} , but quite accurately predicts the transition at higher U_{SG} .

The measurements in Figure 2.11 were done by Kristiansen (2004) in a 16 m pipe with i.d. of 0.06 m. Two different inlet conditions were considered here, stratified and slug flow represented by empty and filled circles, respectively. The dotted vertical lines are the deviation from the average slug length. The figure shows the behaviour of the slug length as a function of U_{SL} , at $U_{SG} = 1$ m/s. It is noticeable that the theoretical model (the solid line) overpredicts the average values of the slug lengths with about a factor of 4 at low U_{SL} . A possible reason for this deviation between predictions and measurements is the short pipe length being not sufficient for developed slug flow (the slug growth rate at $x/D = 219$ is still positive, Kristiansen (2004)). Note that the inlet conditions do not have a significant impact on the slug length in the short loop.

2.5.2 Predictions for declined air–water flow

Figures 2.12 and 2.13 compare theoretical predictions of the slug length with measurements, as a function of U_{SL} for $U_{SG} = 1$ and 3 m/s, respectively. The measurements were also done by Kristiansen (2004) and carried out in the same short flow loop as in Figure 2.11. However, a negative inclination of -0.5° was considered here. Kristiansen (2004) found that the declination of the pipe results in lower growth rates so that slugs reach their final length earlier in the pipe, especially at lower U_{SG} . In the case of Figure 2.12, where $U_{SG} = 1$ m/s, the measured slugs have reached their final length and they are in good agreement with the theoretical predictions. On the other hand, for the measurements in Figure 2.13, carried out at higher U_{SG} , the pipe is too short to obtain a fully developed slug flow. Here, the model overpredicts the slug length with a factor of three at low U_{SL} , and underpredicts it with a factor of two at high U_{SL} .

2.5.3 Predictions for SF_6 gas–ExxsolD80 oil flow under varying pressure

The measurements shown in Figures 2.14–2.15 are those performed by Kristiansen (2004) for different inlet conditions with different fluids in a longer and slightly larger facility (horizontal, 103 m long test loop with an i.d. of 0.069 m). Instead of air/water he used SF_6 (sulphur

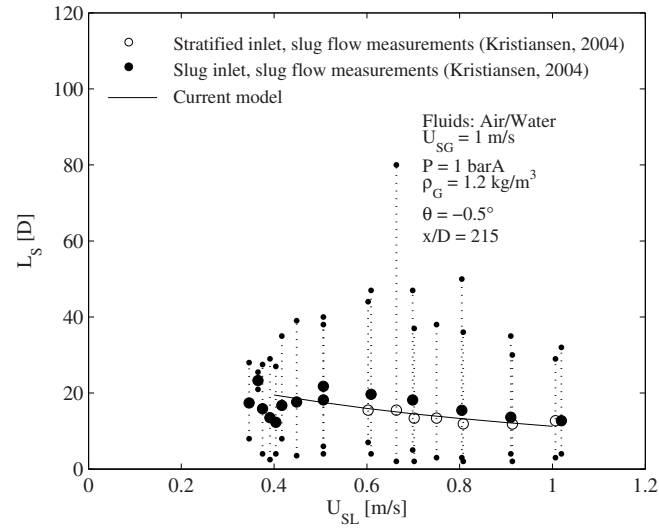


Figure 2.12: Air–water theoretical predictions and measurements of slug length as a function of liquid superficial velocity, $D = 0.06$ m, $\theta = -0.5^\circ$, $P = 1$ barA, $U_{SG} = 1$ m/s.

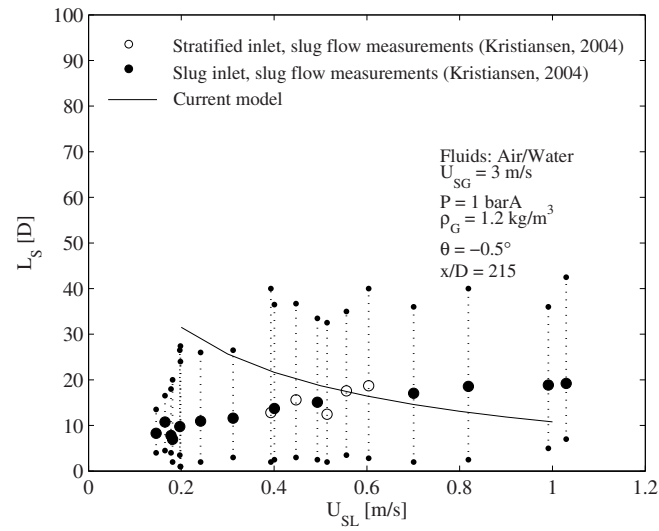


Figure 2.13: Air–water theoretical predictions and measurements of slug length as a function of liquid superficial velocity, $D = 0.06$ m, $\theta = -0.5^\circ$, $P = 1$ barA, $U_{SG} = 3$ m/s.

hexafluoride) gas and *ExxsolD80* (hydrocarbon fluid) liquid at two different pressures. Sulphur hexafluoride is a dense gas, approximately 5.5 times of the air density, that simulates high operation pressure conditions. The figures compare theoretical predictions of $L_{S,f}$ with measurements as a function of U_{SL} at constant U_{SG} and varying pressure. The predictions of $L_{S,f}$ in Figure 2.14 ($P = 1.5 \text{ barA}$ and $\rho_G = 9.1 \text{ kg/m}^3$ simulating $P = 12 \text{ bar}$) are in a good agreement with the slug inlet measurements. However, a deviation between the predictions and the stratified inlet measurements at $U_{SL} < 0.15 \text{ m/s}$ is noticed. The reason behind the deviation is the proximity of the low U_{SL} to the pattern transition value that moves the slug initiation point further downstream in the pipe. As a result, the slugs close to the outlet are not fully developed.

At higher pressure, $P = 3 \text{ barA}$ ($\rho_G = 18 \text{ kg/m}^3$ simulating $P = 23 \text{ bar}$), a deviation is noticed, as well, between predictions and slug inlet measurements at $U_{SL} = 0.1 \text{ m/s}$ (see Figure 2.15). The deviation between the predictions and the stratified inlet measurements becomes even larger and for a wider range of U_{SL} ($U_{SL} < 0.4 \text{ m/s}$). In the stratified inlet case, increasing the pressure results in increasing $U_{SL,crit}$ needed for the transition from stratified to slug flow. Therefore, the delay of the slug initiation point further downstream in the pipe corresponds, as well, to higher values of U_{SL} . That is also why in the case of $P = 3 \text{ barA}$ no slugs appeared for $U_{SL} < 0.17 \text{ m/s}$ at the given U_{SG} (the flow rates are below the critical values required for the pattern transition). In the case of the slug inlet, slugs at $U_{SL} < 0.12 \text{ m/s}$ are unstable (slug stability) and their growth is sensitive to small perturbations at their

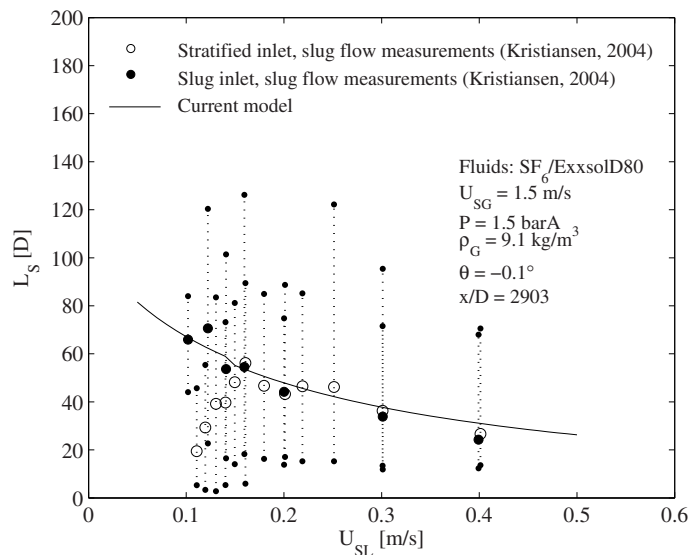


Figure 2.14: SF_6 -*ExxsolD80* theoretical predictions and measurements of slug length as a function of liquid superficial velocity, $D = 0.069 \text{ m}$, $\theta = -0.1^\circ$, $P = 1.5 \text{ barA}$, $U_{SG} = 1.5 \text{ m/s}$.

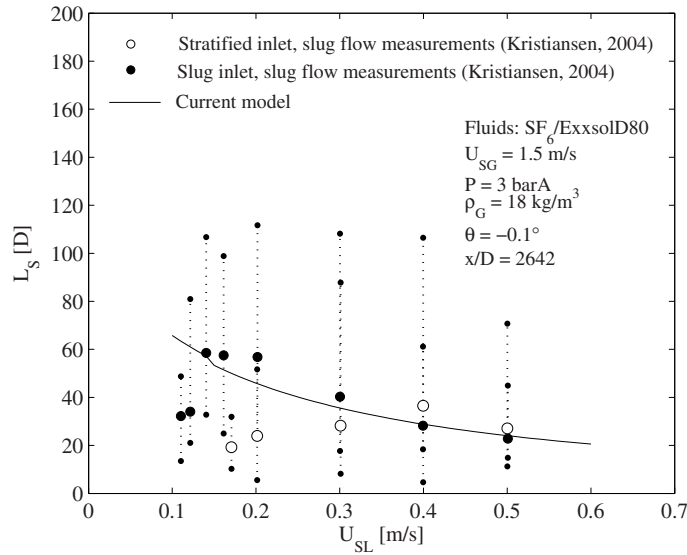


Figure 2.15: SF_6 -ExxsolD80 theoretical predictions and measurements of slug length as a function of liquid superficial velocity, $D = 0.069\text{ m}$, $\theta = -0.1^\circ$, $P = 3\text{ barA}$, $U_{SG} = 1.5\text{ m/s}$.

fronts. Therefore, they can grow or decay accordingly.

2.5.4 Predictions at large mixture velocities

In this subsection we examine the effect of large mixture velocities on the predictions by the proposed model and compare the predictions to available measurements. Unfortunately, in these experiments there were no direct measurements for the slug length but for the slug frequency. For that reason, we used the following approximation, suggested by Woods and Hanratty (1996), for the relation between f_S and $L_{S,f}$ under “fully developed” conditions,

$$\frac{f_S D}{U_{SL}} = 1.2 \left(\frac{L_{S,f}}{D} \right)^{-1}. \quad (2.35)$$

Please note that we shall denote the slug lengths derived from the slug frequency measurements via Eq. (2.35) in the subsequent comparisons by slug “measurements”. Figures 2.16–2.17 compare predictions and measurements for a 20 m length and 0.0763 m i.d. pipe. The slug frequency measurements were done by Woods and Hanratty (1999). In Figure 2.16 we see that the current model overpredicts the measurements at low U_{SL} , underpredicts them at high U_{SL} and successfully predicts them at “intermediate” U_{SL} . Predictions at intermediate liquid flow rates are important for the transition from hydrodynamic to long slug flows as shown in Figure 2.17, a flow map for the long (●) and hydrodynamic (○) slug measurements

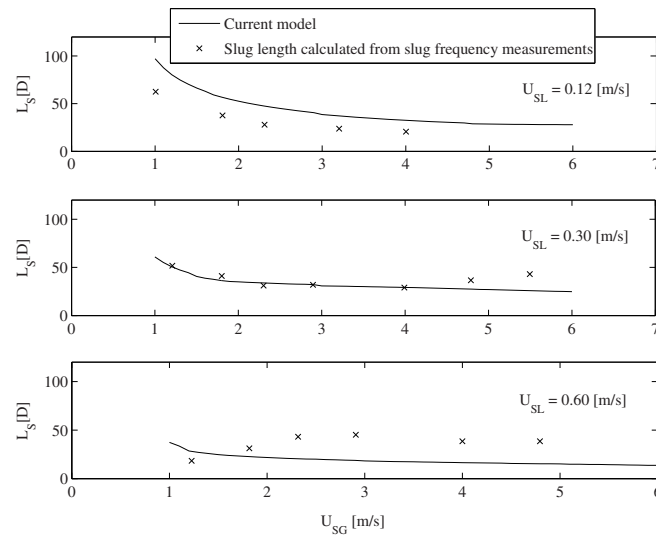


Figure 2.16: Air–water theoretical predictions and measurements of slug length as a function of gas superficial velocity, $D = 0.0763 \text{ m}$, $\theta = 0^\circ$, $P = 1 \text{ barA}$.

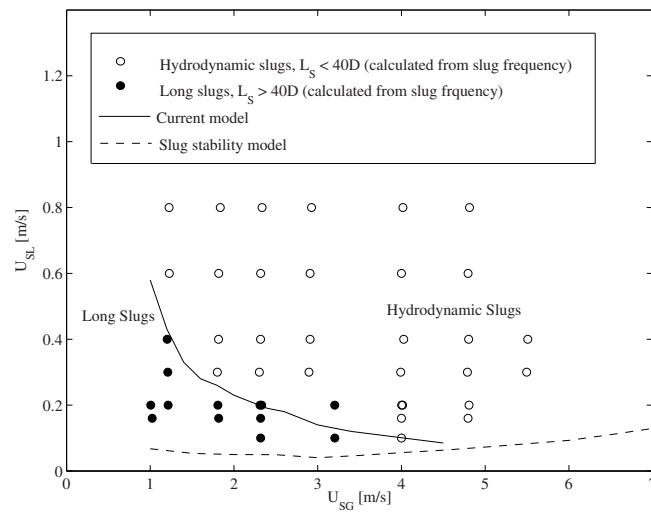


Figure 2.17: Air–water theoretical predictions and measurements of the flow regime transition for different U_{SG} and U_{SL} , $D = 0.0763 \text{ m}$, $\theta = 0^\circ$, $P = 1 \text{ barA}$.

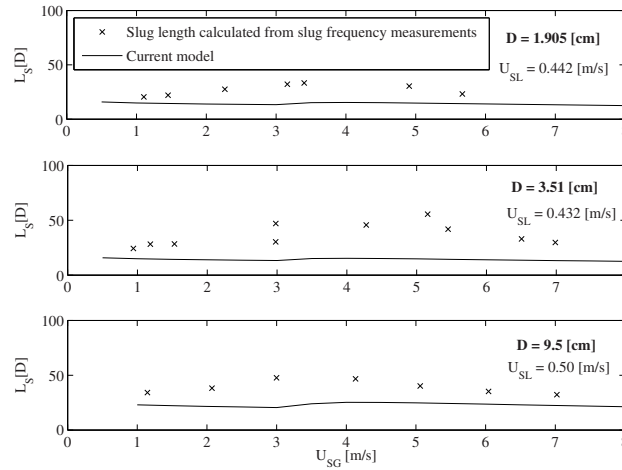


Figure 2.18: Air–water theoretical predictions and measurements of slug length as a function of gas superficial velocity, $\theta = 0^\circ$, $P = 1 \text{ bar}$, top subplot: $D = 0.019 \text{ m}$, middle subplot: $D = 0.0351 \text{ m}$, bottom subplot: $D = 0.095 \text{ m}$.

at different superficial flow rates. The dashed line is the slug stability line, and the solid line ($L = 40D$) represents the transition from long to hydrodynamic slugs.

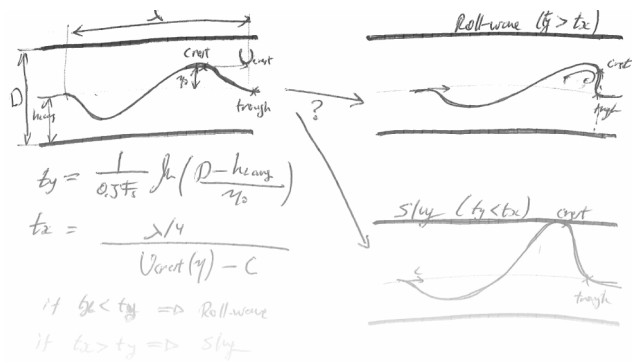
Figure 2.18 compares predictions with measurements in 3 different i.d. pipes: 0.019, 0.0351 and 0.095 m (in the figure from top to bottom, respectively). Each subplot shows $L_{s,f}$ as a function of U_{SG} at relatively high constant U_{SL} . The slug frequency measurements used to calculate the slug length shown in the upper subplot were done by Gregory and Scott (1969) at $U_{SL} = 0.442 \text{ m/s}$; in the middle subplot by Hubbard (1965) at $U_{SL} = 0.432 \text{ m/s}$; and in the bottom subplot by Fan et al. (1993a) at $U_{SL} = 0.5 \text{ m/s}$. The slug growth model underpredicts the measurements in all of the subplots. A possible reason for the disagreement between predictions and measurements is that the mixture velocities are not low enough to neglect the aeration (ϵ reaches 0.39 at $U_{SG} = 7 \text{ m/s}$) as assumed by the model (see Eq. (2.13)). Considering the aeration results in lower liquid velocity in the slug, u_3 , lower mixture velocity, U_{Mix} (Eq. (2.13)), lower bubble velocity, C_B (Eqs. 2.8, 2.9 and 2.10), and therefore larger development time, t_∞ (Eq. 2.34) that results in larger slugs.

2.6 Conclusions

1. Very long slugs, reaching 500 pipe diameter have been observed in gas–liquid horizontal pipe flow measurements. The long slugs appear at low gas flow rates, where the flow development is slow and the differences in liquid level between the front and the tail of a developing slug is large.
2. In the long slug regime, there are two different sub–regimes: (a) stable slugs (fully

developed), that have reached their final length; and (b) growing slugs. The second type appears, at critical liquid flow rates close to the transition from stratified to slug flow.

3. At low gas flow rates the transition from stratified to hydrodynamic slug flow occurs via the long slug regime. At high gas flow rates such a long slug region does not exist and for favourable flow conditions stratified flow directly transforms into hydrodynamic slug flow.
4. A slug growth model was presented. The growth model applies a volumetric balance between the front and the tail of a slug. In the model, the behaviour of the liquid phase at the slug tail is simplified by applying a linear kinematic relation between the back of the slug and the wave upstream. This relation is used to calculate the tail extension and the change in the liquid level. The growth model captures the main factors contributing to the slug growth behaviour. As a result, it accurately predicts the transition from hydrodynamic to long slug regimes for different pipe diameters. However, it underpredicts the average slug length at high mixture velocities. To improve the predictions, gas entrainment should be taken into consideration.
5. The model provides an explanation for a number of important observations in the slug flow regime: (a) in the long slug regime, the slug length decreases with increasing liquid flow rates as a result of the faster development of the liquid level behind the slug (Eqs. (2.27) and (2.34)); (b) increasing the operation pressure results in larger interfacial shear stresses, lower equilibrium liquid level (Eq. (2.24)) and volumetric growth rate (Eq. (2.28)), and thus shorter average slug length – that is why at high pressure only hydrodynamic slugs are observed; (c) further increase of the pressure results in liquid levels approaching the minimum slug stability level, so that no stable slugs (long or hydrodynamic) can appear anymore (unless produced at the inlet).
6. Our study with the long slug growth model raises important questions on: (a) the critical operation pressure and flow development time at which the long slugs appear; and (b) the contribution of the interfacial shear stresses and gas entrainment to the long slug development. Answers to these questions are key issues in reducing the negative effects of long slugs when operating at low pressure and low gas rates. These are subjects of research in progress.



3

Transition to slug flow and roll-waves ¹

In stratified gas-liquid horizontal pipe flow, growing long wavelength waves may reach the top of the pipe and form a slug flow, or evolve into roll-waves. At certain flow conditions, slugs may grow to become extremely long, e.g. 500 pipe diameter. The existence of long slugs may cause operational upsets and a reduction in the flow efficiency. Therefore, predicting the flow conditions at which the long slugs appear contributes to a better design and management of the flow to maximize the flow efficiency.

In this paper we introduce a wave transition model from stratified flow to slug flow or roll-wave regimes. The model tracks the wave crest along the pipe. If the crest overtakes the downstream wave end before hitting the top of the pipe, a roll-wave is formed, otherwise a slug.

For model validation we performed measurements in air-water horizontal pipe flow facilities with internal diameters of 0.052 and 0.06 m. Furthermore, we made numerical calculations using a transient one-dimensional multiphase flow simulator (MAST) which adopts a four-field model. The model presented in this paper successfully predicts the evolution of waves and their transition into either slugs or roll-waves. It also predicts the formation time of slugs and roll-waves with a satisfactory agreement.

¹This chapter is based on Kadri et al. (2009b)

3.1 Introduction

The transportation of gas and liquid in horizontal pipes can lead to a number of flow patterns. A stratified flow pattern has the configuration of a continuous gas phase flowing on the top of the liquid phase. This pattern occurs at relatively low gas and liquid superficial velocities. At higher liquid superficial velocity waves may initiate at the interface. These waves can grow to reach the top of the pipe forming liquid plugs travelling in the pipeline, separated by large gas bubbles. This intermittent regime is characterized as slug flow. However, if the growth rate of the waves is insufficient it can be shown, from momentum and mass balances, that the crests of the growing waves move faster than the troughs (Lighthill and Whitman (1955)). This behaviour might cause the crests to roll over the downstream end of the wave forming roll-waves.

3.1.1 Waves

The wave growth can be described by the Kelvin–Helmholtz instability as follows. The local gas velocity is highest in the neighbourhood of the wave crest so that the local gas pressure drops there. As a result, suction forces elevate the interface further toward the top of the pipe while gravity forces work at the opposite direction tending to stabilize the wave. At sufficient gas velocity the suction forces overcome gravity and the liquid level increases.

Several researchers (such as Jeffreys (1924); Jeffreys (1925a); Benjamin (1959); Lighthill (1962)) developed theories on the basis of transfer of energy from the gas phase to the liquid. They obtained wave growth at lower gas velocities than predicted by the Kelvin–Helmholtz approach. The sheltering hypothesis of Jeffreys (1925a) considers the variable pressure distribution at the water surface and the energy further supplied to the wave due to its geometry. Phillips (1957) proposed a theory for the generation of waves by turbulent wind. Unlike the instability concept of the Kelvin–Helmholtz model, he based his work on the generation and growth of waves by a mechanism of resonance between the components of the surface pressure distribution and the free surface waves. Miles (1957) introduced a mechanism for the generation of surface waves by a parallel inviscid shear flow and obtained a qualitative agreement with observations. Miles (1996) introduced a viscoelastic model for the generation of surface-waves. He concluded that the difference in energy transferred from the wind to the wave using quasi-laminar and viscoelastic models is small over a wide range of wave velocity for a logarithmic mean-wind profile. Belcher (1999) used the sheltering mechanism to explain wave growth considering the displacement over the undulating surface, the pressure variations over the wave and the contribution of the turbulent stresses in the air flow. He and others (Belcher and Hunt (1993); Cohen and Belcher (1999)) claimed that the non-separated sheltering approach is the primary mechanism responsible for the growth and decay of the waves.

3.1.2 Transition to roll-waves

Roll-waves were first described by Cornish (1910) who observed them in water runways in the mountains. Jeffreys (1925b) suggested theoretical relations to predict the initiation

of roll waves by using integral forms of momentum and mass balances and by examining the conditions under which a disturbance will grow. Hanratty and Engen (1957) described the initiation of roll-waves by an air stream blowing over a horizontal flowing water film in a $2.54 \times 30.48 \text{ cm}^2$ channel. The frequency of the observed roll-waves increased for increasing the gas superficial velocity. Hanratty and Hershman (1961) applied the theory proposed by Jeffreys (1925b) to explain roll-wave transition and suggested initiation of roll-waves from predictions of conditions under which long wave disturbances occur in gas-liquid flows. They showed that their appearance is due to an instability in the flow. Soleimani and Hanratty (2003) claimed that the viscous long wavelength (VLW) theory (which is essentially the same as was used by Hanratty and Hershman (1961)) can be used to predict the initiation of roll-waves in a pipe flow. They concluded that as the gas superficial velocity increases the frequency of the roll-waves increases, and a larger critical superficial liquid velocity is required for the transition to slug flow.

3.1.3 Transition to slug flow

Taitel and Dukler (1976) suggested a critical condition for the gas velocity when gravity can no longer restore the fluctuating pressure of the wave, taking into account non-linear effects using inviscid Kelvin-Helmholtz (IKH). The Taitel and Dukler approach is widely used to predict the transition to intermittent flow. This transition can be defined by one (or more) of three criteria: a viscous linear instability of a stratified flow to long wavelength disturbances; the stability of a slug; and a Kelvin-Helmholtz instability of a stratified flow.

The viscous linear stability analysis (viscous Kelvin-Helmholtz - VKH) done by Lin and Hanratty (1986) and by Wu et al. (1987) describes waves on thin films over which air is blowing. They showed that the influence of the interfacial stress and the resisting stresses at the wall should be included. The theory of viscous long wavelength (VLW) predicts the transitions in gas-liquid systems at low gas velocities. It predicts the gas velocity for the appearance of long wavelength waves and their growth into a slug as reported by Woods and Hanratty (2000).

A number of researchers (Lin and Hanratty (1986); Wu et al. (1987); Hall (1992); Crowley et al. (1992); Barnea and Taitel (1994a); Barnea and Taitel (1994b)) claimed that VKH, in general, gives better predictions for the onset of slug flow. McCready (1998) argued that this analysis fails if the viscosity difference between the two fluids is very large. Hurlburt and Hanratty (2002) suggested that the transition to the slug region in a plot with superficial velocities of gas and liquid is predicted by the VLW model for low gas velocities, and by the slug stability model for high gas velocities. They argued that better predictions can be obtained if the interfacial friction factors are better estimated. The work of Andritsos and Hanratty (1987) together with other results (Bontozoglu and Hanratty (1989); Simmons and Hanratty (2001)) provided a correlation for the interfacial friction factor for the air-water flows.

Woods and Hanratty (1999) suggested two main mechanisms for the transition to slug flow: (1) at low gas and liquid velocities, where the liquid flow rate is subcritical, large amplitude gravity waves may reach the top of the pipe forming a slug; whereas (2) at supercritical flow rates, slug formation is determined by coalescing roll-waves and can be described

by a probabilistic process. Kadri et al. (2009a) showed that the long slugs form only at low gas and liquid superficial velocities, i.e. via gravity waves.

In this chapter we consider the transition from stratified flow to slug flow or roll-wave regimes – slugs that may form by coalescing roll-waves are not addressed. In order to determine the evolution of waves we developed a simplified model that tracks the axial and vertical positions of the wave crest of a growing long wavelength wave in gas-liquid horizontal pipe flow. A linear assumption, for the momentum transfer from the gas phase to the wave crest, has been made in order to calculate the axial velocity of the wave crest. Whereas, for the vertical growth an exponential wave growth with a nonlinear growth rate based on slug frequency correlations (Nydal (1991)) is used. If the wave crest approaches its downstream end before it reaches the top of the pipe, the crest rolls over the downstream wave front forming a roll-wave. Otherwise, at sufficiently high superficial velocities, if the wave crest hits the top of the pipe before approaching the downstream wave end, a slug is formed.

Constructing such a simplified theoretical model that successively approximates the transition from waves into slug flow or roll-waves has two major advantages: (I) The computing time of the current model is extremely low. (II) Physical parameters can be easily tracked within the different stages of the model.

For the validation of the model we performed wave growth time measurements using a high speed camera in a 137 m long air-water horizontal pipe flow of an internal diameter (i.d.) of 0.052 m. The measurements provide clearly the behaviour of the wave crest just before hitting the top of the pipe. Another set of experiments was carried out in a 16 m long air-water horizontal pipe flow of 0.06 m i.d. pipe at different gas and liquid superficial velocities. In this set of experiments we tracked the crest of growing waves and measured the slug/roll-wave formation time. The measurements were compared with the theoretical predictions of the current model at different gas and liquid superficial velocities. Moreover, theoretical predictions of different pipe sizes were tested against MAST, a transient one-dimensional multiphase flow simulator whose numerical framework is based on a multi-field approach as described by Bonizzi et al. (2009). MAST is capable to predict transitions from one flow pattern to another retaining the same set of closure laws and governing equations, provided that high spatial resolution of the computational grid is adopted.

A theoretical background including stability of stratified flow and slug stability model is presented in section 3.2. The detailed analysis of the proposed model for the transition from stratified flow to slug flow or roll-wave regimes is given in section 3.3. Section 3.4 provides an overview of the experimental setup and the methods used for performing the measurements. Details on the numerical tests by MAST are given in section 3.5. Comparisons between theory and measurements, and theory and simulations are given in section 3.6. Finally, the conclusions are presented in section 3.7.

3.2 Theoretical background

3.2.1 Stratified flow pattern

A simplified geometric representation of the time-averaged stratified flow is considered prior to the transition to slug flow or roll-wave regimes. The pipe diameter is denoted by D . The

length of the segments of the pipe circumference that are in contact with the gas and with the liquid are, respectively, S_G and S_L . The length of the gas–water interface is presented by S_i . The areas occupied by the gas and the liquid are denoted by A_G and A_L . The parameter h_L is the height of the liquid layer along the centerline. Given the pipe diameter, D , and any other parameter the remaining parameters are calculated using geometric considerations (e.g. Govier and Aziz (1972)).

Based on the simplified geometry, the momentum balances for the gas and liquid phases can be expressed by:

$$-A_G \left(\frac{dp}{dx} \right) - \tau_{WG} S_G - \tau_i S_i + \rho_G A_G g \sin \theta = 0; \quad (3.1)$$

$$-A_L \left[\left(\frac{dp}{dx} \right) - \rho_L g \cos \theta \left(\frac{dh_L}{dx} \right) \right] - \tau_{WL} S_L + \tau_i S_i + \rho_L A_L g \sin \theta = 0; \quad (3.2)$$

where ρ_G and ρ_L are the gas and liquid densities, θ is the inclination angle of the pipe from the horizontal. dp/dx is the pressure gradient, dh_L/dx is the liquid hydraulic gradient, g is the acceleration due to gravitational forces, τ_{WG} and τ_{WL} are the time-averaged resisting stresses of the gas and liquid phases at the wall, and τ_i is the resisting stress at the interface. The stresses τ_{WG} , τ_{WL} and τ_i are defined in terms of friction factors, which are calculated using the Blasius equation if $Re < 10^5$ and the wall roughness effect can be ignored, otherwise the Churchill equation is used (see Churchill (1977)). However, because of the presence of waves at the interface, the interfacial friction factor, f_i , becomes larger than the friction factor for a smooth surface, f_s . A number of previous works (Andritsos and Hanratty (1987); Bontozoglu and Hanratty (1989); Simmons and Hanratty (2001); Hurlburt and Hanratty (2002)) suggest an estimation for interfacial friction factors (near the transition) for air–water flows from the following relations:

$$\frac{f_i}{f_s} = 2, \quad \text{smooth liquid surface} \quad (U - u) \leq (U - u)_{crit}; \quad (3.3)$$

$$\frac{f_i}{f_s} = 5, \quad \text{wavy liquid surface} \quad (U - u) \leq (U - u)_{crit}; \quad (3.4)$$

$$\frac{f_i}{f_s} = 5 + 15 \left(\frac{h_L}{D} \right)^{0.5} \left[\frac{(U - u)}{(U - u)_{crit}} - 1 \right], \quad (U - u) > (U - u)_{crit}; \quad (3.5)$$

where U and u are the actual gas and liquid velocities, and $(U - u)_{crit}$ is the critical relative velocity at which waves become unstable.

Note that the flow is assumed to be varying slowly enough so that pseudo–steady–state assumptions can be made (e.g. $dh_L/dx = 0$ and τ_{WG} , τ_{WL} and τ_i can be related to flow variables). Based on the pseudo–steady–state assumptions, Eqs. (3.1) and (3.2) are used to find the pressure gradient and the height of the liquid layer provided that the superficial velocities of the gas and the liquid are given.

3.2.2 Slug stability theory

Slug stability theory considers the rates of liquid adjoining or detaching from the slug at its front or back. The back of the slug is assumed to propagate together with the bubble at the bubble velocity C_B . The bubble velocity is modelled as a Benjamin bubble (Benjamin (1968)). Following Bendiksen (1984), Woods and Hanratty (1996), Hurlburt and Hanratty (2002) and Soleimani and Hanratty (2003), three main regimes of C_B are defined:

$$C_B = U_{Mix} + 0.542\sqrt{gD} \quad U_{Mix} < 2\sqrt{gD}; \quad (3.6)$$

$$C_B = 1.1U_{Mix} + 0.542\sqrt{gD} \quad 2\sqrt{gD} < U_{Mix} < 3.5\sqrt{gD}; \quad (3.7)$$

$$C_B = 1.2U_{Mix} \quad U_{Mix} > 3.5\sqrt{gD}; \quad (3.8)$$

where the mixture velocity $U_{Mix} = U_{SG} + U_{SL}$, and U_{SG} and U_{SL} are the superficial gas and liquid velocities, respectively.

Slugs are defined *neutrally stable* (following Hurlburt and Hanratty (2002)) when the flow rate of liquid adjoining is equal to the rate at which liquid detaches ($Q_{in} = Q_{out}$). This also requires that the slug front and back velocities are equal, $C_F = C_B$. Applying the two conditions of neutral stability, and making a volumetric flow balance between the liquid entering the front and leaving the back result in a critical liquid area at the front of the slug below which it will be unstable (Hurlburt and Hanratty (2002); Soleimani and Hanratty (2003); Kadri et al. (2009a)):

$$\left(\frac{A_{L1}}{A} \right)_{Crit} = \frac{(C_B - u_3)(1 - \varepsilon)}{(C_B - u_1)}, \quad (3.9)$$

where ε is the void fraction in the slug, and u_1 and A_{L1} are, respectively, the actual liquid velocity and liquid cross-sectional area downstream the slug at station 1 (2.2). For incompressible flow, the term u_3 is calculated from a volumetric balance between the inlet of the pipe and station 3 as follows,

$$U_{Mix} = \varepsilon U_3 + (1 - \varepsilon)u_3, \quad (3.10)$$

where U_3 is the actual gas velocity at station 3. At low mixture velocities aeration is negligible ($\varepsilon = 0$) so that Eq. (3.10) gives $u_3 = U_{Mix}$. From Eq. (3.9) we calculate the minimum liquid height, h_{Lmin} , in front of a stable slug. A more detailed analysis of the slug stability theory can be found in Hurlburt and Hanratty (2002); Soleimani and Hanratty (2003).

3.2.3 The liquid level downstream of the growing wave

The average liquid cross-sectional area of the stratified layer, A_{Lavg} , is calculated from the momentum balances for the stratified flow pattern, Eqs. (3.1) and (3.2). Following Kadri et al. (2009a), substituting $A_L = A_{Lavg}$ and $A_G = A - A_{Lavg}$, Eq. (3.1) is written in the following form:

$$\left(\frac{dp}{dx} \right) = \frac{\tau_{WG}S_G + \tau_i S_i}{A - A_{Lavg}} - \rho_G g \sin \theta. \quad (3.11)$$

Plain stratified flow is reached when the pressure gradients of the two phases on the interface cancel each other. Therefore, substituting Eq. (3.11) in Eq. (3.2) and after basic algebra we obtain,

$$A_{L_{avg}} = A \frac{\tau_{WL} S_L - \tau_i S_i}{\tau_{WL} S_L + \tau_{WG} S_G} + g A_{L_{avg}} (A - A_{L_{avg}}) \left[\rho_L \cos \theta \left(\frac{dh_L}{dx} \right) - (\rho_L - \rho_G) \sin \theta \right]. \quad (3.12)$$

For a fully developed stratified flow Eq. (3.12) reduces to the simple form:

$$A_{L_{avg}} = A \frac{\tau_{WL} S_L - \tau_i S_i}{\tau_{WL} S_L + \tau_{WG} S_G}. \quad (3.13)$$

In this chapter we do not consider the evolution of unstable slugs. Therefore, we only address problems that satisfy the following condition,

$$\left(\frac{A_{L_{avg}}}{A} \right) \geq \left(\frac{A_{L1}}{A} \right)_{Crit}. \quad (3.14)$$

From Eq. (3.13) and geometric consideration we calculate the liquid height of the averaged stratified flow, $h_{L_{avg}}$.

3.3 A roll-wave/slug formation time model

In the model presented here, we address the formation of either slugs or roll-waves from growing waves. The waves are assumed to have a wavelength, λ , large compared to the average liquid height of the stratified flow, $h_{L_{avg}}$. Such waves have an average wave velocity, C , that depends on the liquid level alone,

$$C = \sqrt{gh_{L_{avg}}}. \quad (3.15)$$

The long wavelength waves grow in two different directions:

(1) *Growth in the vertical direction.* The local velocity of the gas phase above the rising wave crest increases. As a result, the pressure drops and local suction forces (associated with the Bernoulli effect) tend to elevate the surface in the neighbourhood of the wave crest, whereas gravity acts in the opposite direction tending to stabilize the wave surface. At sufficiently high gas velocities, the local suction forces overcome the gravitational forces and the liquid level surrounding the crest grows toward the top of the pipe.

(2) *Growth in the axial direction.* It can be shown, from the law of conservation of mass, that the wave crest propagates at a higher axial velocity than the wave trough (Lighthill and Whitman (1955)). If the crest overtakes the downstream wave end, the crest will steepen and roll upon itself creating a roll-wave (Hanratty and Hershman (1961)).

In our model, we calculate the time required for the crest to reach the top of the pipe, t_y , and the time needed for the crest to approach the horizontal displacement of the downstream trough, t_x . If the crest reaches the top of the pipe before it approaches the downstream trough, the wave grows into a slug. On the other hand, if the crest approaches the downstream trough first, a roll-wave is generated. This is the outline of the model presented here:

$$\text{if } t_y < t_x \quad \text{the wave evolves into a slug,} \quad (3.16)$$

if $t_x < t_y$ the wave evolves into a roll-wave. (3.17)

Note that, depending on the height of the liquid layer, a slug formed can either be a hydrodynamic slug with an average length of $30D$ or a long growing slug that may reach lengths that are 10 times greater.

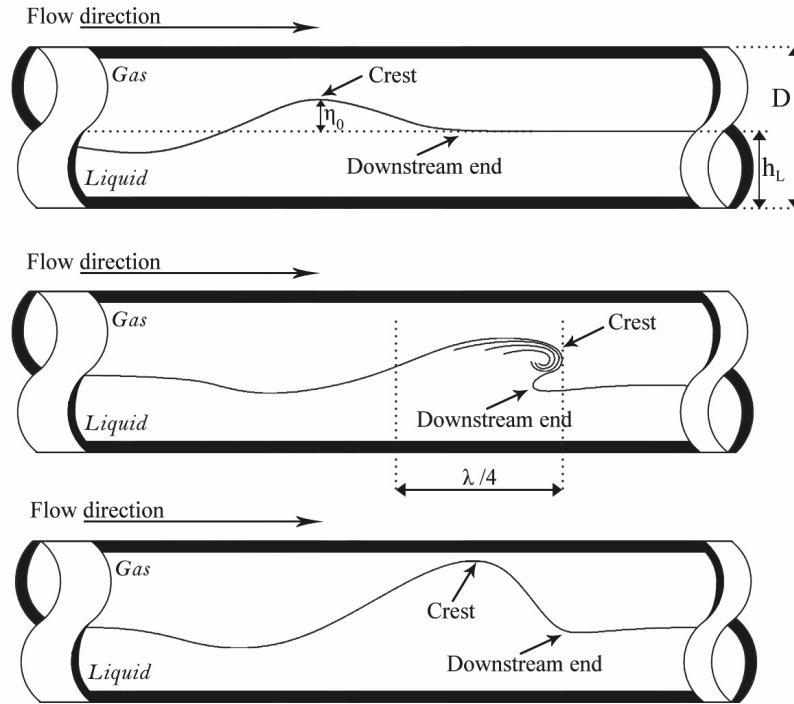


Figure 3.1: Pictorial representation of a growing wave (top); the wave crest overtakes the downstream wave end forming a roll-wave (middle); the wave crest reaches the critical liquid height near the top of the pipe forming a slug (bottom).

3.3.1 The vertical growth time

We consider a long wavelength wave propagating over the average liquid height, $h_{L,avg}$, as given in Fig. 3.1 (top). In the figure, the term η_0 represents the initial amplitude of the wave. Following Kadri et al. (2007a) and Kadri et al. (2007b), the growth rate of the amplitude is defined as

$$\frac{d\eta}{dt} = K\eta, \quad (3.18)$$

where t is the time, η is the amplitude of the wave, the parameter K is a nonlinear growth defined as $K = C_1 f_S$ (Kadri et al. (2007b)), and f_S is the slug frequency calculated with the

correlation suggested by Nydal (1991):

$$\mathbf{f}_S = 0.088 \frac{(U_{SL} + 1.5)^2}{gD}. \quad (3.19)$$

The definition of K based on the slug frequency is a logical choice, since the slug time ($1/\mathbf{f}_S$) is an actual limit for the average growth time of waves that evolve into slugs. The smaller the slug frequency is, the greater the growth time becomes. The parameter C_1 is a constant that was chosen as $C_1 = 0.3$ for the best agreement with air–water horizontal pipe flow measurements (Kadri et al. (2007b)). Solving Eq. (3.18) and substituting $K = 0.3\mathbf{f}_S$ results in,

$$\eta(t) = \eta_0 e^{0.3\mathbf{f}_S t}. \quad (3.20)$$

The initial amplitude, η_0 , is estimated from the pressure fluctuations at the surface caused by turbulence (Phillips (1957); Longuet-Higgins (1952)). Therefore, and to a first approximation, we consider the initial wave amplitude, η_0 , to be proportional to the turbulence length scale, l_T . The proportionality between η_0 and l_T is expressed as function of D alone (see appendix). Thus, we write $\eta_0 = C_2 D$, where C_2 is the proportionality constant. A range of $0.01 < C_2 < 0.03$ is obtained, and for a maximum vertical growth time, the minimum value of the proportionality constant, $C_2 = 0.01$, is considered.

Using the amplitude growth rate (Eq. (3.20)), the time needed for the crest to hit the top of the pipe, t_y , is calculated. By substituting $t = t_y$ and $\eta(t = t_y) = D - h_{L_{avg}}$ in Eq. (3.20), we obtain the following relation for t_y :

$$t_y = \frac{1}{0.3\mathbf{f}_S} \ln \frac{D - h_{L_{avg}}}{\eta_0}. \quad (3.21)$$

3.3.2 The axial growth time

A roll-wave is formed when the crest overtakes the downstream wave end (see Fig. 3.1 (middle)). The distance between the crest and the downstream wave end is $\lambda/4$, as shown in the figure. The downstream end of the wave propagates with the wave at the propagation velocity C . Whereas due to the contribution of the momentum of the gas phase, the crest has an axial velocity:

$$U_{crest}(\eta) = \frac{\rho_G U + \rho_L C}{\rho_G + \rho_L}, \quad (3.22)$$

where U is the actual mean velocity of the gas phase at the crest, $U \equiv U_{SG}(A/A_G)$. Note that the cross-sectional area of the gas phase, A_G , at the crest decreases when the wave amplitude η grows, and therefore $U_{crest} = f(\eta)$.

The time needed for the crest to approach the downstream wave end can be determined from the relative velocity, and the distance between the crest and the downstream wave end,

$$t_x = \frac{\lambda/4}{U_{crest}(\eta) - C}. \quad (3.23)$$

Following Kadri et al. (2009a), the term λ is calculated from the wave velocity ($\lambda = C/f_w$) and the relation $f_w = c_w f_S$ by Tronconi (1990) for the slug and the wave frequencies, f_S and f_w , as follows,

$$\lambda = \frac{C}{c_w f_S}, \quad (3.24)$$

where c_w is a constant equal to 2 for air–water systems (Tronconi (1990)). Note that Woods and Hanratty (1999) reported slug frequency measurements to be inconsistent with the relation between slug frequency and wave frequency by Tronconi (1990) (e.g. Eq. (3.24)). However, here we use Eq. (3.24) only to estimate a realistic value of λ , which plays no role for predicting the vertical growth time (3.21).

3.4 Experiments

Experiments have been carried out in two multiphase flow laboratory facilities. The first facility, located at the *Kramers Laboratorium of Fysische Technologie* (KLFT) at TU Delft, The Netherlands, is denoted as the KLFT flow loop. In this facility, we investigated the behaviour of wave crests of growing waves just before they evolve into slugs. The second facility is the NTNU (Norwegian University of Science and Technology) flow loop located in Trondheim, Norway. Here, we tracked growing waves using a moving camera, and measured the time needed for initial disturbances to evolve into either roll-waves or slugs. Descriptions of the experimental setup of each facility are given in the following sub-sections.

3.4.1 The KLFT flow loop

The flow loop used in the experiments consists of a 137 m long horizontal pipeline with a 0.052 m i.d. pipe. The pipe is made of Perspex (Plexiglass) to allow visual observations of the flow conditions. The experiments are performed at atmospheric pressure with gas and liquid being air and water, respectively. The two phases are combined at the inlet in a Y-shaped section. The gas enters from the top in a horizontal direction, in order to prevent the impact of gas-jet coming from above. At the outlet, the last element of the pipe is connected to a short near-horizontal hose. The hose enters a larger diameter pipe through which the liquid returns down to the storage tank positioned 5 m below, and the gas is allowed to escape. A sketch of the experimental setup is given in Fig. 3.2. In the sketch L_{pipe} stands for the length of the pipeline test section.

The shape and movement of the growing waves are measured by means of a high speed camera (Olympus, i-SPEED). The camera is positioned at 4 locations along the pipe at: 2–3.5, 4, 7.5, and 13 m from the inlet (see Fig. 3.2). The locations are denoted by 1, 2, 3 and 4, respectively. The camera is setup such that the field of view in one image covers a length of 0.5 m, while still having high enough resolution to resolve the gas–liquid interface accurately. The frame rate of the camera is 955.5 frames per second (*fps*), with an uncertainty of 2 *fps*. Images of the growing waves were evaluated by tracking their position in time. At location 1, we tracked the crest of growing waves just before they hit the top of the pipe creating slugs. For that matter, the camera at position 1 had to be located between 2–3.5 m from the inlet depending on the gas and liquid superficial velocities. At the other three locations we

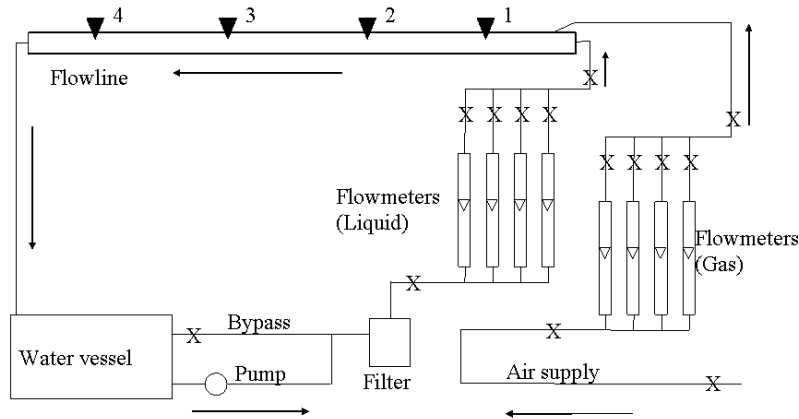


Figure 3.2: Sketch of the KLFT experimental setup. Air–water horizontal pipe flow, $L_{pipe} = 137\text{ m}$, $D = 0.052\text{ m}$. The valves are indicated by \times . The 4 positions of the camera are indicated by \blacktriangledown . Distance from the inlet: (1) 2–3.5 m; (2) 4 m; (3) 7.5 m; and (4) 13 m.

tracked the downstream front and back of the slugs formed to ensure that the behaviour of the liquid downstream and upstream the slugs is similar in all measurements. The experiments were performed at constant gas and liquid superficial velocities being 1.5–3 and 0.2–0.4 m/s, respectively. Fig. 3.3 presents three images by the camera capturing the propagation of a growing wave (see top picture), the “jump” of the crest reaching the top of the pipe (middle picture), and the propagation of the formed slug (bottom picture). It is noticeable that the exit geometry and the fact that the measurements were performed at the initial part of the pipe ensure independence of the liquid holdup from any outlet effect.

The aim of this set of measurements is to show the development of the growing waves, especially during the “jump”. Although the model presented in this paper does not consider this “jump”, we show that the difference between the slug growth time calculations using the model and the measurements is negligible. Hence, the slug growth time can be approximated by calculating the time needed for the crest to reach the top of the pipe.

3.4.2 The NTNU flow loop

The experiments in the NTNU flow loop were done for a two phase air–water horizontal pipe flow. The loop test is 16 m long with a 0.06 m i.d. pipe. The pipe is made of straight transparent Plexiglass and configured as an open loop system so that the pressure at the outlet is atmospheric. The two phases are combined at the inlet in a Y-shaped section, where the gas enters at 45° from the top and the liquid is introduced axially. At the outlet, the liquid is allowed to drop downwards. A sketch of the experimental setup is given in Fig. 3.4.

Two different measurement techniques were installed. The first consists of 4 ring probes located along the pipe at: 3.39, 5.91, 10.77, and 13.13 m from the inlet. The probes were

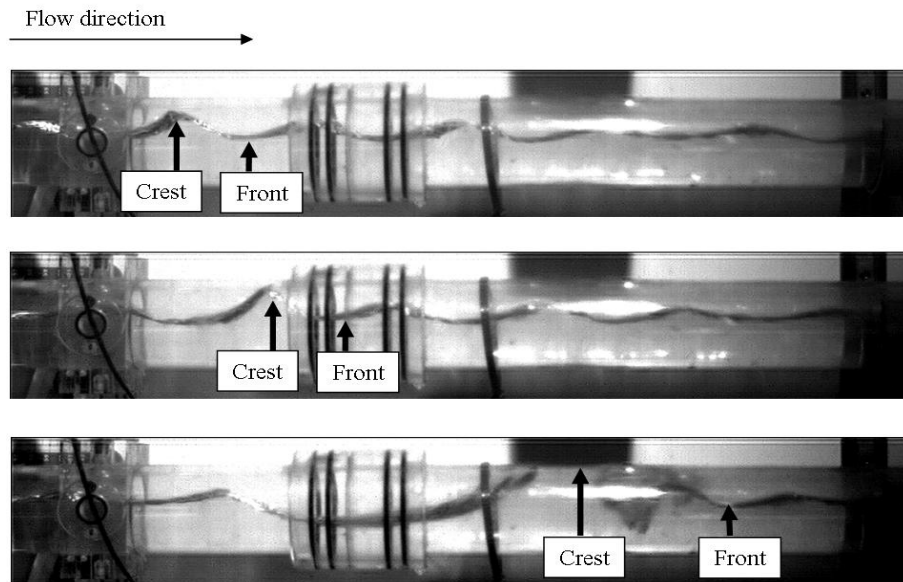


Figure 3.3: Three images captured by the camera. Top: the propagation of a growing wave. Middle: the “jump” of the crest reaching the top of the pipe. Bottom: slightly after the slug is formed.

used to record the time dependent liquid height behaviour. The probes were primarily used as slug detectors. In the second measurement technique the growing waves were tracked using a moving camera (webcam) (see Fig. 3.4). The camera slides over a track along the pipeline at a speed that is manually controlled. The time that takes the waves to evolve into either slugs or roll-waves was measured.

Two sets of experiments were performed, each at different constant superficial liquid velocities, 0.17 and 0.22 m/s , and varying superficial gas velocities, 0.5 – 6 m/s . For consistency, the following procedure was applied to all measurements: (a) the superficial gas and liquid velocities are set to the desired values – the liquid valve was 50% opened for $U_{SL} = 0.17$ m/s and 75% for $U_{SL} = 0.22$ m/s , and the liquid pump frequency was 30 – 35 Hz ; (b) the pump frequency is reduced to 10 Hz for 10 seconds – this was necessary in order to reduce the liquid level close to $h_{L,avg}$, and to have a smoother interface; (c) the pump is set back to the original value and the time measurement starts; and (d) each time measurement is stopped when the crest of a growing wave rolls over the downstream wave end or hits the top of the pipe. The stopping criterion is based on visual observations and verified using the time dependent liquid height measurements. Note that only the first slug or roll-wave were considered in each measurement. Therefore, the exit effects of slugs or roll-waves are irrelevant. It is also worth noting that perturbations that may appear at the interface due to procedures (b) and (c) result

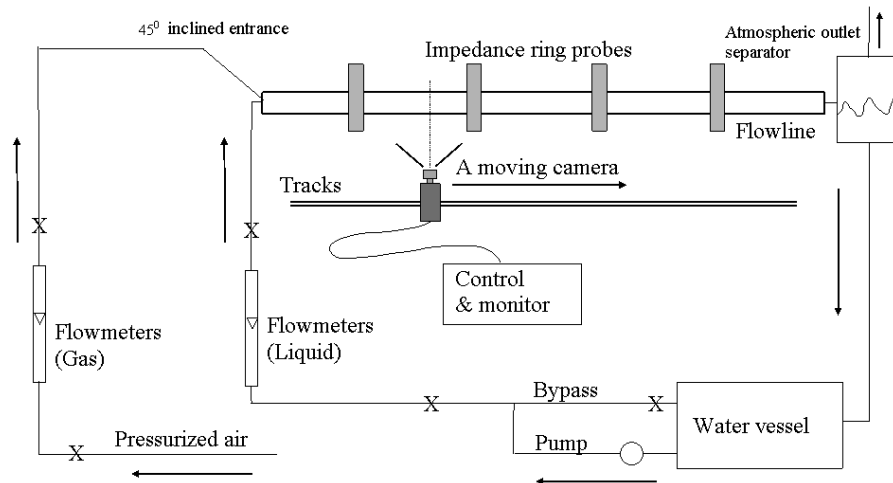


Figure 3.4: Sketch of the NTNU experimental setup, the position of the impedance ring probes, and the moving camera track. Air–water horizontal pipe flow, $L_{pipe} = 16\text{ m}$, $D = 0.06\text{ m}$. The valves are indicated by \times .

in shorter growth times in the measurements. However, the appearance time of perturbations on a “perfectly” smooth interface is associated with a turbulence time scale in gas and liquid, that is much shorter than the wave growth time. Therefore, the effect of induced perturbations on the total measuring time is negligible.

3.5 Numerical tests

The numerical code used to conduct computational tests is MAST (Multiphase Analysis and Simulation of Transitions). The simulator, in the case of gas–liquid flows, solves the governing equations of the flow (mass, momentum and pressure) for each field which locally maybe generated inside each control volume (liquid continuous, liquid dispersed – droplets, gas continuous, gas dispersed – bubbles). In this approach, mass conservation is enforced.

The governing equations of the flow are discretised on a staggered grid arrangement using a fully explicit discretisation in time and a first order upwind scheme for the spatial terms. The developed methodology allows the prediction of the flow pattern which prevails in each computational node retaining the same set of closure laws and governing equations. Hence, different fields may exist from control volume to control volume, depending on the flow pattern which prevails. Qualitatively we identify the local flow pattern that prevails in each computational cell as follows:

1. Stratified flow: stratified layers (of continuous gas and continuous liquid with possibly some entrained gas–dispersed gas field) with low void fraction fluctuations (no distinction is made between wavy and smooth regimes).

2. Annular flow: stratified layers (a layer of continuous gas with dispersed liquid and a layer of continuous liquid) where the liquid layer tends to wet the whole perimeter of the pipe wall and the gas flows in the core.
3. Slug flow: stratified layers with large void fraction fluctuations which do bridge the pipe, causing regions with very thin stratified gas layers (i.e. the liquid film is dominated by the presence of two stratified layers – continuous gas with possibly dispersed liquid, and continuous liquid with in general dispersed bubbles; the slug body is dominated by a continuous liquid film with dispersed gas with a very thin continuous gas layer on top).
4. Bubbly flow: the pipe is fully bridged with no regions where there are stratified gas layers that are not very thin (continuous liquid with dispersed gas bubbles)

Unstable waves may grow until the pipe is fully bridged and a slug is generated. Slug-ging is predicted because the governing equations are capable to capture the viscous Kelvin–Helmholtz instabilities that lead to flow pattern transition from stratified to slug flow (Issa and Kempf (2003)). In order to ensure that these instabilities are not smeared out by numerical diffusion, a fine numerical mesh is adopted with a spatial resolution of some pipe diameters. The growth of the instabilities is then an outcome of the transient numerical solution of the equations. When slugging occurs, regardless of its specific nature (hydrodynamic, terrain-induced or severe), trains of slugs are generated automatically. Provided that reasonable closure laws (i.e. friction factors) are adopted, MAST has the capability to predict the correct flow pattern that results from the boundary and geometry conditions under investigation.

Fig. 3.5 shows typical profiles of the liquid holdup and gas velocity at different time instants for a wave which grows and eventually leads to hydrodynamic slugging for gas–liquid horizontal pipe flow. The pipe is 137 m long with 0.052 m i.d. (the KLFT facility), the gas and liquid phases are air and water travelling at $U_{SG} = 8$ m/s and $U_{SL} = 0.3$ m/s, respectively.

Slugs of different sizes may be generated, depending on the pipe geometry and flow conditions, leading to a slug length distribution. The simulator, MAST, gives estimates of the average slug length as shown in figure 5 of the paper by Bonizzi et al. (2009), where predictions by MAST are compared with the measurements of Nydal et al. (1992) for air–water flow in a horizontal 0.05 m i.d. pipe at $U_{SL} = 0.6$ and 2.4 m/s.

The robustness of the slug criterion can be appreciated by referring to figure 7 of the paper by Bonizzi et al. (2009), where predictions of the critical height of the liquid layer at the transition to slug flow for air–water horizontal pipe flow at atmospheric pressure are plotted against U_{SG} and compared with measurements by Andritsos et al. (1989) and the theoretical transition boundary according to Hurlburt and Hanratty (2002). The accuracy of the criteria used for identification, noting that the closure relationships are not adjusted, is satisfactory. For the tests presented in this paper, the closures proposed by Taitel and Dukler (1976) were selected.

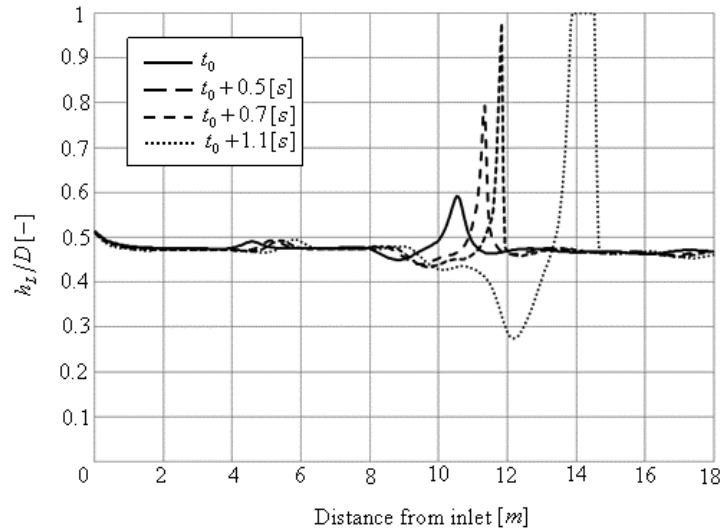


Figure 3.5: Hydrodynamic instabilities in the KLFT loop calculated by MAST, for air–water 0.052 m i.d. pipe, $U_{SG} = 8 \text{ m/s}$ and $U_{SL} = 0.3 \text{ m/s}$.

3.6 Results

In this section we compare theoretical calculations, of the wave growth and the formation time of slugs and roll-waves, with measurements and simulations. A summary of the properties of the different systems is found in Table 3.1. For all calculations presented in this paper the lowest initial wave amplitude was applied in order to obtain the largest growth time of the wave crest, hence $C_2 = 0.01$ is chosen (see appendix).

3.6.1 Crest growth near the pipe top

Measurements of growing waves just before they hit the pipe top for air–water horizontal flow are presented in Fig. 3.6. The measurements were carried out in a 137 m long pipe with 0.052 m i.d. at the KLFT flow loop. A description of the experimental setup is found in section 3.4.1. The sub-plots in Fig. 3.6 show the liquid holdup at the crest, $(h_L/D)_{crest}$, as function of time, t , at $U_{SG} = 1.85 \text{ m/s}$ and different superficial liquid velocities. The average liquid holdup is denoted by (\times) , whereas the minimum and maximum values of the holdup are represented by the error-bars. The solid line represent theoretical predictions of the crest growth from η_0 . The wave grows exponentially until the top of the pipe is reached. A zoom over the measurement region is given on the right hand side of each sub-plot.

In the sub-plots (a), (b) and (c) we see that the time needed for a growing crest before the “jump” is two orders of magnitude greater than the time needed for the crest to hit the top of the pipe (during the “jump”). This observation is true for all superficial velocities of gas

Table 3.1: Summary of system properties.

	Air-water system
Pipe diameter [m]	0.025, 0.052, 0.06, 0.095
Pressure [Pa]	$1 \times 10^5, 2 \times 10^5$
Interfacial tension [N/m]	0.07
Gas density [kg/m ³]	1.2
Gas viscosity [kg/ms]	1.8×10^{-5}
Liquid density [kg/m ³]	1000
Liquid viscosity [kg/ms]	0.001

and liquid in sub-plots (a), (b) and (c) of Fig. 3.6.

The measurements in sub-plots (a), (b) and (c) (in the zoom area) are for $U_{SG} = 1.85$ m/s and $U_{SL} = 0.2, 0.3$ and 0.4 m/s, respectively. Here we see that increasing the superficial liquid velocity (at fixed U_{SG}) results in a shorter “jump time” being: 0.09, 0.06 and 0.04 s for sub-plots (a), (b) and (c), respectively. The “jump time” in subplot (b) is about two times slower than in subplot (c), and slightly faster than the “jump time” in subplot (a). A possible reason for this behaviour is the following. The stratified (initial) liquid height is larger for larger U_{SL} (Eq. (3.13)), and the actual gas velocity at the crest is constant for fixed U_{SG} . However, the total mass of liquid above the stratified liquid level is smaller for larger U_{SL} (and so is the potential energy). Therefore, the suction forces (e.g. Bernoulli effect) acting on the crest will result in a higher growth rate of the crest for larger U_{SL} .

In the case of sub-plot (b), the wave crest moves with an average velocity $U_{crest} = 0.7$ m/s, and the “jump” occurs after approximately 17 seconds. Thus, the wave crest moves a distance of 12 m, from the inlet, just before the slug is formed. This formation distance is well predicted by MAST, as shown by the dashed line ($t_0 + 0.7$ s) in Fig. 3.5

3.6.2 Prediction of roll-wave/slug formation time

Theoretical calculations of the time needed for the wave crest to evolve into a roll-wave or a slug (t_x and t_y , respectively) are compared with measurements and numerical calculations by MAST in Fig. 3.7. The measurements were carried out in a 16 m pipe with a 0.06 m i.d. at NTNU. A description of the experimental setup and the numerical calculations are found in sections 4.2 and 5, respectively. Fig. 3.7 presents the time needed for a growing wave to form either a slug or a roll-wave as a function of the superficial gas velocity, U_{SG} . In the figure, the superficial liquid velocity $U_{SL} = U_{SL_{min}}$, where $U_{SL_{min}}$ is the minimum velocity required for the transition to slug flow. $U_{SL_{min}}$ is calculated iteratively from the gas and liquid momentum balances (Eqs. (3.1) and (3.2)) for the liquid height $h_{L_{min}}$. The stars (*) represent slug measurements, the plus signs (+) are roll-wave observations, the bullets (●) and the circles (○) are simulations by MAST for slugs and roll-waves, respectively. The dashed lines (---) are theoretical calculations of t_x (Eq. (3.23)), and the solid lines (—) represent theoretical calculations of t_y (Eq. (3.21)). The arrows indicate the curves for which either t_x or t_y is shortest, indicating a transition boundary from stratified to slug or roll-waves, respectively.

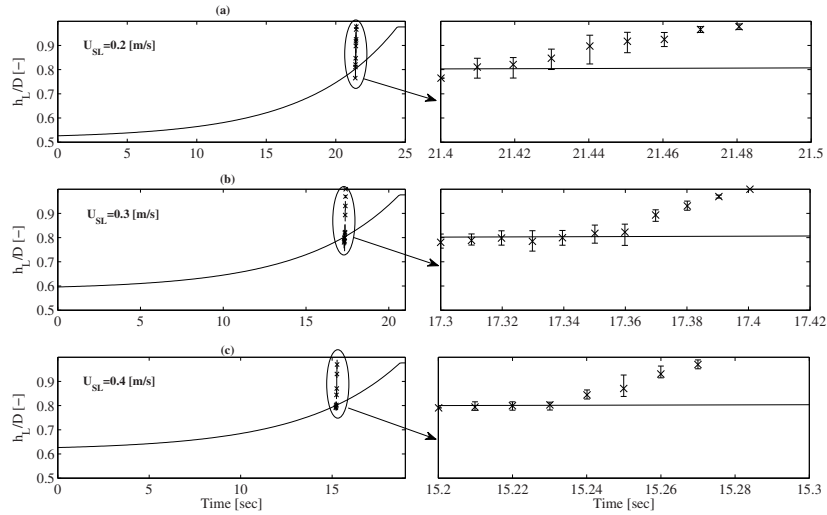


Figure 3.6: Prediction of the wave crest growth, and time measurements (\times) of the crest during the “jump”, just before a slug is formed, for air–water flow in a horizontal $D = 0.052$ m pipe and $U_{SG} = 1.85$ m/s.

In Fig. 3.7 the model predicts that the slug/roll–wave formation time increases and then decreases with U_{SG} , and the intersection point between (t_x and t_y) successfully predicts the transition from growing regular gravity waves to roll–waves. Note that slugs may still form in the roll–wave region by coalescence between roll–waves or if the superficial liquid velocity is further increased. Increasing the superficial liquid velocity results in shorter transition times from stratified way to slug flow. This is clearly observed at low U_{SG} , which is not surprising since introducing larger U_{SL} results in a larger initial liquid height. Therefore, the distance between the wave crest and the top of the pipe becomes shorter. At sufficient liquid height, the wave crest will be unable to approach the downstream wave end before hitting the top of the pipe. Thus, a slug is formed.

3.6.3 Formation time predictions for different pipe diameters

We have performed simulations with MAST for horizontal air–water flow in pipes with diameters of 0.025, 0.052, and 0.095 m. The aim of the simulations is to investigate the diameter scaling of the transitions from stratified to slug and roll–wave regimes, where no experimental data is available for the flow regime transitions considered. Figs. 3.8, 3.9 and 3.10 compare theoretical predictions of t_y and t_x with the simulations. The simulations for the slug flow and roll–wave cases are denoted by (\blacksquare) and (\square), respectively. The solid (—) and the dashed lines (---) represent theoretical calculations of t_x and t_y , respectively. The simulations and the model predictions have been performed at $U_{SL} = U_{SLmin}$. Note that increasing the pipe

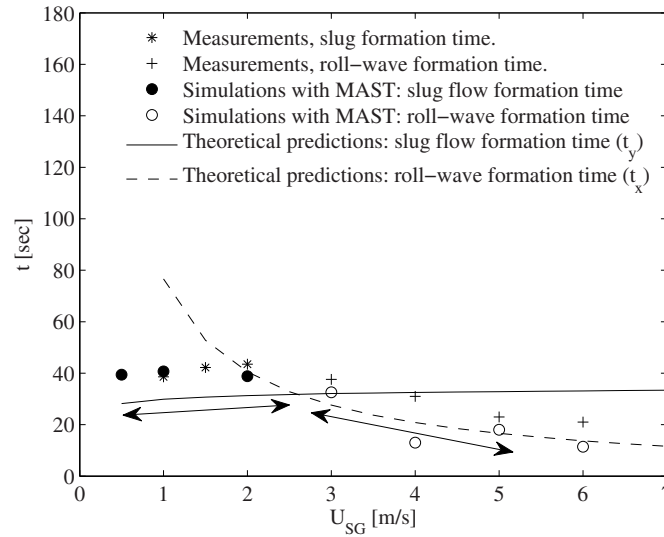


Figure 3.7: Theoretical predictions of t_y and t_x , compared with slug and roll-wave measurements for air-water horizontal pipe flow at $U_{SL} = U_{SL_{min}}$ and $D = 0.06$ m.

size requires larger $U_{SL_{min}}$ for the transition from stratified to slug flow.

In Fig. 3.8 the calculations were done for a 0.025 m i.d. pipe. At low U_{SG} , the time needed for the wave to hit the top of the pipe (t_y) grows with U_{SG} . A possible reason for that is the lower initial liquid height of the stratified flow due to the increase of the superficial gas velocity (Eq. (3.13)). The lower the initial height is, the larger the (vertical) distance needed to be travelled by the wave crest in order to hit the top of the pipe, and thus t_y increases. At large U_{SG} , and if U_{SL} is low enough, roll-waves are formed. Their formation is related to the relative velocity between the crest and the downstream wave end as given by Eq. (3.22). By increasing U_{SG} , the crest moves faster toward the downstream wave end resulting in shorter time for the formation of roll-waves.

For a larger pipe $D = 0.052$ m, presented in Fig. 3.9, we notice that the time needed for the wave to reach the top of the pipe increases. This can be explained by the larger vertical distance to be travelled by the wave crest due to the larger pipe diameter. The same behaviour is found for the pipes with diameters of 0.06 and 0.095 m presented in Figs. 3.7 and 3.10.

3.6.4 Critical Froude number for the transition

A significant result of the model is the relation between the pipe size and the transition from regular gravity waves (forming slug flow) to roll-wave regions. Defining $U_{SG_{crit}}$ as the critical superficial gas velocity where $t_y = t_x$, we find that $U_{SG_{crit}}$ increases with pipe size. In Figs. 3.8, 3.9, 3.7, and 3.10, $U_{SG_{crit}} \simeq 2.3, 3.4, 3.6$ and 4.1 m/s, respectively. Defining a Froude number

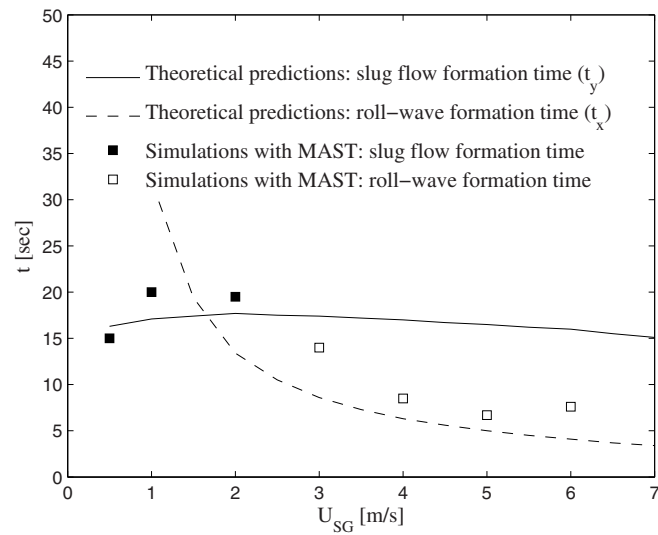


Figure 3.8: Simulations and theoretical predictions of t_y and t_x for air–water horizontal pipe flow at $U_{SL} = U_{SL_{min}}$ and $D = 0.025$ m.

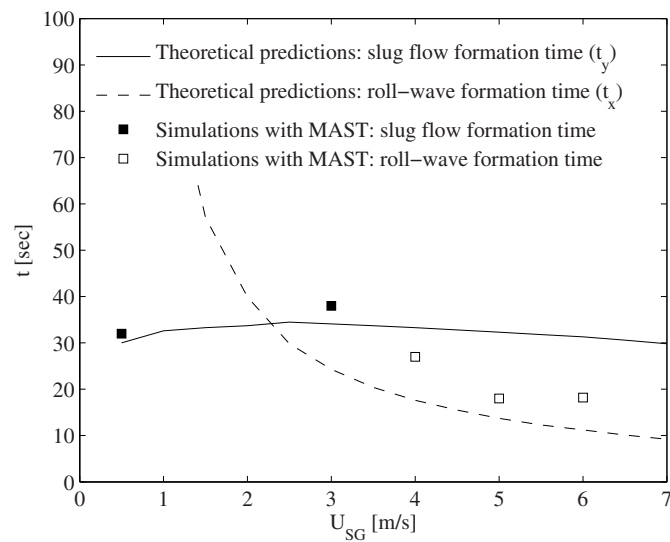


Figure 3.9: Simulations and theoretical predictions of t_y and t_x for air–water horizontal pipe flow at $U_{SL} = U_{SL_{min}}$ and $D = 0.052$ m.

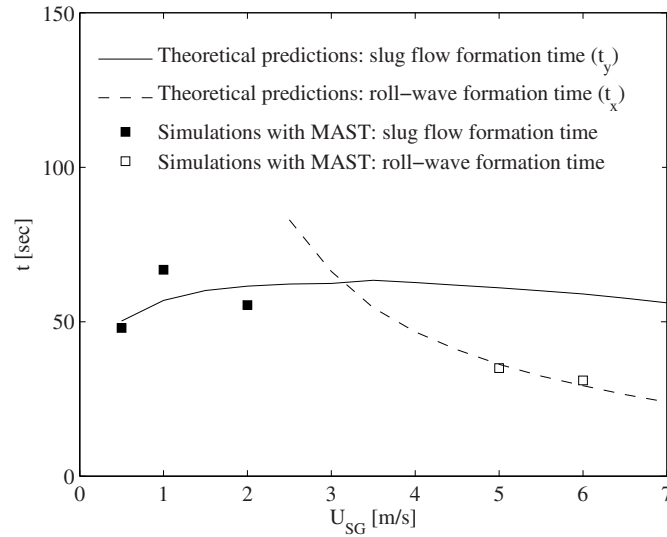


Figure 3.10: Simulations and theoretical predictions of t_y and t_x for air–water horizontal pipe flow at $U_{SL} = U_{SL_{min}}$ and $D = 0.095$ m.

$Fr_{crit} = \sqrt{\rho_G U_{SG_{crit}}^2 / (\Delta\rho g D)}$, where $\Delta\rho = \rho_L - \rho_G$, we obtain that $Fr_{crit} \simeq 0.15$ is the critical Froude number at which the transition from slug flow (formed by gravity waves) to roll-waves occurs, for the different pipe diameters and $U_{SL_{min}}$ in Figs. 3.8, 3.9, 3.7, and 3.10.

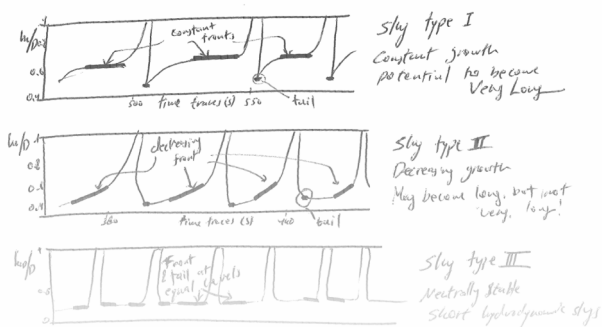
This result agrees well with previous work by Woods and Hanratty (1999) who showed that the flow becomes supercritical, at $U_{SG} > 4$ m/s (that is at $Fr_{crit} > 0.16$), and slug formation is determined by coalescing roll-waves, whereas at lower U_{SG} slugging is reached when large wavelength waves reach the top of the pipe. They also noted that the minimum U_{SG} required for the transition from stratified to slug flow increases with the pipe size, which agrees with the behaviour of $U_{SG_{crit}}$ for the transition from slug flow to roll-wave region, as aforementioned.

3.7 Conclusions

1. The evolution of long wavelength waves in horizontal pipes may result in different flow patterns in the pipe. If the wave crest reaches the top of the pipe a slug may form. However, if the crest overtakes the downstream wave end (before it reaches the top of the pipe) a roll wave is formed.
2. A “jump” in the liquid phase toward the top of the pipe is observed just before the wave crest bridges the pipe. A possible reason for this “jump” is the suction forces acting in the neighbourhood of the crest. The suction forces may become large enough to

elevate the liquid surface as the actual gas velocity becomes relatively high due to the exponential decrease of the gas cross-sectional area at the crest.

3. Measurements carried out in a 137 m long horizontal pipeline with a 0.052 m i.d. show that the time required for a wave to reach the height at which the crest “jumps” toward the top of the pipe, is much longer than the “jump time”. Increasing the superficial liquid velocity results in shorter “jump” time.
4. A wave transition model was presented. The model is based on calculating the time required for a long wavelength wave with a small initial amplitude, on the order of the turbulent length scale, to grow and reach the top of the pipe (see Eq. (3.21)), and the time it takes the axial propagation of the wave crest to overtake the downstream wave end (see Eq. (3.23)). The model predicts the transition from stratified flow to slug flow or roll-wave regimes for different pipe diameters and different gas and liquid superficial velocities.
5. The model predicts a number of important observations regarding the behaviour of slug/roll-wave formation time: (a) increasing the superficial liquid velocity results in shorter transition times from stratified wavy to slug flow; (b) at relatively low U_{SG} , the formation of slug/roll-wave time increases with increasing U_{SG} , which is a result of the lower initial stratified height; however, (c) at relatively high U_{SG} , due to the domination of inertial forces, the formation time decreases with increasing U_{SG} and a roll-wave is formed; and (d) increasing the pipe size results in larger axial growth compared to the growth of the vertical direction, making the appearance of long slugs less likely.
6. Numerical simulations have been carried out using a transient one-dimensional multi-phase flow simulator in order to investigate the diameter scaling of the transitions from stratified to slug and roll-wave regimes. Comparing predictions by the model with the simulations we found that increasing the pipe diameter results in larger formation times for both t_y and t_x . However, since t_x is function of both vertical and axial displacements of the crest, its sensitivity to a change in the pipe diameter is greater. As a result, larger U_{SG} is required for the transition from slug flow (formed by regular gravity waves) to roll-wave regimes.
7. Based on predictions by the model presented in this paper we obtained a critical densimetric gas Froude number, $Fr \simeq 0.15$, for the transition from regular growing gravity waves, to roll-wave regimes. The critical Froude number was obtained for superficial velocities close to the transition to slug flow.
8. The accuracy of the modelling could be improved if the interfacial friction factor at transition, the wave length, and the gas entrainment were better known over a wider range of flow conditions. The theories applied in the modelling are sensitive to the value of the interfacial friction factor which is of a critical importance at all flow rates. Whereas, the accuracy in the wave length and the gas entrainment (which was neglected in this paper) becomes important at relatively large flow rates.



4

Operation pressure and slug length¹

Slug flow is commonly observed in gas production offshore fields. At high operation pressure only short hydrodynamic slugs are observed. However, as the offshore fields become older, the operation pressure becomes lower and long slugs may form. At near atmospheric pressures the long slugs may reach a size of 500 pipe diameters or more. Such slugs can cause serious operational failures due to the strong fluctuating pressure. Identifying the operation pressure conditions at which the long slugs appear, may reduce or prevent these negative effects.

In this chapter we process and analyse gas–liquid flow measurements in order to investigate the different slug types and their sensitivity to the operation pressure. The measurements were performed by Kristiansen (2004) in a 103 m long pipe with an internal diameter of 0.069 m and an inclination of -0.1° from the horizontal. Three types of slugs were categorized according to the difference in liquid levels (liquid excess) between the slug front and tail. The long slugs were found to have the largest liquid excess after formation, whereas the hydrodynamic slugs had no liquid excess. The analysis of the measurements provides a detailed overview on the effect of pressure on the long slug length, and a safe operation region where long slugs will not appear.

¹This chapter is based on Kadri et al. (2009c)

4.1 Introduction

The cocurrent flow of gas and liquid in horizontal and near horizontal pipes results in a number of flow patterns. A *stratified flow* occurs at relatively low gas and liquid flow rates whereby the gas moves on top of the liquid. At higher rates of gas and liquid a *slug flow* pattern might exist where plugs of liquid move downstream separated by elongated bubbles moving along the top of the pipe. Although mostly short hydrodynamic slugs are observed, long slugs with sizes reaching 500 pipe diameters or more may form if the operation pressure becomes sufficiently low, e.g. in older gas production offshore fields. Such long slugs induce strong pressure fluctuations large enough to cause severe operational failures. Therefore, identifying the transition to the long slugs and the critical pressure at which they may appear, will be helpful in preventing or reducing such future operational failures.

Two main theoretical approaches are used to predict the transition from stratified to slug flow: stability of stratified flow and stability of slug flow. The *stability of stratified flow* was initially used by Hanratty and Hershman (1961) to describe waves on thin films over which air is blowing. A number of researchers (Wallis and Dobbins (1973); Lin and Hanratty (1986); Wu et al. (1987)) followed this analysis to investigate the viscous wavelength wave instability (VLW). The VLW theory successfully predicts that increasing the pipe size requires larger gas flow rates for the transition from stratified to slug flow in air–water horizontal pipe flow. The *stability of slug flow* considers the amount of liquid entering and leaving the slug. The slug becomes *neutrally stable*, not growing neither decaying, when a volumetric liquid balance is reached between the slug front and tail. This balance results in a minimum liquid area at the front, below it the slug becomes unstable (Bendiksen (1984); Ruder et al. (1989); Woods and Hanratty (1996)).

Slug lengths have been reported to be in a range of 12–30 D for horizontal air–water flow (Dukler and Hubbard (1975); Nicholson et al. (1978); Nydal et al. (1992)). This type of slugs is known as hydrodynamic slugs. Kristiansen (2004) found a similar range of slug lengths for gas–liquid near horizontal pipe flow when introducing slugs at the inlet. However, when introducing stratified flow at the inlet he observed both short hydrodynamic and long slugs. Zoetewij (2007) observed very long slugs reaching 500 pipe diameters. The long slugs form at relatively low gas and liquid velocities, where two sub–regimes are observed: neutrally stable, and growing slugs (Kadri et al. (2009a)).

In this chapter we analyse measurements performed by Kristiansen (2004) in a 103 m long gas–liquid near horizontal pipe flow with an internal diameter of 0.069 m . The measurements were performed with air or high density gas at atmospheric and higher operation pressures. The analysis of the measurements is unique in the sense that it provides a simple mechanism for the appearance of different slug types in the long slug regime. Slugs were categorized into three types according to the difference in liquid levels (*liquid excess*) between the front and tail: (1) slugs with large and initially constant excess; (2) slugs with decreasing excess; and (3) slugs with no excess. Slugs with large liquid excess can grow to become very long, whereas slugs that have no liquid excess are the shortest. We also found that small changes in the liquid excess, at the formation time, may result in large differences in slug length. Moreover, we identified the operation pressures at which the growing and stable slugs may appear.

A background on the theoretical approaches, stability of stratified flow and slug stability, is given in section 4.2. Section 4.3 provides a description of the experimental facility and methods used for performing the measurements. A discrimination method between slug types is given in section 4.4. In section 4.5 we present results of the effect of slug types on the slug length at atmospheric and high operation pressures. Finally, the conclusions are presented in section 4.6.

4.2 Background

4.2.1 Stratified flow pattern

An idealized model of the stratified flow pattern is represented by a simplified geometry. The diameter of the pipe is D . The height of the liquid layer along the centerline is h_L . The length of the segments of the pipe circumference in contact with the gas and liquid are S_G and S_L , respectively. The length of the gas–water interface is presented by S_i . The areas occupied by the gas and the liquid are A_G and A_L , respectively. Given the pipe diameter, these parameters can be calculated, from measurements of h_L , by using geometric relations (e.g. Govier and Aziz (1972)). The momentum balances for the gas and the liquid flows are as follows,

$$-A_G \left(\frac{dp}{dx} \right) - \tau_{WG} S_G - \tau_i S_i + \rho_G A_G g \sin \theta = 0, \quad (4.1)$$

$$-A_L \left[\left(\frac{dp}{dx} \right) - \rho_L g \cos \theta \left(\frac{dh_L}{dx} \right) \right] - \tau_{WL} S_L + \tau_i S_i + \rho_L A_L g \sin \theta = 0, \quad (4.2)$$

where ρ_G and ρ_L are the gas and the liquid densities, θ is the inclination angle of the pipe from the horizontal, dp/dx is the pressure gradient, dh_L/dx is the liquid hydraulic gradient, and g is the acceleration due to gravity. The time-averaged stress of the gas and liquid phases at the wall and the stress at the interface, τ_{WG} , τ_{WL} and τ_i , are defined in terms of friction factors, and calculated using the Blasius equation if $Re < 10^5$ and the wall roughness effect can be ignored, otherwise the Churchill equation is used (see Churchill (1977)). Due to the presence of waves at the interface, the interfacial friction factor becomes larger than the friction factor for a smooth surface. In this chapter we use an estimation for the interfacial friction factor suggested by Hurlburt and Hanratty (2002). For given flow rates of liquid and gas Eqs. (4.1) and (4.2) are used to find the pressure gradient and the height of the liquid layer. However, these equations do not determine the stability of the stratified flow.

4.2.2 Average liquid area

The average liquid area, $A_L = A_{L_{avg}}$, is calculated from the momentum balances for the stratified flow pattern, Eqs. (4.1) and (4.2). Substituting $A_L = A_{L_{avg}}$ and $A_G = A - A_{L_{avg}}$, Kadri et al. (2009a) wrote Eq. (4.1) in the following form,

$$\left(\frac{dp}{dx} \right) = \frac{\tau_{WG} S_G + \tau_i S_i}{A - A_{L_{avg}}} - \rho_G g \sin \theta. \quad (4.3)$$

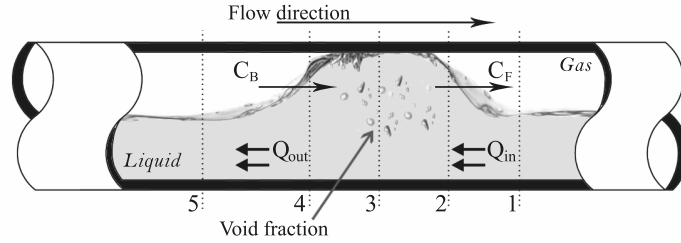


Figure 4.1: Sketch of a slug.

The average liquid area is the initial plain stratified flow in the pipe. This occurs when the pressure gradients of the two phases on the interface cancel. Substituting Eq. (4.3) in Eq. (4.2) and assuming a fully developed horizontal pipe flow Kadri et al. (2009a) obtained a relation for $A_{L_{avg}}$ as follows,

$$A_{L_{avg}} = A \frac{\tau_{WL}S_L - \tau_i S_i}{\tau_{WL}S_L + \tau_{WG}S_G}. \quad (4.4)$$

The average liquid height $h_{L_{avg}}$ is calculated using Eq. (4.4) and geometric relations (e.g. Govier and Aziz (1972)). Eq. (4.4) successfully predicts the inverse proportionality between the gas flow rates and $h_{L_{avg}}$.

4.2.3 Slug stability model

The slug stability model considers the rates of liquid adjoining or detaching from the slug at its front or rear. Slugs are stable (not decaying) when the rates of liquid adjoining are not less than the rates at which liquid detaches. Figure 4.1 gives an illustration of a slug moving with front velocity C_F over a stratified liquid layer at station 1 of area A_{L1} and actual velocity u_1 . The volumetric flow rate of liquid adjoining the slug is

$$Q_{in} = (C_F - u_1)A_{L1}. \quad (4.5)$$

The rear of the slug is assumed to behave as a bubble moving with a velocity C_B . The volume fraction of the gas in the slug is ϵ . The volumetric flow rate of the liquid detaching from the slug is

$$Q_{out} = (C_B - u_3)(1 - \epsilon)A \quad \text{at station 3.} \quad (4.6)$$

The parameter u_3 is the actual liquid velocity at stations 3. Assuming neutral stability, $Q_{in} = Q_{out}$ and $C_F = C_B$, and making use of Eqs. (4.5) and (4.6), the following relation is obtained for the area of the stratified layer:

$$\left(\frac{A_{L1}}{A} \right)_{crit} = \frac{(C_B - u_3)(1 - \epsilon)}{(C_B - u_1)}, \quad (4.7)$$

for the area of the stratified flow at the front. Using Eq. (4.7) and geometric relations, the critical height, $h_{L_{crit}}$, at the slug front required for the slug to be neutrally stable is obtained. A detailed analysis of the slug stability model is well documented by Hurlburt and Hanratty (2002); Soleimani and Hanratty (2003).

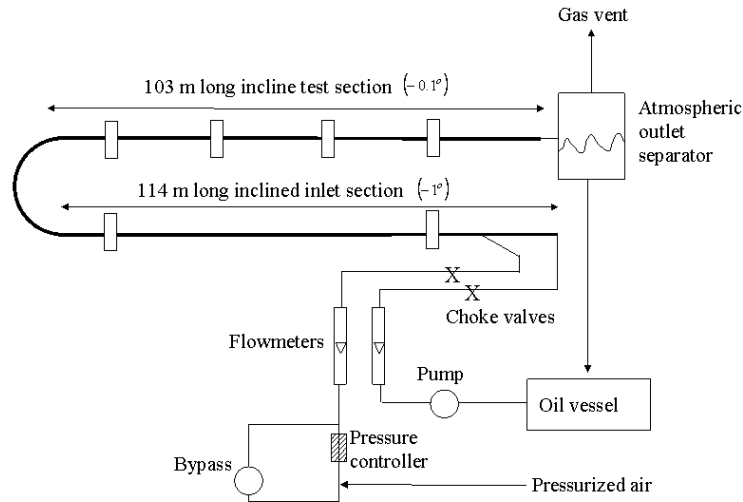


Figure 4.2: Sketch of the SINTEF experimental setup for an open loop configuration.

4.3 Experiments

The experiments analysed in this chapter have been carried out by Kristiansen (2004) who investigated the transition from stratified to slug flow in multiphase pipe flow. The multiphase flow laboratory facility that was used is the SINTEF (The Foundation for Scientific and Industrial Research) flow loop located in Trondheim, Norway.

The flow loop was configured as an open loop when operating at atmospheric experiments, and as a closed system for experiments at higher pressures. The loop is 217 m long with 0.069 m internal diameter near-horizontal pipe. A sketch of the experimental setup is given in Figures 4.2 and 4.3 for open and closed loop configurations, respectively. The inlet is 114 m long adjusted with an inclination of -1° from the horizontal to ensure stratified flow at the inlet. The inlet ends in a 180° u-turn, and the last 103 m is the test section with an inclination of -0.1° . The geometry configuration of the flow loop is given in Figure 4.4.

The fluids used in the experiments were air or sulphur hexafluoride (SF_6) gas, and oil (*ExxsolD80*). Air was used when operating at atmospheric conditions, whereas SF_6 in higher pressure experiments. Sulphur hexafluoride (SF_6) is a dense gas with density approximately 5.5 times that of air, simulating high pressure conditions (natural gas up to 65 bar).

The liquid height was measured using 6 single-energy narrow-beam gamma densitometers, at locations: 19.37, 100.17, 128.30, 161.42, 182.32, and 200.32 m from the inlet. The gamma densitometers were calibrated using a two-point calibration in single-phase liquid and gas, respectively. The slug length was calculated at the sensors in the test section (last 4 sensors). Note that the slug length measurements presented in this chapter are slug length calculations at the last sensor downstream, where the development time is the largest.

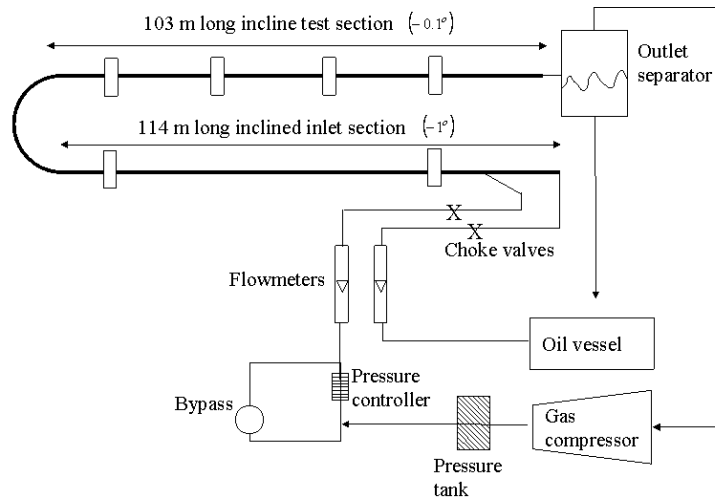


Figure 4.3: Sketch of the SINTEF experimental setup for a closed loop configuration.

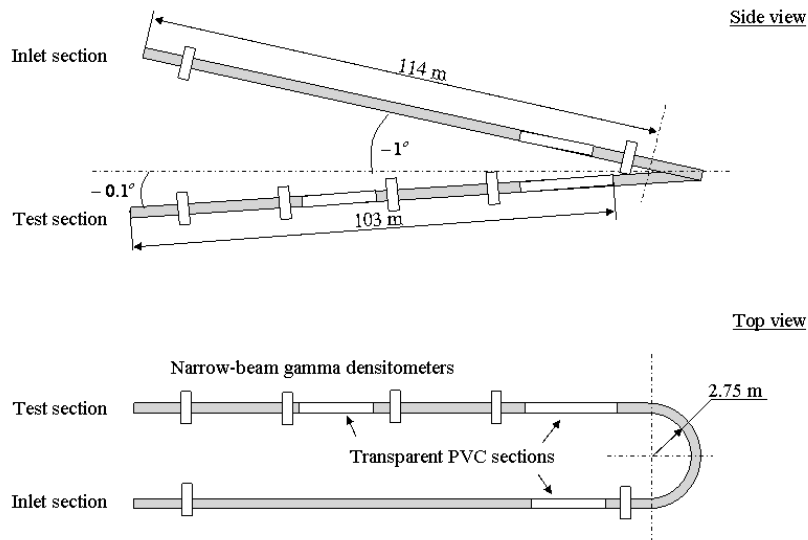


Figure 4.4: Side and top views of the geometry configuration of the flow loop.

The tests were performed in series with constant gas rate and increasing liquid rate, always starting in stratified flow. The full description of the test conditions can be found in Kristiansen (2004). A summary for the test conditions and fluids properties is shown in Table

4.1.

All measurements presented in this chapter have been processed according to the different slug types presented in the next section. The processed measurements are addressed as “measurements”.

Table 4.1: Summary of test conditions and fluids properties.

Pipe diameter [m]	0.069
Pipe length [m]	217.24
Test section length [m]	103
Inlet section inclination [deg]	-1
Test section inclination [deg]	-0.1
Gas phase	Air or SF_6 gas
Liquid phase	<i>ExxsolD80</i> oil
Gas density [kg/m^3]	1.2, 9, 19, 46, 52
Liquid density [kg/m^3]	810
Air viscosity [kg/ms]	1.8×10^{-5}
Gas (SF_6) viscosity [kg/ms]	1.5×10^{-5}
Liquid viscosity [kg/ms]	0.0018
Interfacial tension ($\sigma_{oil/air}$) [N/m]	0.025
Interfacial tension (σ_{oil/SF_6}) [N/m]	0.021
Pressure [$barA$]	1, 1.5, 3, 7, 8
U_{SG} [m/s]	0.2–8
U_{SL} [m/s]	0.05–0.5

4.4 Definition of slug types by liquid excess

The slug formation is associated with liquid depletion at the tail of the slug (Woods and Hanratty (1999)). The slug becomes *neutrally stable*, neither growing nor decaying, when a volumetric balance between the liquid detaching, at the tail, and joining, at the front, is reached. For a constant gas density and a continuous liquid phase, it can be shown from conservation of mass of the liquid phase that the liquid heights at the tail and front should be equal in order to reach neutral stability. That happens when the slug front approaches the tail of a second slug downstream, and the liquid excess becomes zero (i.e. that is why the first slug in the pipe can grow indefinitely).

4.4.1 Discrimination between slug types in measurements

Figure 4.5 presents an example of time traces of three different slug types measured with the first sensor downstream. In Figure 4.5(a), the liquid height at the slug front is constant along a relatively large distance downstream, and remarkably higher than the liquid height at the tail. This observation indicates that such a slug is not influenced by the presence of a second slug (probably far) downstream. Such slugs are defined as *type I*. In Figure 4.5(b),

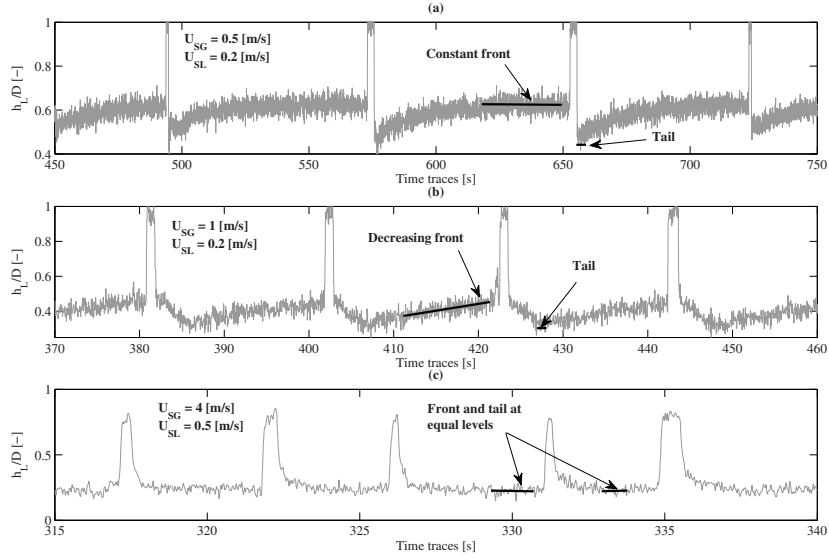


Figure 4.5: Time traces of different slug types in SF_6 gas-oil pipe flow, $D = 0.069$ m, $\theta = -0.1^\circ$, $P = 1.5$ barA ($\rho_G = 9$ kg/m³): (a) type I, (b) type II, and (c) type III.

the liquid height at the front decreases as a slug moves downstream. In this case, the slug growth is dependant on the downstream liquid depletion due to the existence of a second slug downstream. This type of slugs is defined as *type II*. In Figure 4.5(c), the liquid at the front and at the tail are equal, indicating a fully developed slug where the slug front approaches the tail of a second slug downstream. This type of slugs is denoted as *type III*.

The overall slug type of each measurement is denoted as one of the three types only if at least 90% of the individual slugs share the same type. Otherwise, the overall slug type is addressed as “undefined”.

4.4.2 Measurements of the liquid excess, Δh_L

In order to calculate the average liquid excess of the different slug types the following steps are made: (1) The time traces of the liquid height are examined at the first sensor where slugs are observed, at constant gas and liquid flow rates. (2) The average liquid height at the tail, h_{Ltail} , is calculated from the average height around the lowest point in the tail of each slug in the time traces. (3) The average liquid height at the front, h_{Lfront} , is calculated from the average over a distance on the order of $10D$ from the front of all slugs in the time traces. (4) The average liquid excess of each measurement is calculated as follows,

$$\Delta h_L = h_{Lfront} - h_{Ltail}. \quad (4.8)$$

4.4.3 Theoretical predictions of the liquid excess, Δh_L

4.4.3.1 Slugs type I

At low gas and liquid flow rates, where the slug frequency is relatively low, a forming slug is far enough from a second slug downstream, as mentioned above. As a result, the liquid height at the front is not affected by the presence of the second slug. In this case, the liquid height at the front is the average height of the stratified flow, $h_{L_{front}} = h_{L_{avg}}$, whereas the liquid height at the tail is the minimum height calculated by slug stability ($h_{L_{tail}} = h_{L_{crit}}$). Therefore, the liquid excess of slugs *type I* is calculated as follows,

$$(\Delta h_L)_{typeI} = h_{L_{avg}} - h_{L_{crit}}, \quad (4.9)$$

where $h_{L_{avg}}$ and $h_{L_{crit}}$ are calculated from Eqs. (4.4) and (4.7), respectively. A comparison between the predicted and measured liquid heights is given in Figure 4.6(a).

4.4.3.2 Slugs type II

Increasing the gas or liquid flow rates results in higher slug frequency (e.g. Gregory and Scott (1969)). At a sufficiently high frequency the liquid height at the front of the slug is affected by the presence of another slug downstream, so that the average liquid height at the front is lower than the initial height as presented in Figure 4.6(b). In this case, Δh_L is approximated by the average height between $h_{L_{avg}}$ and $h_{L_{crit}}$ as follows,

$$(\Delta h_L)_{typeII} = \frac{h_{L_{avg}} - h_{L_{crit}}}{2}. \quad (4.10)$$

Eq. 4.10 presents an upper limit of $(\Delta h_L)_{typeII}$.

4.4.3.3 Slugs type III

Further increase of the flow rates results in the generation of a larger number of slugs. In this case, a forming slug reaches neutral stability immediately after formation. Thus, the liquid height at the front and tail are approximately the same (see Figure 4.6(c)), thus:

$$(\Delta h_L)_{typeIII} = 0. \quad (4.11)$$

4.5 Results

In this section we compare theoretical predictions of the liquid excess, Δh_L , of the different slug types with (the processed) measurements. Additionally, we present a flow map and slug length measurements, at atmospheric and higher operation pressures, and identify the conditions at which the long slugs form.

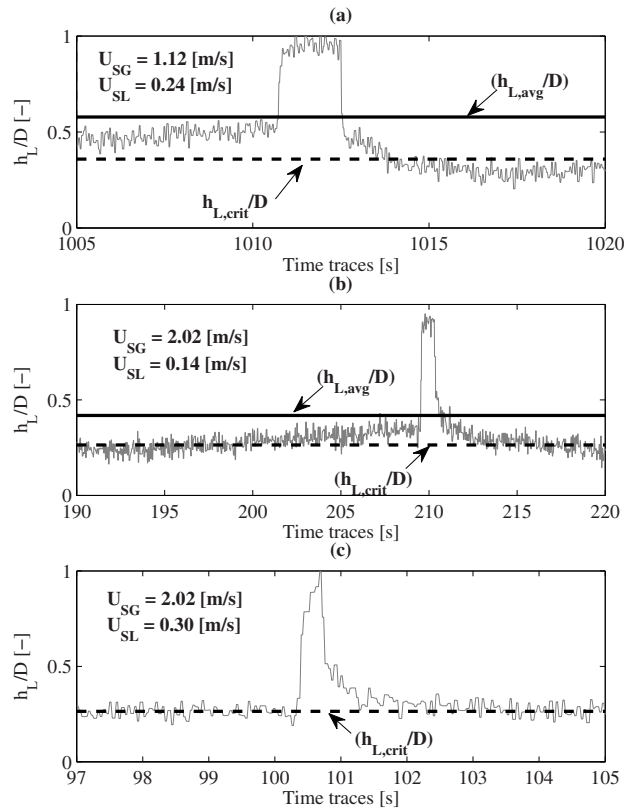


Figure 4.6: Time traces of different slug types in air-oil pipe flow, $D = 0.069$ m, $\theta = -0.1^\circ$, $P = 1$ bar: (a) type I, (b) type II, and (c) type III. The experiments were performed by Kristiansen (2004)

4.5.1 Slug types and the normalized liquid excess, $\Delta h_L/D$

Figure 4.7 compares $\Delta h_L/D$ of the three slug types at atmospheric pressure and different U_{SG} . The gas and liquid phases are air and oil (*ExxsolD80*), and the pipe diameter $D = 0.069$ m. Slugs type I are represented by filled triangles (\blacktriangle), type II by circles (\circ), and type III by stars ($*$). The solid (—), dashed-dotted (—·—), and dashed (---) lines are the theoretical predictions of $(\Delta h_L)_{typeI}$, $(\Delta h_L)_{typeII}$, and $(\Delta h_L)_{typeIII}$, calculated by Eqs. (4.9), (4.10), and (4.11), respectively. The agreement between the theoretical predictions and measurements of the different slug types is satisfactory. However, Eq. (4.9) underpredicts and shows a wrong trend of $(\Delta h_L)_{typeI}$ at $U_{SG} < 1$ m/s. This discrepancy is due to the undeveloped liquid height at the tail, which drops below $h_{L,crit}$ when a slug forms and, at low gas flow rates, slowly rebuilds to reach $h_{L,crit}$. This observation indicates a larger growth rate in slugs type I (due

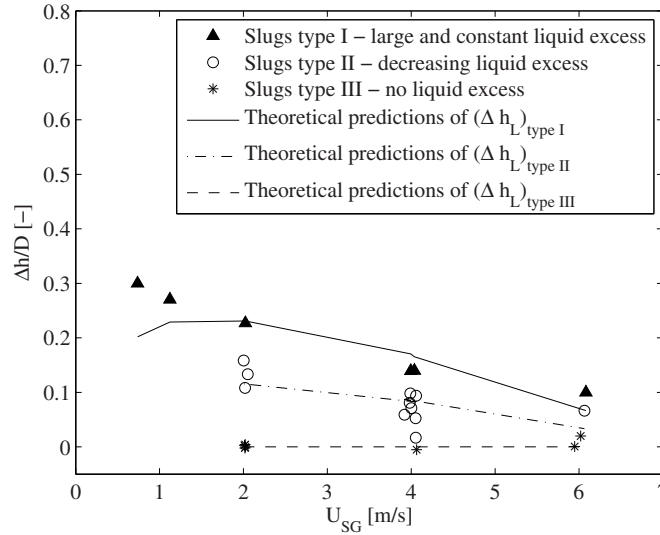


Figure 4.7: Measurements and predictions of Δh_L for the different slug types, in air–oil pipe flow, $D = 0.069 \text{ m}$, $\theta = -0.1^\circ$, $P = 1 \text{ bar}$. The data were derived from experiments done by Kristiansen (2004)

to the larger liquid excess) and a slower development (due to the lower flow rates). In the figure, we see that slugs *type I* have the largest liquid excess, *type III* have approximately zero excess, and the excess in *type II* is intermediate.

It is worth noting that the measurements presented in Figure 4.7 were performed at different U_{SL} . At constant U_{SG} , slugs *type I* have the lowest U_{SL} , whereas slugs *type III* have the largest. The flow rates flow map is further discussed in the next sub–section.

4.5.2 The length of the different slug types at atmospheric pressure

A stable slug (i.e. not decaying) has an initial length of $8D < L_S < 16D$ (e.g. Dukler et al. (1985)), regardless to its type. Since the slug is moving at velocities larger than the downstream liquid it absorbs any liquid excess between the slug tail and front. This is the key difference between the three types. A slug *type III* becomes neutrally stable immediately after formation, so that it does not grow further. However, slugs *type I* and *type II* will grow further until the tail of a second slug downstream is approached, where $\Delta h_L = 0$ is satisfied.

The sub–plots in Figure 4.8 show a flow map (on the left) and slug length measurements (on the right) in air–oil near horizontal pipe flow at atmospheric operation pressure. Here we are interested in the transition between the short hydrodynamic and the long slugs. Slugs with $L_S > 40D$ are defined as long. The transition between the short hydrodynamic and the long slugs is presented by the gray bold–solid line. The dashed line (– –) is the predictions by slug stability model for the transition from stratified to slug flow. In Figure 4.8, we obtain

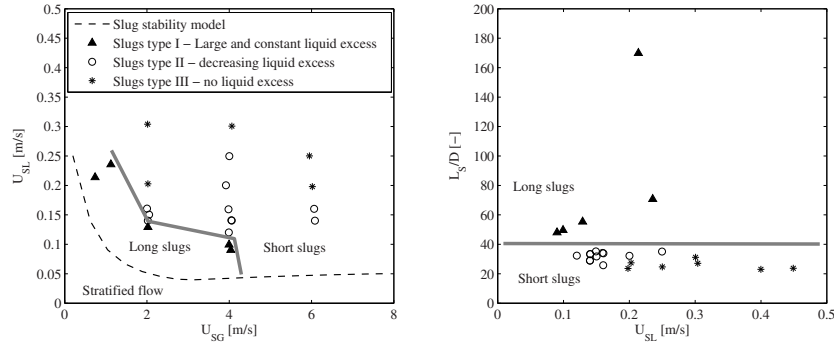


Figure 4.8: Flow regime transition data for different U_{SL} (on the left) and L_S/D (on the right) in air-oil pipe flow, $D = 0.069$ m, $\theta = -0.1^\circ$, $P = 1$ bar. The data were derived from experiments done by Kristiansen (2004)

that only slugs *type I* have grown to become long ($L_S > 40D$). Slugs *type II* are mostly larger than slugs *type III*. However, both types are hydrodynamic ($L_S < 40D$). In the flow map, we also find that slugs *type I* (the only long slugs here) are found at relatively small U_{SG} and U_{SL} . This observation is in agreement with the detailed measurements and theoretical calculations of the long slug regime by Kadri et al. (2009a).

4.5.3 The length of the different slug types at $P = 1.5$ barA ($\rho_G = 9$ kg/m³)

In Figure 4.9, the gas phase is SF_6 at the operation pressure $P = 1.5$ barA (the effective density, $\rho_G = 9$ kg/m³, simulates an operating pressure of 12 bar). In the slug length measurements (on the right) we notice that all slugs *type I* are long, as in the atmospheric case in Figure 4.8. However, part of the slugs *type II* are also long, unlike the atmospheric case. On the other hand, all slugs *type III* are short. It is worth noting that slugs *type III* may double their length when two slugs collide and merge as a single slug. It is also remarkable, that the long slugs *type II* differ fundamentally from the long slugs *type I*. Long slugs *type II* form at flow rates large enough to create large waves downstream. The growth of the long slugs *type II* involves collisions with these large waves, resulting in an increased turbulent front.

An interesting observation was found at measurements of similar flow rates but with a small difference in the initial liquid excess that resulted in large differences in the final slug length. As an example, in the flow map of Figure 4.9 there are two measurements at $U_{SL} = 0.17$ m/s, and $U_{SG} = 1$ m/s denoted as $M1$ and $M2$, where $(\Delta h_L)_{M1}$ is 3% larger than $(\Delta h_L)_{M2}$. Although the difference between $(\Delta h_L)_{M1}$ and $(\Delta h_L)_{M2}$ is relatively small, the difference of the final slug length in the two measurements is remarkably large: $(L_S/D)_{M1} = 112$, whereas $(L_S/D)_{M2} = 72$.

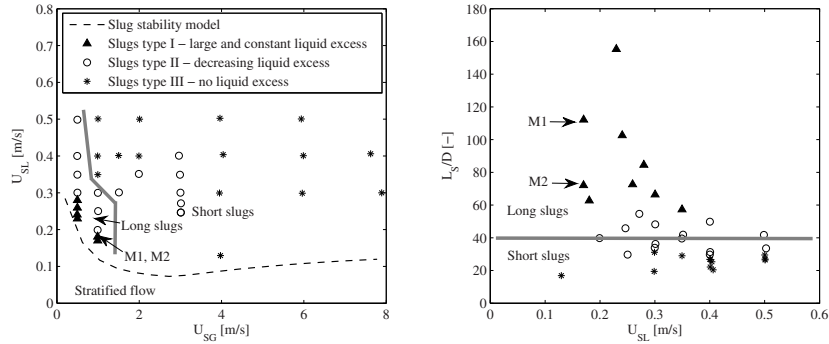


Figure 4.9: Flow regime transition data for different U_{SL} (on the left) and L_S/D (on the right) in SF_6 gas-oil pipe flow, $D = 0.069$ m, $\theta = -0.1^\circ$, $P = 1.5$ barA (the effective density, $\rho_G = 9$ kg/m³, simulates an operating pressure of 12 bar). The data were derived from experiments done by Kristiansen (2004)

4.5.4 The length of the different slug types at $P = 3$ barA ($\rho_G = 18.5$ kg/m³)

Operating at higher pressure results in higher critical flow rates and $h_{L_{crit}}$ required for the transition to slug flow (Eq. (4.7)), on the one hand, and lower flow rates and $h_{L_{avg}}$ of the stratified flow (Eqs. (4.1), (4.2) and (4.4)), on the other hand. As a result, the slug flow region “shrinks”. This shrinkage can be seen by comparing the flow maps presented in Figures 4.9 and 4.10.

In the flow map of Figure 4.10, we find that increasing the operation pressure, $P = 3$ barA (the effective density, $\rho_G = 18.5$ kg/m³, simulates an operating pressure of 23 bar),

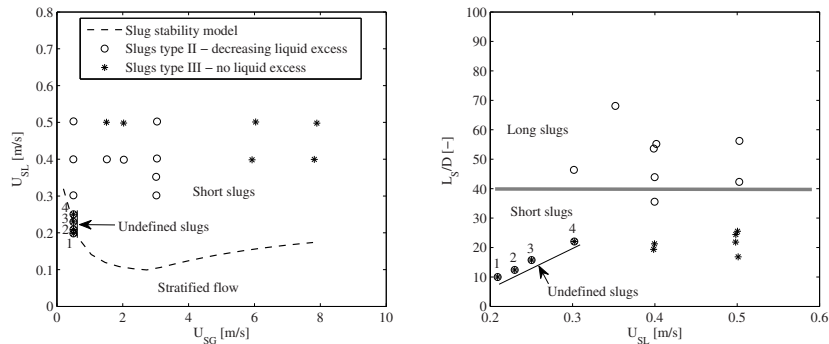


Figure 4.10: Flow regime transition data for different U_{SL} (on the left) and L_S/D (on the right) in SF_6 gas-oil pipe flow, $D = 0.069$ m, $\theta = -0.1^\circ$, $P = 3$ barA (the effective density, $\rho_G = 18.5$ kg/m³, simulates an operating pressure of 23 bar). The data were derived from experiments done by Kristiansen (2004)

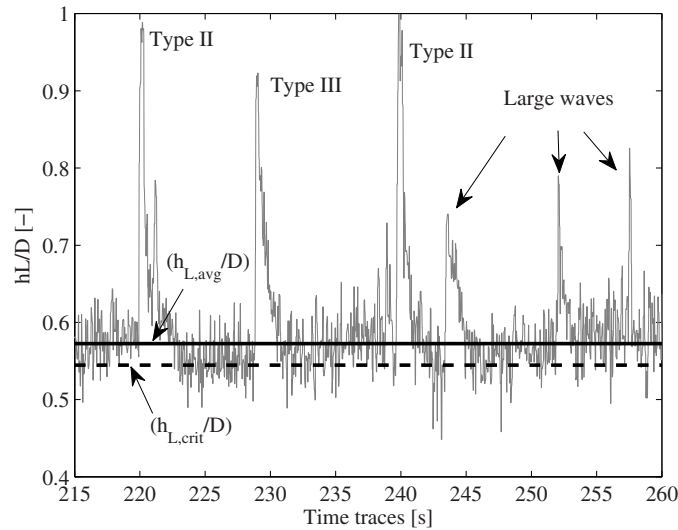


Figure 4.11: Time traces of SF_6 gas-oil pipe flow, $D = 0.069\text{ m}$, $\theta = -0.1^\circ$, $P = 3\text{ barA}$ (the effective density, $\rho_G = 18.5\text{ kg/m}^3$, simulates an operating pressure of 23 bar). The experiments were performed by Kristiansen (2004)

results in the appearance of slugs only at higher U_{SL} , as shown in the flow map. In this set of measurements no slugs *type I* were observed in the same measurements, and all long slugs are *type II* with lengths that do not exceed $70D$. At low flow rates, slugs *type II* and *type III*, and waves were observed, simultaneously. Such slug measurements, at which multiple slug types appeared, were indicated as “undefined slugs” in Figure 4.10. Time traces of these slugs show the combination of slugs *type II*, *type III*, and large waves, as presented in Figure 4.11. These slugs form close to the inlet (of the test section) and propagate at relatively low velocities. As a result, the slugs are being formed within, relatively, small distances, leading to a larger slug frequency compared with that of the long slugs. In addition, increasing U_{SL} results, contrary to slugs *type I*, in increasing L_S (see slug numbers in Figure 4.10).

4.5.5 Effect of pressure on the long slugs – summary

Figure 4.12 summarizes the effect of pressure on the presence of the long slugs in the pipe. In the figure, the bullets (\bullet) represent measurements of the maximum slug length in the pipe at the given flow conditions. For a gas density of air at atmospheric and near atmospheric operation pressures, the long slugs (*a* and *b*) are the longest in the long slug region ($L_S > 150D$). On the other hand, at gas density $18.5 < \rho_G < 52\text{ kg/m}^3$ simulating operation pressure of $23 < P < 65\text{ bar}$, the long slugs are neutrally stable and their length did not exceed $L_S = 70D$. Above $\rho_G = 52\text{ kg/m}^3$ ($P > 65\text{ bar}$), no long slugs have been observed.

From Figures 4.8, 4.9, 4.10, and 4.12 we conclude that the average slug length decreases

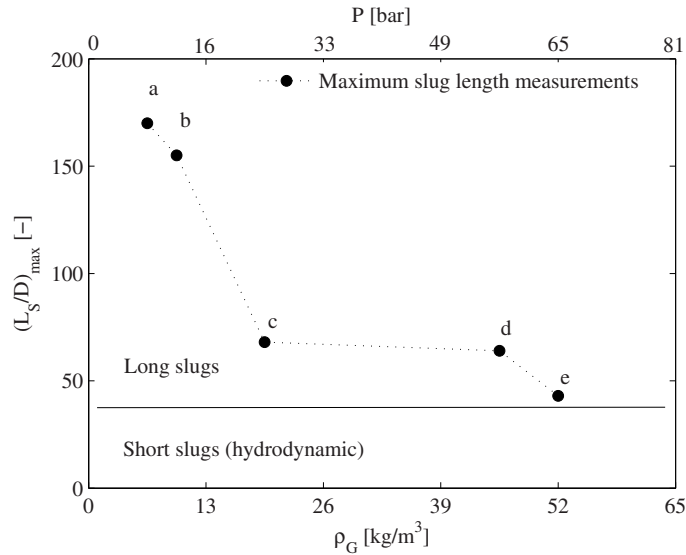


Figure 4.12: Largest normalized slug length, $(L_S/D)_{max}$, as function of gas density and simulated pressure in gas–liquid pipe flow, $D = 0.069$ m, $\theta = -0.1^\circ$. The data were derived from experiments done by Kristiansen (2004)

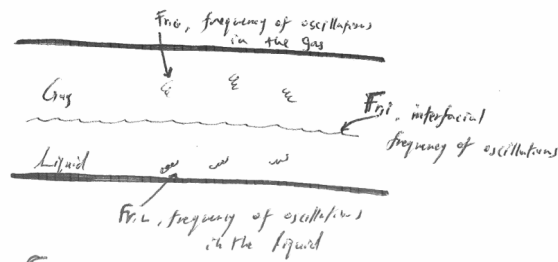
when increasing the operation pressure, at constant U_{SG} and U_{SL} . This conclusion is in agreement with findings by Ujang et al. (2006), who examined the pressure effect on the slug frequency at flow conditions and a pipe diameter similar to these presented in this chapter. Ujang et al. (2006) reported that the slug frequency is not sensitive to a change in the operation pressure. When increasing the operating pressure Δh_L decreases (Eqs. (4.4) and (4.7)), and since the slug frequency remains constant the slug length has to decrease in order to conserve the liquid mass.

4.6 Conclusions

1. Slug flow measurements have been analysed in order to investigate the sub–regimes in the long slug regime, and the effect of pressure on the appearance of the long slugs.
2. Slugs have been categorized into three types according to the liquid excess between the front and tail: (1) *type I*– slugs that are unaffected by the presence of other slugs downstream. They have relatively large and constant initial liquid excess. Due to the large liquid excess, this type of slugs may become extremely long $O(100D)$; (2) *type II*– slugs moving over a depleted liquid layer due to the passage of other slugs. Thus, these slugs have a decreasing liquid excess. Depending on the flow conditions, the length of this type of slugs varies from short hydrodynamic to long; and (3) *type III*– fully developed slugs with no liquid excess. These slugs are the shortest, being 8–16D

long at low flow rates, but double their lengths at larger flow rates due to collisions and merging with other slugs.

3. Theoretical predictions by stratified and slug stability models correctly predict Δh_L of the different slug types. However, the models underpredict $(\Delta h_L)_{type I}$ at $U_{SG} < 1 \text{ m/s}$.
4. At atmospheric pressure, the long slugs were found to be *type I*. When increasing the liquid flow rates, the frequency of slugs *type I* increases, and neutral stability is reached earlier in the pipe, due to the presence of a larger number of slugs. As a result, the slug length decreases.
5. Increasing the operation pressure results, on one hand, in larger flow rates that are required for the transition from stratified to slug flow. On the other hand, the stratified liquid height decreases (due to the larger gas density), and slugs become neutrally stable earlier. As a result, slugs become shorter and the long slug sub-regime “shrinks”.
6. Slugs *type II* may also become long ($L_S > 40D$). However, the mechanism behind their growth is related to the collision and absorption of large waves travelling downstream.
7. Slugs *type I* have not been observed at $\rho_G \geq 18.5 \text{ kg/m}^3$ ($P \geq 23 \text{ bar}$). At $18.5 < \rho_G < 46 \text{ kg/m}^3$ ($23 < P < 65 \text{ bar}$) the long slugs were only *type II*, neutrally stable at the outlet, with lengths less than $70D$. At $\rho_G = 52 \text{ kg/m}^3$ ($P = 65 \text{ bar}$) only short hydrodynamic slugs (*type III*) were found.
8. Slight changes in the liquid excess can lead to large difference in the final slug length, and thus slug frequency.



$$\frac{F_{r,i}}{V_i} = \sqrt{\frac{\rho_g}{\rho_l}} \left(\frac{F_{r,g}}{V_{r,g}} - \frac{F_{r,l}}{V_{r,l}} \right)$$

slug frequency: $F_{slug} = \sum P_k > F_{r,i}$
 probability of slug initiation if bigger at location k

5

A probabilistic slug frequency model ¹

In this chapter we show that the slug frequency is related to the frequency of the turbulent eddies generated in the viscous boundary layers of gas and liquid at the pipe wall. The turbulent eddies in each phase generate resonance oscillations that perturb the surface and create interfacial periodic fluctuations. We found that the slug frequency is characterized by these oscillations. However, the history of other turbulent eddies in the downstream part of the pipe is destroyed by passing slugs, preventing the formation of new slugs during and after their passage. As a result, the frequency of slug formation in the downstream part of the pipe is reduced. A probabilistic model is provided by making use of frequency of vortices, integral scales of turbulence, and probabilistic effects of the properties of developing slugs along the pipe. The model can act as a fundamental scientific guideline toward the design of gas–liquid horizontal pipe flow. Predictions by the model were compared with slug frequency measurements, found in literature, with a satisfactory agreement.

¹This chapter is based on Kadri et al. (2009d)

5.1 Introduction

A slug flow pattern is commonly observed when transporting gas and liquid in horizontal and near-horizontal pipe flows. Slug flow is characterized by plugs of liquid moving downstream separated by elongated bubbles moving along the top of the pipe.

The formation of slugs follows from surface waves evolving on the gas-liquid interface. One of the explanations of the occurrence of the surface waves is the presence of turbulence in the gas and liquid layers. The turbulent pressure and velocity fluctuations drive the wave formation, where the turbulence near the interface is usually maintained by a sheared mean flow (Teixeira and Belcher (2006)). At low Froude numbers there is no vertical motion in the turbulence over a depth comparable with the integral scale of the turbulence, and energy redistributes into horizontal fluctuations (Teixeira and Belcher (2006); Hunt and Graham (1978); Magnaudet (2003); Pan and Banerjee (1995)). At larger Froude numbers of the gas and liquid phases, the pressure fluctuations associated with the turbulence cause a resonant forcing of the free surface modes, which then grow indefinitely (Phillips (1957)). If the flow rates are sufficiently high, the evolving waves can reach the top of the pipe and form slug flow. On the other hand, the interfacial waves may grow in the turbulent layer towards the bottom of the pipe. However, their growth is unlikely to be of a considerable order, since the liquid momentum dominates and the gas turbulence is relatively weak.

Predictions of the flow conditions

Two main theories are involved for predicting the necessary flow conditions at which slugs may form: theories on the stability of stratified flow and the stability of slugs.

Hanratty and Hershman (1961) used the stability of stratified flow to describe waves on thin films over which air is blowing. Their analysis was followed by Kordyban and Ranov (1970), Wallis and Dobbins (1973), Taitel and Dukler (1976) Lin and Hanratty (1986), and Wu et al. (1987) who used the Kelvin-Helmholtz instabilities by analysing small sinusoidal perturbations on the interface of the stratified flow. This approach gives a criterion for the transition from stratified-smooth to wavy flow. On the other hand, the stability of slug flow concerns a volumetric balance between the liquid flow rate shedding from the back of a slug and the liquid rate accumulating on the front. This balance results in a minimum liquid area at the front that is required for a slug to be stable (Ruder et al. (1989); Bendiksen and Espedal (1992), Hurlburt and Hanratty (2002)). In this approach, the back of the slug is modelled as a bubble (Benjamin (1968)), which is supported by measurements and photographs by Woods and Hanratty (1996).

The two stability theories provide predictions of the flow conditions that are necessary. However, they do not provide prediction of slug length or frequency. In this chapter, we use the predictions by the two theories to obtain the properties of a stable slug flow.

Prediction of slug frequency

Slug frequency has been investigated by several researchers in the last decades. Gregory and Scott (1969) modelled the slug frequency as a function of the superficial gas and liquid velocities and the liquid Froude number. The correlation by Gregory and Scott (1969) is based on slug flow measurements performed in a wide range of pipe diameters, at relatively large liquid flow rates. Similar correlations based on additional data have been suggested by a number of researchers (e.g. Greskovich and Shrier (1972); Heywood and Richardson

(1979); Zabaras (1999)). Tronconi (1990) presented a semi-mechanistic model postulating that the slug frequency is one-half of the frequency of the unstable waves responsible for slug initiation. Woods and Hanratty (1999) reported that the postulation by Tronconi (1990) is inconsistent with their experimental data. Nydal (1991) carried out measurements at very large liquid flow rates and suggested a slug frequency correlation directly proportional to the squared liquid Froude number. Zabaras (1999) presented a review of eight slug frequency prediction methods: seven correlations and the mechanistic model by Taitel and Dukler (1976). The correlations were found unsatisfactory, and the mechanistic model was computationally too demanding. Zabaras (1999) suggested a correlation which is basically the correlation by Gregory and Scott (1969) extended to include positive pipe inclinations, relative to the horizontal.

In this chapter we present a probabilistic model for predicting the slug frequency. The proposed mechanism for the onset of the slug formation is that periodic pulsations of turbulent eddies, occurring in the boundary layer, result in periodic turbulence fluctuations at the interface. Slugs are assumed to be triggered at distances of the order of the turbulence mixing length, and at the frequency of pulsation of the eddies at the interface. However, the formation of slugs is influenced by the passage of other slugs that have already been formed upstream in the pipe. Such slugs prevent the triggering of new slugs. Therefore, a probabilistic model is obtained for the formation of slugs, which is dependent on the frequency of oscillations and the properties of the stable slug flow. For the validation of the model we compared predictions of the slug frequency with measurements found in the literature (Fan et al. (1993a); Fan et al. (1993b)), for gas-liquid horizontal pipe flows.

An interesting result is that the behaviour of the slug frequency with a change in the flow rates is similar to that of the frequency of oscillations in the gas phase, whereas the intensity of slugging is dominated by the momentum of the liquid phase.

Theoretical background including stability of stratified and slug flow is given in section 5.2. The proposed slug frequency model is presented in section 5.3. Section 5.4 provides comparisons between predictions by the slug frequency model and measurements, and a discussion. Finally, the conclusions are presented in section 5.5.

5.2 Background

5.2.1 Stratified flow pattern

An idealized model of the stratified flow pattern is represented by a simplified geometry as given in Figure 5.1A. The diameter of the pipe is D . The height of the liquid layer along the centerline is h_L . The length of the segments of the pipe circumference in contact with the gas and liquid are S_G and S_L , respectively. The length of the gas-water interface is presented by S_i . The areas occupied by the gas and the liquid are A_G and A_L , respectively. Given the pipe diameter, these parameters can be calculated, from measurements of h_L , by using geometric relations (e.g. Govier and Aziz (1972)). The momentum balances for the gas and the liquid flows are as follows,

$$-A_G \left(\frac{dp}{dx} \right) - \tau_{WG} S_G - \tau_i S_i + \rho_G A_G g \sin \theta = 0, \quad (5.1)$$

The gas and liquid Reynolds number given in Eq. (5.4) are given by

$$Re_G = \frac{D_{HG}U}{\nu_G}; \quad Re_L = \frac{D_{HL}u}{\nu_L}, \quad (5.9)$$

where ν_G and ν_L are the kinematic viscosities of gas and liquid, and D_{HG} and D_{HL} are the hydraulic diameters defined as

$$D_{HG} = \frac{4A_G}{S_G + S_i}; \quad D_{HL} = \frac{4A_L}{S_L}. \quad (5.10)$$

5.2.2 Average liquid area

The average liquid area, $A_L = A_{L_{avg}}$, is calculated from the momentum balances for the stratified flow pattern, Eqs. (5.1) and (5.2). Substituting $A_L = A_{L_{avg}}$ and $A_G = A - A_{L_{avg}}$, Kadri et al. (2009a) wrote Eq. (5.1) in the following form,

$$\left(\frac{dp}{dx} \right) = \frac{\tau_{WG}S_G + \tau_i S_i}{A - A_{L_{avg}}} - \rho_G g \sin \theta. \quad (5.11)$$

The average liquid area is the initial plain stratified flow in the pipe. This occurs when the pressure gradients of the two phases on the interface cancel. Substituting Eq. (5.11) in Eq. (5.2) and assuming a fully developed horizontal pipe flow Kadri et al. (2009a) obtained a relation for $A_{L_{avg}}$ as follows,

$$A_{L_{avg}} = A \frac{\tau_{WL}S_L - \tau_i S_i}{\tau_{WL}S_L + \tau_{WG}S_G}. \quad (5.12)$$

The average liquid height $h_{L_{avg}}$ is calculated using Eq. (5.12) and geometric relations (e.g. Govier and Aziz (1972)). Eq. (5.12) successfully predicts the inverse proportionality between the gas flow rates and $h_{L_{avg}}$.

5.2.3 Slug stability model

The slug stability model considers the rates of liquid adjoining or detaching from the slug at its front or rear. Slugs are stable (not decaying) when the rates of liquid adjoining are not less than the rates at which liquid detaches. Figure 5.1B gives an illustration of a slug moving with front velocity C_F over a stratified liquid layer at station 1 of area A_{L1} and actual velocity u_1 . The volumetric flow rate of liquid adjoining the slug is:

$$Q_{in} = (C_F - u_1)A_{L1}. \quad (5.13)$$

The rear of the slug is assumed to behave as a bubble moving with a velocity C_B . The volumetric flow rate of the liquid detaching from the slug is:

$$Q_{out} = (C_B - u_3)(1 - \epsilon)A \quad \text{at section 3.} \quad (5.14)$$

The parameter u_3 is the actual liquid velocity at stations 3, and ε is the volume fraction of the gas in the slug (Woods and Hanratty (1998); Woods and Hanratty (1996)):

$$\varepsilon = 0.8 \left[1 - \frac{1}{\left(1 + (U_{Mix}/8.66)^{1.39}\right)} \right], \quad (5.15)$$

where U_{Mix} is the mixture velocity ($U_{Mix} = U_{SG} + U_{SL}$, where U_{SG} and U_{SL} are the superficial gas and liquid velocities, respectively). Assuming neutral stability, $Q_{in} = Q_{out}$ and $C_F = C_B$, and making use of Eqs. (5.13) and (5.14), the following relation is obtained,

$$\left(\frac{A_{L1}}{A} \right)_{crit} = \frac{(C_B - u_3)(1 - \varepsilon)}{(C_B - u_1)}, \quad (5.16)$$

for the area of the stratified flow at the front. Using Eq. (5.16) and geometric relations, the critical height, h_{Lcrit} , at the slug front required for the slug to be neutrally stable is obtained. The detailed analysis of slug stability model is well documented by Hurlburt and Hanratty (2002); Soleimani and Hanratty (2003).

5.3 Slug frequency model

Slug flow is an outcome of a complex two-phase flow field that contains periodic and nonperiodic-chaotic events. These events can be either dependent or independent, and variant or invariant with transformations in space-time. The complex flow field evolves in space-time through different stages: (1) stratified flow; (2) stratified-wavy; (3) transition to slug flow; (4) development of slugs; and (5) periodic "fully" developed slug flow. Solving the flow dynamics of the different stages involves many computational challenges. Instead, we consider slugging as a steady periodic event that is invariant for constant flow conditions. We postulate that slug flow (and so slug frequency) is an outcome of two main factors: (1) dominant independent periodic events that occur at the initial stage in stratified flow; (2) and the effect of slugging on these events.

5.3.1 Frequency of turbulent eddies in gas and liquid

The dominant initial independent periodic events in stratified flow are the quasi-ordered motions in the wall boundary layer of each fluid. Such motions create periodic ejections of slow moving fluid from the viscous sublayer to the external region of the boundary layer (Surkov (1985)); Roshko (1976)); Ginevskii et al. (1978)); Alshamani et al. (1982)). The regions of the quasi-ordered motion are characterised by high intensity pulsation and an increase of the scale of turbulence with a pairwise combination of eddies (Surkov (1985)). Each region occupies a viscous sublayer in the wall boundary layer. The distance from the wall to the external boundary of the eddy formation region is proportional to the thickness of the boundary layer, whereas the distance to the internal boundary is proportional to the thickness of the viscous sublayer (Grabovskii and Surkov. (1984)):

$$k_1 \frac{y}{u_\tau} \leq y \leq k_2 \delta, \quad (5.17)$$

where y is the distance from the wall, ν is the kinematic viscosity of the fluid, δ is the viscous boundary layer, and u_τ is the friction velocity:

$$u_\tau = \sqrt{\frac{\tau_w}{\rho}}, \quad (5.18)$$

where ρ is the fluid density and τ_w is the time-averaged stress of the fluid defined in Eq. (5.3). The coefficient k_1 was evaluated in accordance with data by Surkov (1985): $k_1 = 11$ being the average maximum intensity of pulsations (for gas or liquid). For the case of gas-liquid pipe flow, a maximum distance from the wall is considered for the increase of turbulence in each phase, $k_2\delta = D_H$, where D_H is the hydraulic diameter of the phase defined in Eq. (5.10).

The discrete eddy is represented in the form of a circular fluid disk, where the angular velocity is one-half of the vorticity (Wu et al. (2006)). Therefore, the frequency of rotation is determined by the averaged tangential velocity of a point about the axis of rotation in the following form:

$$\omega = \frac{1}{2} \frac{d\langle \mathbf{u} \rangle}{dy}. \quad (5.19)$$

The frequency of oscillations generated by a discrete eddy into the surrounding medium is assumed to be of the order of magnitude of the frequency of rotation of the eddy. Thus,

$$\mathbf{f}_r = \frac{1}{2\pi} \omega. \quad (5.20)$$

Assuming that the source of oscillations is located at an antinode of the stationary wave, the family of n resonance frequencies can be expressed by:

$$\mathbf{f}_r^n = \frac{2n-1}{4\pi} \frac{u_\tau k_1}{y}. \quad (5.21)$$

The first harmonic, in Eq. (5.21), dominates the resonance frequencies, since the wave damping factor grows proportionally to the square root of the frequency (Lighthill (1978)). Thus, for the frequency of oscillations in gas and liquid we obtain the following relations:

$$\mathbf{f}_{r,G} = \frac{u_{\tau,G} k_1}{4\pi y}, \quad \mathbf{f}_{r,L} = \frac{u_{\tau,L} k_1}{4\pi y}. \quad (5.22)$$

Eq. (5.22) provides uncorrelated quantities of two independent periodic events (frequency of oscillations in gas and liquid). However, since slug flow is an interfacial periodic event (involving both gas and liquid), quantities $\mathbf{f}_{r,G}$ and $\mathbf{f}_{r,L}$ need to be coupled as a single periodic event, which we define as an interfacial oscillation frequency, $\mathbf{f}_{r,i}$. The scale of y is considered to be of the same order of magnitude for the two phases. This consideration is valid for the flow rates considered in this chapter where non of the phases is relatively thin.

5.3.2 Interfacial frequency of turbulent eddies, $\mathbf{f}_{r,i}$

From similarity consideration we define an interfacial frequency of turbulent eddies that obeys the same laws in Eq. (5.22), thus,

$$\mathbf{f}_{r,i} \triangleq \frac{u_{\tau,i} k_1}{4\pi y}. \quad (5.23)$$

We also introduce an interfacial velocity:

$$u_{\tau,i} = \sqrt{\frac{\tau_i}{\rho_L}}. \quad (5.24)$$

Substituting τ_i (from Eq. (5.3)) into Eq.(5.24), and expressing the result as function of $\mathbf{f}_{r,G}$ and $\mathbf{f}_{r,L}$, we obtain

$$u_{\tau,i} = \frac{2\pi}{k_1} \sqrt{f_i} \left(\frac{\mathbf{f}_{r,G}}{\sqrt{f_{WG}}} - \frac{\mathbf{f}_{r,L}}{\sqrt{f_{WL}}} \right). \quad (5.25)$$

Finally, substituting Eq. (5.25) into Eq. (5.23) gives a relation for an interfacial frequency:

$$\frac{\mathbf{f}_{r,i}}{\sqrt{f_i}} = \sqrt{\frac{\rho_G}{\rho_L}} \left(\frac{\mathbf{f}_{r,G}}{\sqrt{f_{WG}}} - \frac{\mathbf{f}_{r,L}}{\sqrt{f_{WL}}} \right). \quad (5.26)$$

5.3.3 Triggering of slug precursors

Slug flow evolves from turbulent fluctuations at the interface into growing waves that reach the top of the pipe. Therefore, at the initial stage, a slug precursor can be triggered at the same frequency of the turbulent eddies at locations $i = 1, \dots, n$ along the pipe, as shown in Figure 5.2. The length of the pipe is l_{pipe} , and the distance between every two neighbouring slug precursors is the average turbulence scale length, l_T . For a fully developed pipe flow l_T is estimated as follows,

$$l_T = 0.07D. \quad (5.27)$$

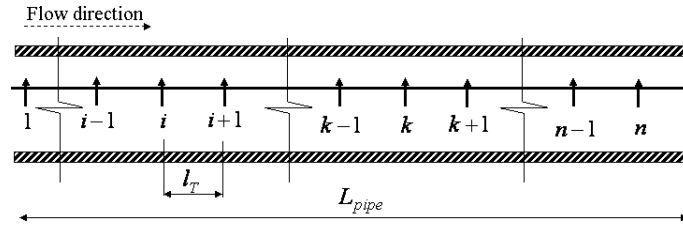


Figure 5.2: Sketch of triggering slug precursors along the pipe.

5.3.4 Conditional probability of slug formation

We assume that a precursor slug will form if triggered at any location k unless another slug (or slug precursor) is passing at that location, at the triggering time, as illustrated in Figure 5.2. The passing slug unit (slug and bubble) is referred to as a “dead-zone”. The initial length of the “dead-zone” is defined as the length passed by a perturbation moving with the interface at the velocity C_R for a time period $\Delta t = 1/\mathbf{f}_{r,i}$:

$$l_{dead} = C_R \Delta t, \quad (5.28)$$

The wave velocity C_R is calculated from the classical Kelvin–Helmholtz analysis of a stratified flow (e.g. Simmons and Hanratty (2001)):

$$C_R = \frac{\rho_G U h_L + \rho_L u H}{\rho_L H + \rho_G h}, \quad (5.29)$$

where h and H are the height of the liquid and gas.

Figure 5.3 shows examples of triggering slug precursors that form slugs (a and d), and others that fail to form (b and c) due to its existence in the dead-zone at the triggering time. With t_k being the time at which a slug precursor is triggered at location k , we define a factor $m_{i,k}$ which is a measure for the effect of a slug at location i on the triggered slug precursor,

$$m_{i,k} = \max \left[0, \frac{\min [t_k, t_{i,w}] - t_{i,F}}{\Delta t} \right], \quad (5.30)$$

where $t_{i,w}$ is the time that takes the upstream wave behind a slug at location i to reach the triggered slug precursor at location k ,

$$t_{i,w} = \frac{(k-i)l_T}{C_R}, \quad (5.31)$$

whereas $t_{i,F}$ is the time needed for the front of a slug at location i to reach the triggered slug precursor at location k ,

$$t_{i,F} = \frac{(k-i)l_T - l_{dead}}{C_F}. \quad (5.32)$$

Eq. (5.30) provides the number of slugs that may form upstream and their passage will prevent the formation of a slug precursor that is triggered at location k , within the time interval $(t_{i,w} - t_{i,F})$. Therefore, the conditional probability of forming a slug (if triggered) at location k is:

$$\mathbb{P}_k = 1 - \sum \frac{m_{i,k} \mathbb{P}_i}{n}, \quad (5.33)$$

where $\mathbb{P}_1 = 1$ is the conditional probability of forming a slug, if triggered, at location 1. Averaging the probability of slug formation along the pipe $\langle \mathbb{P}_k \rangle$, the slug frequency is obtained as follows,

$$\mathbf{f}_S = \langle \mathbb{P}_k \rangle \mathbf{f}_{r,i}. \quad (5.34)$$

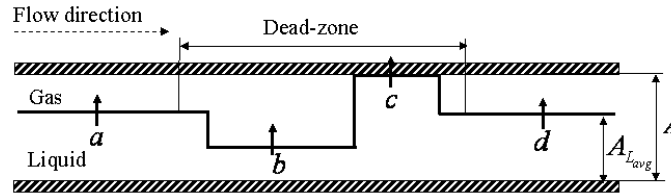


Figure 5.3: An example for triggering slug precursors at different locations a , b , c , and d . The triggering at locations a and d may form slugs, whereas triggering at b and c , in the “dead zone”, fails to form slugs.

Note that an expression for the average fully developed slug length can be obtained by making use of the bubble velocity and Eqs. (5.26), (5.33) and (5.34):

$$L_S = \frac{C_B}{\sqrt{f_i}} \sqrt{\frac{\rho_L}{\rho_G}} \frac{\sqrt{f_{WL}} \mathbf{f}_{r,G} - \sqrt{f_{WG}} \mathbf{f}_{r,L}}{\sqrt{f_{WL} f_{WG}} \langle 1 - \sum_{i=1}^{k-1} \frac{m_{i,k} \mathbb{P}_i}{n} \rangle}}. \quad (5.35)$$

5.4 Results

Theoretical calculations of the frequency of oscillations in the gas and liquid phases, and at the interface are given in Figure 5.4. The calculations were performed for air–water flow in a 20 m long pipe with 0.095 m i.d. The subplots (a) and (b) indicate constant $U_{SL} = 1.2$ m/s and $U_{SG} = 3.5$ m/s, respectively. The dashed and dotted curves are calculations of the frequency of the oscillations generated in the gas and liquid (Eq. (5.22)), respectively; whereas the solid curve is the calculation of the frequency at the interface (Eq. (5.26)). In Figure 5.4, the frequency of the oscillations generated in the gas phase, $\mathbf{f}_{r,G}$, is order of magnitude larger than that in the liquid, $\mathbf{f}_{r,L}$, or at the interface, $\mathbf{f}_{r,i}$. However, the behaviour of $\mathbf{f}_{r,i}$ with the flow rates is similar to that of $\mathbf{f}_{r,G}$. This indicates that the momentum of the liquid phase dictates the magnitude of the interfacial oscillations, whereas the intensity of eddy ejections in the gas phase dictates the behaviour of $\mathbf{f}_{r,i}$ with the flow rates.

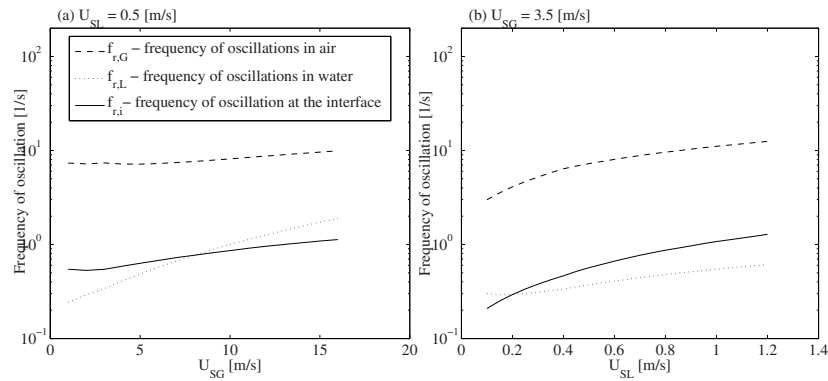


Figure 5.4: Theoretical calculations of the frequency of oscillations in air and water, and at the interface. $D = 0.095$ m, $l_{pipe} = 20$ m. (a) Constant liquid flow rate, $U_{SL} = 0.5$ m/s. (b) Constant gas flow rate, $U_{SG} = 3.5$ m/s.

The relative scale of the dominating instabilities in each phase can be obtained by a frequency Strouhal number which is defined by the identity: $St = \mathbf{f}_r D_H / \mathbf{u}$, where D_H is the hydraulic diameter, defined in Eq.(5.10), and \mathbf{u} is the average actual velocity of the fluid. Figure 5.5 shows the change of the frequency Strouhal number of the gas (solid curves) and liquid (dashed curves), as function of U_{SG} . Curves with the symbols (\times) are predictions for relatively low U_{SL} , whereas the other curves are for large U_{SL} . The larger frequency Strouhal number indicates smaller-scale instabilities from the separation of the shear layer (Kim and

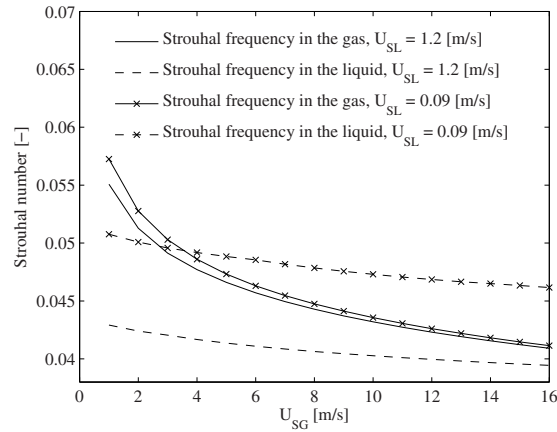


Figure 5.5: Strouhal number in air (solid curves) and water (dashed curves). $D = 0.095$ m, $l_{pipe} = 20$ m, curves without symbols: $U_{SL} = 1.2$ m/s, curves with \times : $U_{SL} = 0.09$ m/s.

Durbin (1988)). In the case of large U_{SL} the gas phase is dominated by smaller-scale instabilities compared with the liquid phase, for all gas flow rates. However, at $U_{SL} = 0.09$ m/s the liquid phase is dominated by larger-scale instabilities at $U_{SG} \leq 4$ m/s, and smaller-scale at $U_{SG} > 4$ m/s (compared with the gas phase). As the liquid flow rate decreases, the actual gas velocity only indirectly changes (due to the decrease of the liquid level), therefore the gas Strouhal number increases slightly. However, the actual liquid velocity decreases significantly and the liquid Strouhal number increases dramatically, especially at low U_{SG} where the change of the liquid level is enormous. At low flow rates, the small-scale instabilities are associated with low oscillation frequency (see Figure 5.4). As a result, ripples and large wavelength waves are generated at the surface. Slugs that evolve from such large wavelength waves and low frequencies may become very long (Kadri et al. (2009a)).

Figure 5.6 presents theoretical calculations with the above model of the conditional probability of slug formation as function of the location on the pipe. The pipe is horizontal, 137 m long with a diameter of 0.052 m, and the fluids are air and water with $U_{SG} = 3.5$ m/s. The probability of slug formation corresponds to Eq. (5.33). In Figure 5.6, the probability monotonically decreases downstream in the pipe, which is due to the more probable passage of slugs formed upstream (see Eq. (5.33)). Increasing U_{SL} results in a smaller turbulence length scale, l_T , and the number of the slug precursors (triggering locations) increases. Thus, the probability of slug formation increases.

Theoretical predictions of slug frequency are compared with measurements in Figure 5.7. The measurements were carried out by Fan et al. (1993a) and Fan et al. (1993b) (published in Woods et al. (2006)) at $U_{SL} = 0.5, 0.8$ and 1.2 m/s, and a range of $U_{SG} = 1 \dots 16$ m/s. The pipe is 20 m long with a diameter $D = 0.095$ m. The agreement between predictions and measurements is satisfactory. Eq. (5.34) successfully predicts that the slug frequency increases with increasing U_{SG} . However, a systematic overprediction is noticed as U_{SL} decreases. It is

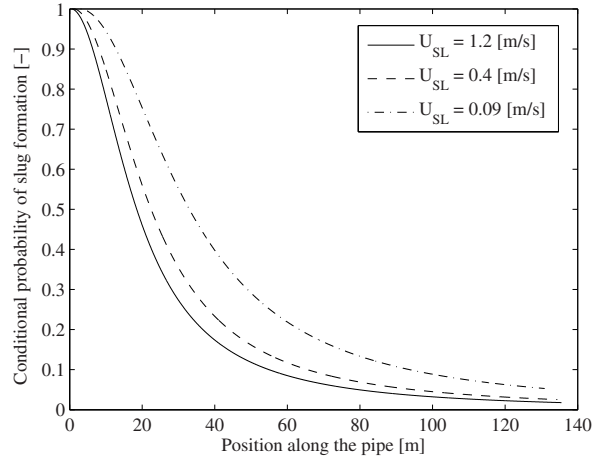


Figure 5.6: Theoretical predictions of the conditional probability of slug formation in air-water horizontal pipe flow. $U_{SG} = 3.5 \text{ m/s}$, $D = 0.052 \text{ m}$, $l_{pipe} = 137 \text{ m}$.

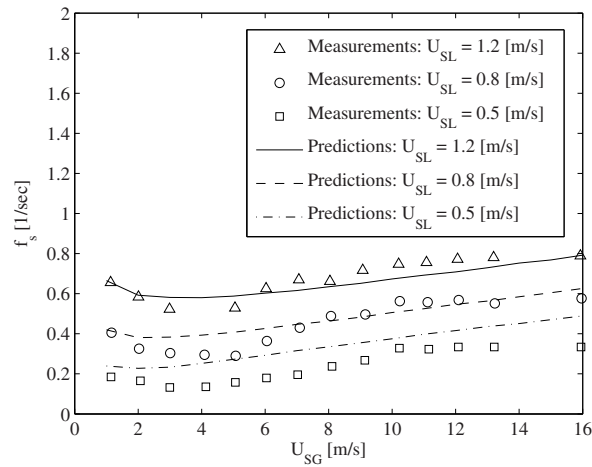


Figure 5.7: Theoretical predictions and measurements of slug frequency at fixed $U_{SL} = 1.2 \text{ m/s}$ and varying U_{SG} . $D = 0.095 \text{ m}$, $l_{pipe} = 20 \text{ m}$. The measurements were performed by Fan et al. (1993a) and Fan et al. (1993b).

also noticeable that the region $U_{SG} > 10 \text{ m/s}$ is a transition region to annular flow. In order to improve the accuracy of the predictions of slug frequency, the effect of annular flow needs to be considered.

Figure 5.8 compares theoretical predictions with measurements in pipes with diameters of

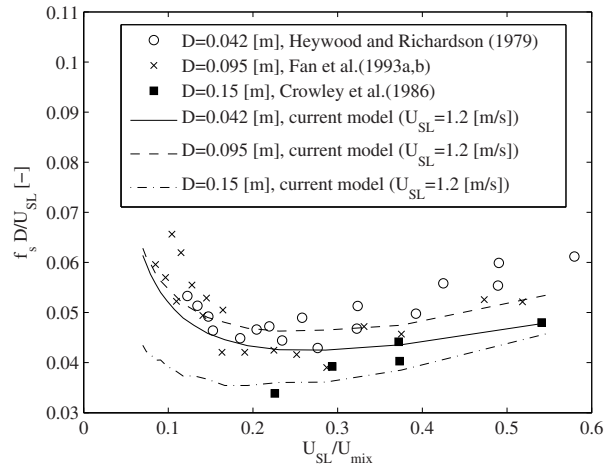


Figure 5.8: Theoretical predictions and measurements of slug frequency for different pipe diameters.

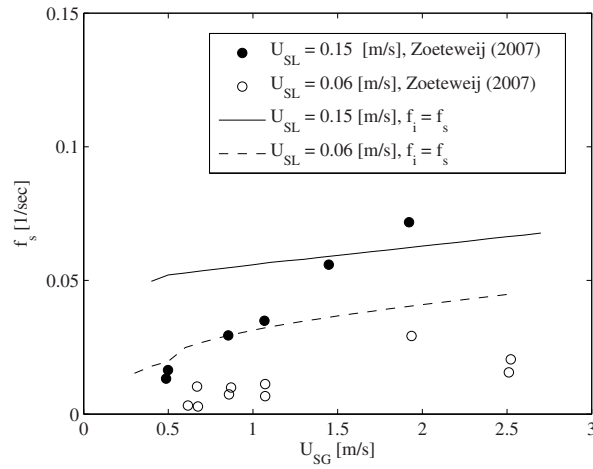


Figure 5.9: Theoretical predictions and measurements of slug frequency at low fixed U_{SL} and varying U_{SG} . $D = 0.052$ m, $l_{pipe} = 137$ m. The measurements were performed by Zoetewij (2007).

0.042 m (Heywood and Richardson (1979)), 0.095 m (Fan et al. (1993a); Fan et al. (1993b)) and 0.15 m (Crowley et al. (1986)). The ordinate is $f_s D / U_{SL}$ and the abscissa is U_{SL} / U_{Mix} . The current model successfully predicts the slug frequency for the different pipe diameters.

In the case of (very) low flow rates, slugs evolving from long wavelength waves (as mentioned previously) may grow to become several hundreds pipe diameter (Kadri et al. (2009a)).

Such slugs are not desirable due to the strong pressure fluctuations and separation difficulties they cause. The long slugs are characterised by a very low slug frequency that behaves in a “different” way compared to the case of large flow rates (Zoetewij (2007)): in the long slug region (at low flow rates) the slug frequency becomes a monotonically increasing function of U_{SG} (without a minimum). Predictions for the behaviour of f_S with U_{SG} are compared with measurements in Figure 5.9. In the figure, the bullets (●) and circles (○) are slug frequency measurements at $U_{SL} = 0.06$ and 0.15 m/s, respectively; whereas the solid and dashed curves are the corresponding predictions. The model predicts that f_S increases with U_{SG} , however, at $U_{SL} = 0.15$ m/s the trend becomes wrong. A possible reason for the wrong capture of the trend is the lack of precise interfacial friction values at very low flow rates.

5.5 Conclusions

1. Slug frequency in gas–liquid horizontal pipe flow was investigated and derived by the frequency of vortices in the two phases. Turbulent eddies, generated in the viscous boundary layer of the pipe wall, generate resonance oscillations that perturb the surface and create interfacial periodic fluctuations. Slug frequency is characterized by these fluctuations.
2. At varying flow rates, slug frequency is found to behave similar to the frequency of oscillations in the gas phase. However, the scale of frequency is dominated by the liquid momentum.
3. The history of turbulent eddies (slug precursors) in the downstream part of the pipe is destroyed by passing slugs, preventing the formation of new slugs. As a result, the frequency of slug formation in the downstream part of the pipe is reduced.
4. A probabilistic model was provided by making use of frequency of vortices, integral scales of turbulence, and probabilistic effects of the properties of developing slugs along the pipe. Predictions by the model were compared with slug frequency measurements, found in literature, with a satisfactory agreement.
5. The probability of forming a slug decreases in the downstream part of the pipe as a result of the passage of other slugs formed upstream earlier.
6. The model was validated by comparing slug frequency calculations with measurements found in literature. The agreement between predictions and measurements is satisfactory at $U_{SG} < 10$ m/s. However, at large gas or low liquid flow rates the model over-predicts the slug frequency. A possible reason for this deviation between predictions and measurements is the transition to annular flow, gas entrainment, and liquid breakup that is not considered in the chapter.
7. The model predicts the change in the behaviour of the slug frequency in the long slug region, i.e. at very low gas and liquid flow rates. However, the trend becomes wrong as the liquid flow rate increases. The accuracy of predictions by the model could be improved if the interfacial friction factor was better estimated at very low flow rates.

6

Conclusions and final remarks

The aim of this thesis was to investigate slug flow characteristics in stratified gas–liquid flow in horizontal and near horizontal pipes. The focus of the research was on the long liquid slugs that may grow up to several hundreds of pipe diameter causing undesired system vibration and serious operational failures. Simplified theoretical models, numerical simulations and experiments have been carried out to investigate the following subjects: (1) the slug growth and the long slug region; (2) a detailed investigation of mechanisms in wave evolution (gravity and roll–waves) and their effect on the long slugs; (3) the effect of the operation pressure (on the long slugs); (4) the role of turbulence.

6.1 Slug growth and the long slug region

Very long slugs reaching 500 pipe diameter have been observed in gas–liquid horizontal pipe flow measurements. The long slugs appear at low gas and liquid flow rates, where the slug frequency is relatively low and the difference in liquid level between the front and tail (liquid excess) of a slug is large. As a result, decreasing the gas or liquid flow rate, in the long slug region, produces larger slugs. The long slug regime can be divided in two main sub-regimes: (a) long fully developed slugs; and (b) long growing slugs. The long growing slugs, were observed at flow rates close to the transition from stratified to slug flow, where the slug frequency is lowest and the liquid excess is largest.

A dynamic slug growth model was presented. The model calculates the transient growth of a slug by applying a volumetric balance between the front and tail of the slug. The liquid at the front is calculated from the gas and liquid momentum equations. However, at the tail, the dynamics of the liquid level was simplified by a linear kinematic relation between the tail and the following upstream wave.

The model provides an explanation for a number of important observations in the slug flow regime: (a) in the long slug regime, the slug length decreases with increasing liquid flow rates as a result of the faster development of the liquid level behind the slug; (b) increasing the operation pressure results in larger interfacial shear stresses, lower equilibrium liquid level and volumetric growth rate, and thus shorter average slug length – that is why at high pressure only hydrodynamic slugs are observed; (c) further increase of the pressure results in liquid levels approaching the minimum slug stability level, so that no stable slugs (long or hydrodynamic) can appear anymore (unless produced at the inlet).

6.2 Evolution of waves and transition to slug flow or roll–waves.

Slugs may form either directly by growing gravity waves that bridge the pipe, or by coalescing roll–waves. These are two different mechanisms for the formation of slug flow. Slugs that form by roll–wave coalescence are short ($L_s < 40D$) and have relatively a large frequency, whereas slugs that form by growing large amplitude gravity waves are growing slugs that can become long. Therefore, it is important to identify and predict the conditions at which the crest of a growing wave bridges the pipe, and the condition where the crest approaches the downstream end of the wave producing a roll–wave.

In order to predict the evolution of waves into either slug flow or roll–waves, we developed a time–difference wave transition model. The model calculates the time required for a long wavelength wave to grow and reach the top of the pipe, and the time needed for the wave crest to approach its downstream end. The model predicts the transition from stratified flow to slug flow or roll–wave regimes for different flow conditions and pipe diameters. It also predicts a number of important observations regarding the behaviour of slug/roll–wave formation time: (a) increasing the liquid flow rates results in shorter transition times from stratified wavy to slug flow; (b) at relatively low U_{SG} , the formation of slug/roll–wave time increases with increasing U_{SG} , which is a result of the lower initial stratified height; however (c) at relatively high U_{SG} , due to the domination of inertial forces, the formation time decreases with increasing U_{SG} and a roll–wave is formed; and (d) increasing the pipe size

results in larger axial growth compared to the growth in the vertical direction, making the appearance of long slugs less likely.

Based on predictions by the time-difference model we obtained a critical densimetric gas Froude number, $Fr \simeq 0.15$, for the transition from slug flow to roll-wave regimes. The critical Froude number was obtained for flow rates close to the transition to slug flow.

6.3 The effect of operation pressure

In order to evaluate the effect of the operation pressure on the long slugs, air-oil and SF_6 gas-oil pipe flow measurements by Kristiansen (2004) were investigated. The measurements were carried out at $P = 1-8 \text{ bar}$ with high density SF_6 gas simulating a pressure up to 65 bar.

Slugs have been categorized into three types according to the liquid excess between the front and tail: (1) *type I*- slugs that are unaffected by the presence of other slugs downstream. They have relatively large and constant initial liquid excess. Due to the large liquid excess, this type of slugs may become extremely long $O(100D)$; (2) *type II*- slugs moving over a depleted liquid layer due to the passage of other slugs. Thus, these slugs have a decreasing liquid excess. The length of this type of slugs vary from short hydrodynamic to long depending on the flow conditions; and (3) *type III*- fully developed slugs with no liquid excess. These type of slugs are the shortest, being 8-16D at low flow rates and doubling their length at larger flow rates due to collisions and merging with other slugs.

At atmospheric pressure, the long slugs were found to be *type I*. When increasing the liquid flow rates, the frequency of slugs *type I* increases, and neutral stability is reached earlier in the pipe, due to the presence of a larger number of slugs. As a result, the slug length decreases.

Slugs *type I* have not been observed at $\rho_G \geq 18.5 \text{ kg/m}^3$ ($P \geq 23 \text{ bar}$). At $18.5 < \rho_G < 46 \text{ kg/m}^3$ ($23 < P < 65 \text{ bar}$) the long slugs were only *type II*, neutrally stable at the outlet. At $\rho_G = 52 \text{ kg/m}^3$ ($P = 65 \text{ bar}$) only hydrodynamic slugs (*type III*) were found.

Slight changes in the liquid excess can lead to large difference in the final slug length, and thus slug frequency.

6.4 Slug flow and turbulence

Slug frequency in gas-liquid horizontal pipe flow was investigated and derived by the frequency of vortices in the two phases. Turbulent eddies, generated in the viscous boundary layer of the pipe wall, generate resonance oscillations that perturb the surface and create interfacial periodic fluctuations. Slug frequency is characterized by these fluctuations.

At varying flow rates, the slug frequency is found to behave similar to the frequency of oscillations in the gas phase. However, the scale of frequency is dominated by the liquid momentum.

The history of turbulent eddies downstream of the pipe is destroyed by passing slugs, preventing the formation of new slugs. As a result, the frequency of slug formation downstream of the pipe is reduced.

A probabilistic model was provided by making use of frequency of vortices, integral scales of turbulence, and probabilistic effects of the properties of developing slugs along the pipe. Predictions by the model were compared with slug frequency measurements, found in literature, with a satisfactory agreement. The probability of forming a slug decreases downstream the pipe as a result of the passage of other slugs formed upstream earlier.

The model was validated by comparing slug frequency calculations with measurements found in literature. The agreement between predictions and measurements is satisfactory at $U_{SG} < 10 \text{ m/s}$. However, at large gas flow rates the model overpredicts the slug frequency. A possible reason for this deviation between predictions and measurements is the transition to annular flow.

The model predicts that the slug frequency increases with U_{SG} in the long slug region. However, the trend becomes wrong as the liquid flow rate increases. The interfacial friction factor plays an important role in the derivation of the slug frequency ($f_s f_i^{1/2}$). The accuracy of predictions by the model could be improved if the interfacial friction factor was better estimated at very low flow rates.

6.5 Final remarks

Studying the characteristic length and time scales of slug flow in horizontal pipes, with a particular focus on the long slugs, gave some insight into the dominating effects in stratified and slug flow regimes.

It is possible to derive slugging, considered as a periodic problem, from the dominating periodic events in stratified flow. However, mapping these events as a single “interfacial” periodic event results in the involvement of the interfacial friction factor. A basic understanding of the interfacial friction factor could lead to more accurate predictions of the flow-field, in general, and slug flow in particular.

It might be useful to repeat the periodicity approach presented in chapter 5 for other periodic flow patterns in pipe flow, e.g. annular flow, constructing a theoretical model for each pattern. Then, combining the different models may give a general overview on the transportation of gas and liquid in pipelines. Moreover, once all periodic events are treated, the chaotic part of the flow-field should be related to the remaining non-periodic events.

Bibliography

- Alshamani, K.M.M, Laivsi, J.L., Edwards, F.J., 1982. Sound excitation of the boundary region in a channel with a turbulent flow. *Raket. Tekh. Kosmon.* 20, 41–48.
- Andritsos, N., Hanratty, T.J., 1987. Influence of interfacial waves in stratified gas–liquid flows. *AIChE J.* 33, 444–454.
- Andritsos, N., Williams, L., Hanratty, T.J., 1989. Effect of liquid viscosity on the stratified–slug transition in horizontal pipe flow. *Int. J. Multiphase Flow* 15, 877–892.
- Barnea, D., Taitel, Y., 1994a. Interfacial and structural stability of separated flow. *Int. J. Multiphase Flow* 20, 387–414.
- Barnea, D., Taitel, Y., 1994b. Non–linear interfacial instability of separated flow. *Chem. Eng. Sci.* 49, 2341–2349.
- Belcher, S., 1999. Wave growth by non–separated sheltering. *Eur. J. Mech. B/Fluids* 18, 447–462.
- Belcher, S., Hunt, J., 1993. Turbulent shear flow over slowly moving waves. *J. Fluid Mech.* 251, 119–148.
- Bendiksen, K.H., 1984. An experimental investigation of the motion of long bubbles in inclined tubes. *Int. J. Multiphase Flow* 10, 467–483.
- Bendiksen, K.H., Espedal, M., 1992. Onset of slugging in horizontal gas–liquid pipe flow. *Int. J. Multiphase Flow* 18, 234–247.
- Benjamin, T.B., 1959. Shear flow over a wavy boundary. *J. Fluid Mech.* 6, 161–205.
- Benjamin, T.B., 1968. Gravity currents and related phenomena. *J. Fluid Mech.* 31, 209–248.
- Bonizzi, M., Andreussi, P., Banerjee, S., 2009. Flow regime independent, high resolution multi–field modelling of near–horizontal gas–liquid flows in pipelines. *Int. J. Multiphase Flow* 35, 34–46.

- Bontozoglu, V., Hanratty, T.J., 1989. Wave height estimation in stratified gas–liquid flows. *AIChE J.* 35, 1346–1350.
- Bradshaw, P., 1976. Topics in applied physics. Turbulence 12(3) Chapter 3. Springer, Berlin.
- Churchill, S.W., 1977. Friction–factor equation spans all fluid–flow regimes. *Chem. Eng.* 7, 91.
- Cohen, J., Belcher, S., 1999. Turbulent shear flow over fast–moving waves. *J. Fluid Mech.* 386, 345–371.
- Cornish, V., 1910. Waves of sea and other water waves. T. Fisher, Unwin, London, England.
- Crowley, C.J., Sam, R.G., Rothe, P.H., 1986. Investigation of two–phase flow in horizontal and inclined pipes at large pipe size and high gas density. Report prepared for the American Gas Association by Creae Inc.
- Crowley, C.J., Wallis, G.B., Barry, J.J., 1992. Validation of a one–dimensional wave model for the stratified–to–slug flow regime transition, with consequences for wave growth and slug frequency. *Int. J. Multiphase Flow* 18, 249–271.
- Dukler, A.E., Hubbard, M.G., 1975. A model for gas–liquid slug flow in horizontal tubes. *Ind. Eng. Chem. Fundam.* 14, 337–347.
- Dukler, A.E., Maron, D.M., Brauner, N., 1985. A physical model for predicting the minimum stable slug length. *Chem. Eng. Sci.* 40, 1379–1385.
- Fan, G.W., Lusseyran, F., Hanratty, T.J., 1993. Initiation of slugs in horizontal gas–liquid flows. *AIChE J.* 39, 1741–1753.
- Fan, Z., Ruder, Z., Hanratty, T.J., 1993b. Pressure profiles for slugs in horizontal pipelines. *Int. J. Multiphase Flow* 19, 421–437.
- Ginevskii, A.S., Vlasov, E.F., Kolesnikov, A.V., 1978. Aeroacoustic Interaction [in Russian], Mashinostroenie, Moscow.
- Govier, G.W., Aziz, K., 1972. *The Flow of Complex Mixtures in Pipes*. Van Nostrand Reinhold Co, NY, p.563.
- Grabovskii, A.M., Surkov, S.V., 1984. Frequency spectra of turbulent pulsations and stability of the laminar boundary layer, *Inzh. Fiz. Zh.* 46, 900–905.
- Gregory, G.A., Scott, D.S., 1969. Correlation of liquid slug velocity and frequency in horizontal cocurrent gas–liquid slug flow. *AIChE J.* 15, 933–935.
- Greskovich, E.J., Shrier, A.L., 1972. Slug frequency in horizontal gas–liquid slug flow. *Ind. Eng. Chem. Proc. Design Dev.* 11, No. 2, 317–318.
- Hall, A., 1992. *Multiphase Flow of Oil, Water and Gas in Horizontal Pipes*. Ph.D. thesis, University of London.

- Hanratty, T.J., 2004. Final report on gas–liquid flow in pipelines. University of Illinois, Urbana.
- Hanratty, T.J., Engen, J., 1957. Interaction between a turbulent air stream and a moving water surface. *AIChe J.* 3, 299–304.
- Hanratty, T.J., Hershman, A., 1961. Initiation of roll waves. *AIChe J.* 7, 488–497.
- Heywood, N.I., Richardson, J.F., 1979. Slug flow of air–water mixtures in a horizontal pipe: Determination of liquid holdup by gamma–ray absorption. *Chem. Eng. Sci.* 34, 17–30.
- Hubbard, M.G., 1965. An analysis of horizontal gas liquid slug flow. Ph.D. thesis, University of Houston.
- Hunt, J.C.R., Graham, J.M.R., 1978. Free–stream turbulence near plane boundaries. *J. Fluid Mech.* 84, 209–235.
- Hurlburt, E.T., Hanratty, T.J., 2002. Prediction of the transition from stratified to slug and plug flow for long pipes. *Int. J. Multiphase Flow* 28, 707–729.
- Jeffreys, H., 1924. On the formation of water waves by wind. *Proc. Royal Soc.* A107, 189–205.
- Jeffreys, H., 1925a. On the formation of water waves by wind. *Proc. Royal Soc.* A110, 241–247.
- Jeffreys, H., 1925b. The flow of water in an inclined channel of rectangular section. *Phil. Mag.* (6) 49, 793–807.
- Issa, R.I., Kempf, M.H.W., 2003. Simulation of slug flow in horizontal and nearly horizontal pipes with the two–fluid model. *Int. J. Multiphase Flow* 29, 69–95.
- Kadri, U., Mudde, R.F., Oliemans, R.V.A., 2009c. Influence of the operation pressure on slug length in near horizontal gas–liquid pipe flow. Submitted to: *Int. J. Multiphase Flow*.
- Kadri, U., Mudde, R.F., Oliemans, R.V.A., 2007a. On the prediction of the transition from stratified flow to roll waves and slug flow in horizontal pipes. *Proceedings 13th International Conference on Multiphase Production Technology, Edinburgh, Scotland* 13, pp. 65–78.
- Kadri, U., Mudde, R.F., Oliemans, R.V.A., 2007b. On the development of waves into roll waves and slugs in gas–liquid horizontal pipe flow. *Proceedings 6th International Conference on Multiphase Flow, Leipzig, Germany* 6, 332.
- Kadri, U., Mudde, R.F., Oliemans, R.V.A., 2008b. A growth model for dynamic slugs in gas/liquid horizontal pipes. In *proc. BHR Conf., Banff, Canada*, pp. 241–254.
- Kadri, U., Mudde, R.F., Oliemans, R.V.A. 2009d. Prediction of slug frequency by a probabilistic model from periodic interfacial turbulence fluctuations in gas/liquid pipe flow. Submitted to: *SPE J.*

- Kadri, U., Bonizzi M., Mudde, R.F., Oliemans, R.V.A., Andreussi P., 2009b. Prediction of the transition from stratified to slug flow or roll-waves in gas-liquid horizontal pipes. *Int. J. Multiphase Flow*, doi:10.1016/j.ijmultiphaseflow.2009.07.002.
- Kadri, U., Zoetewij, M.L., Mudde, R.F., Oliemans, R.V.A., 2009a. A growth model for dynamic slugs in gas-liquid horizontal pipes. *Int. J. Multiphase Flow* 35, 439-449.
- Kim, K.J., Durbin, P.A., 1988. Observations of the frequencies in a sphere wake and of drag increase by acoustic excitation. *Phys. Fluids* 31, 3260-3265.
- Kordyban, E., Ranov, T., 1970. Mechanism of slug formation in horizontal two-phase flow. *J. Basic Eng.* 92, 857-864.
- Kristiansen, O., 2004. Experiments on the transition from stratified to slug flow in multi-phase pipe flow. Ph.D. thesis, Norwegian University of Science and Technology (NTNU), Trondheim.
- Lighthill, M., 1962. Physical interpretation of the mathematical theory of wave generation by wind. *J. Fluid Mech.* 14, 385-398.
- Lighthill, M.J., 1978. *Waves in fluids*, Cambridge/New York, Cambridge University Press, pp. 221-229
- Lighthill, M., Whitman, G., 1955. On kinematics of waves: Part 1 and 2. *Proc. Royal Soc. London.* A229, 281-345.
- Lin, P.Y., Hanratty, T.J., 1986. Prediction of the initiation of slugs with linear stability theory. *Int. J. Multiphase Flow* 12, 79-98.
- Longuet-Higgins, M.S., 1952. On Statistical Distribution of the Heights of Sea Waves. *J. Mar. Res.*, 11:245-266.
- Magnaudet, J., 2003. High-Reynolds number turbulence in a shear-free boundary layer: re-visiting the Hunt-Graham theory. *J. Fluid Mech.* 484, 167-196.
- McCready, M.J., 1998. Introduction to hydrodynamic stability. Lecture notes (version 3/16/98), University of Notre Dame.
- Miles, J., 1957. On the generation of surface waves by shear flows. *J. Fluid Mech.* 3, 185-204.
- Miles, J., 1996. Surface-wave generation: a viscoelastic model. *J. Fluid Mech.* 322, 131-145.
- Oliemans, R.V.A., 1987. Modelling of gas-condensate flow in horizontal and inclined pipes. In: *ASME Pipeline Engineering Symposium-ETCE*. pp. 72-81.
- Nydal, O.J., 1991. An experimental investigation of slug flow. Ph.D. thesis, University of Oslo, Department of Mathematics, Oslo, Norway.
- Nydal, O.J., Pintus, S., Andreussi, P., 1992. Statistical characterization of slug flow in horizontal pipes. *Int. J. Multiphase Flow* 18, 439-453.

- Nicholson, M.K., Aziz, K., Gregory, G.A., 1978. Intermittent two phase flow in horizontal pipes: predictive models. *The Can. J. of Chemical Eng.* 56, 653–663.
- Pan, Y., Banerjee, S., 1995. A numerical study of free-surface turbulence in channel flow. *Phys. Fluids* 7, 1649-1664.
- Phillips, O., 1957. On the generation of waves by turbulent wind. *J. Fluid Mech.* 2, 417–445.
- Roshko, A., 1976. Structure of turbulent shear flows: a new point of view. *Raket. Tekh. Kosmon.* 14, 8–20.
- Ruder, Z., Hanratty, P.J., Hanratty, T.J., 1989. Necessary conditions for the existence of stable slugs. *Int. J. Multiphase Flow* 15, 209–226.
- Scott, S.L., Shoham, O., Brill, J.P., 1987. Modelling slug growth in large diameter pipes. In: 3rd International Conference on Multiphase Flow, The Hague, Netherlands. BHRA Vol. 1, 55–64.
- Simmons, M.J.H., Hanratty, T.J., 2001. Transition from stratified to intermittent flow in small angle upflows. *Int. J. Multiphase Flow* 27, 599–616.
- Soleimani, A., Hanratty, T.J., 2003. Critical liquid flows for the transition from the pseudo-slug and stratified patterns to slug flow. *Int. J. Multiphase Flow* 29, 51–67.
- Surkov, S.V., 1985. Cascade character of the growth of turbulent eddies. *Inzh.–Fiz. Zh.* 48, 561–568.
- Taitel, Y., Dukler, A., 1976. A model for predicting flow regime transitions in horizontal and near horizontal gas-liquid flow. *AIChE J.* 22, 47–55.
- Teixeira, M.A.C., Belcher, S.E., 2006. On the initiation of surface waves by turbulence shear flow. *Dynamics of Atmospheres and Oceans* 41, 1–27.
- Tronconi, E., 1990. Prediction of slug frequency in horizontal two-phase slug flow. *AIChE J.* 36, 701–709.
- Ujang, P.M., Lawrence, C.J., Hale, C.P., Hewitt, G.F., 2006. Slug initiation and evolution in two-phase horizontal flow. *Int. J. Multiphase Flow* 32, 527–552.
- Wallis, G.B., Dobbins, J.E., 1973. The onset of slugging in horizontal stratified air-water flow. *Int. J. Multiphase Flow* 1, 173–193.
- Woods, B.D., 1998. Slug formation and frequency of slugging in gas-liquid flows. Ph.D. thesis, University of Illinois, Urbana.
- Woods, B.D., Hanratty, T.J., 1996. Relation of slug stability to shedding rate. *Int. J. Multiphase Flow* 22, 809–828.

- Woods, B.D., Hanratty, T.J., 1999. Influence of Froude number on physical processes determining frequency of slugging in horizontal gas–liquid flows. *Int. J. Multiphase Flow* 25, 1195–1223.
- Woods, B.D., Hanratty, T.J., 2000. Mechanism of slug formation in downwardly inclined pipes. *Int. J. Multiphase Flow* 26, 977–998.
- Woods, B.D., Fan, Z., Hanratty, T.J., 2006. Frequency and development of slugs in a horizontal pipe at large liquid flows. *Int. J. Multiphase Flow* 32, 902–925.
- Wu, H.L., Pots, B.F.M., Hollenberg, J.F., Meerhoff, R., 1987. Flow pattern transitions in two–phase gas/condensate flow at high pressure in an 8–inch horizontal pipe. *Proc. BHRA Conf.*, The Hague, The Netherlands, pp. 13–21.
- Wu, J.Z., Ma, H.Y., Zhou, M.D., 2006. *Vorticity and vortex dynamics*, Springer Berlin Heidelberg, pp. 67–68.
- Zabaras, G.J., 1999. Prediction of slug frequency for gas–liquid flows. In: *Annual Technical Conference*, SPE 56462. pp. 181–188.
- Zoetewij, M.L., 2007. Long liquid slugs in horizontal tubes. Development study and characterisation with electrical conductance techniques. Ph.D. thesis, Delft University of Technology, Department of Multi–Scale Physics, Delft, The Netherlands.



Calculation of the wave growth coefficient, C_2

In this appendix, the calculation of the wave growth coefficient, C_2 , is presented:

The initial wave amplitude, η_0 , is assumed to be half the turbulence length scale, l_T , in a fully developed pipe flow:

$$\eta_0 = \frac{l_T}{2}, \quad (\text{A.1})$$

where

$$l_T = 0.07D_{HG}. \quad (\text{A.2})$$

The parameter D_{HG} is the hydraulic diameter of the gas phase give by

$$D_{HG} = \frac{4A_G}{S_i + S_G}. \quad (\text{A.3})$$

From Eq. 3.13, we calculate the range of the normalized average gas area for the flow rates and pipe diameters considered in this paper as follows,

$$0.2 \lesssim \frac{A_{G_{avg}}}{D^2} \lesssim 0.7. \quad (\text{A.4})$$

Using geometric relations to calculate S_i and S_G (e.g. Govier and Aziz (1972)) we obtain:

$$2 \lesssim \frac{S_i + S_G}{D} \lesssim 3. \quad (\text{A.5})$$

Substituting Eqs. A.4–A.5 into Eq. A.3 results in a lower and upper values of D_{HG} as function of the pipe diameter:

$$0.4D \lesssim D_{HG} \lesssim 0.9. \quad (\text{A.6})$$

Substituting Eqs. A.6–A.2 into Eq. A.1 we obtain the following range for the initial amplitude:

$$0.01D \lesssim \eta_0 \lesssim 0.03D. \quad (\text{A.7})$$

In order to obtain the maximum growth time of the crest we consider the smallest possible initial wave amplitude, $\eta_0 = 0.01D$. Hence, the constant $C_2 = 0.01$. It is noticeable that when operating at larger pressure the lower value of D_{HG} increases, due to momentum considerations. As a result C_2 should be modified ($C_2 > 0.01$). However, C_2 cannot be larger than 0.03 since the upper value of D_{HG} decreases with the pressure, due to the increase in the minimum liquid height downstream that is required for the formation of slugs (Eq. 3.9). As a result, the upper value of C_2 decreases with the pressure (thus $0.01D < C_2 < 0.03D$).

Publications

U. Kadri, R.F. Mudde and R.V.A. Oliemans, 2009. Prediction of slug frequency by a probabilistic model from periodic interfacial turbulence fluctuations in gas/liquid pipe flow. Preprint submitted to SPE J.

U. Kadri, R.F. Mudde and R.V.A. Oliemans, 2009. Influence of the operation pressure on slug length in near horizontal gas–liquid pipe flow. Preprint submitted to Int. J. Multiphase Flow.

U. Kadri, R.F. Mudde and R.V.A. Oliemans, M. Bonizzi, P. Andreussi, 2009. On the evolution of waves into roll–waves and slugs in gas–liquid horizontal pipe flow. Int. J. Multiphase Flow, doi:10.1016/j.ijmultiphaseflow.2009.07.002.

U. Kadri, M.L. Zoetewij, R.F. Mudde and R.V.A. Oliemans, 2009. A growth model for dynamic slugs in gas–liquid horizontal pipes. Int. J. Multiphase Flow 35, 439–449.

U. Kadri, R.F. Mudde and R.V.A. Oliemans, 2009. Slugs, turbulence and the butterfly effect. Proceedings 14th International Conference on Multiphase Production Technology, Cannes, France 14, pp. 319–330.

U. Kadri, R.F. Mudde and R.V.A. Oliemans, 2008. A theoretical growth model for hydrodynamic slugs in gas/liquid horizontal pipes. Proceedings 22nd International Congress of Theoretical and Applied Mechanics (ICTAM2008), Adelaide, Australia 22, pp. 113.

L. Badarnah, U. Kadri, U. Knaack, 2008. A bio–inspired ventilating envelope optimized by air–flow simulations. The World Sustainable Building (SB) Conference series, Melbourne, Australia, pp. 29.

U. Kadri, R.F. Mudde and R.V.A. Oliemans, 2008. A growth model for dynamic slugs in gas/liquid horizontal pipes. Proceedings 6th North American Conference on Multiphase Technology, Banff, Canada 6, pp. 241–254.

U. Kadri, R.F. Mudde and R.V.A. Oliemans, 2008. The effect of the liquid level on the characteristics of forming slugs. Proceedings 7th International ERCOFTAC Symposium on Engineering Turbulence Modelling and Measurements, Limassol, Cyprus 7.

U. Kadri, R.F. Mudde and R.V.A. Oliemans, 2007. On the prediction of the transition from stratified flow to roll waves and slug flow in horizontal pipes. Proceedings 13th International Conference on Multiphase Production Technology, Edinburgh, Scotland 13, pp. 65–78.

U. Kadri, R.F. Mudde and R.V.A. Oliemans, 2007. On the development of waves into roll waves and slugs in gas–liquid horizontal pipe flow. Proceedings 6th International Conference on Multiphase Flow, Leipzig, Germany 6, 332.

Acknowledgements

Advisors

My deep gratitude goes to my advisors, René Oliemans and Rob Mudde, for the delightful discussions, and continuous guidance, encouragement, and supervision. After this formality, it is time for honesty. Before starting my PhD, I was offered PhD positions at other locations, all had research titles much more attractive and exciting than “Long slugs ...”. However, it was not difficult for me to make the “right” choice. I chose the “right” supervisors.

Staff

I would like to thank all the support staff including Thea, Amanda, Angela, Wouter, Jaap (van Raamt), Jaap (Kamminga) and Jan for their support, whether directly or indirectly related to the research and research facilities.

Colleagues

I thank Maria for the unforgettable atmosphere she made, Ruurd for his valuable advises and tips, Jos for providing 3D-shooter games and Lan addiction *support* group, Marcos for arranging sports activities, Marco for the experiments and the “slug” discussions, Michael for providing excellent working atmosphere, Andrea for justifying the atmosphere in the Italian way, Volkert for the valuable advices, discussions and willingness to help, Annekatrien for providing an emergency-information support point on how to deal with the Dutch systems, Özgür for the precious spontaneous scientific discussions we had almost about any object (except humans) that moved around, Federico for “taking care” of MY neighbourhood and for surviving the “head-shot”, Anton for being on holidays for a sufficient period of time that was required to finalize my thesis, Mohammad for carrying my 200 kg washing machine, the successive roommates, Reza, Gallelio and Duong for the relaxed working environment, as well other PhD’s among which Amer, Adrian, Davide, Hamid, Laurens and Farzad who contributed to this environment, Chris, Luis, and other professors for the *open door* policy (does not necessarily mean that someone is inside). For the third year PhD students, when you lastly start seeing the light in the tunnel, take a deep breath, turn around, run as fast as you can, and climb the closest platform you find.

Others

I thank my PhD users’ committee for their critical remarks and their valuable suggestions during the meetings we had. I thank Prof. Ole Jørgen Nydal for the hospitality at his group,

and Dr. Olav Kristiansen for providing the detailed measurements of his PhD thesis, that had a valuable contribution to the research. I thank Dr. Marco Bonizzi and Prof. Paolo Andreussi for the fruitful cooperation we had.

Friends

My friends withstanding back home, and those enduring foreignness, never skimmed or scrimped a moment of being real friends. Thank you.

Family

The deepest gratitude goes to my family, and in particular to you, my parents. For your ability to discern what is true and right, inculcating in me the dedication and discipline of a free man with independent insights, the guidance with wisdom and continuous prayers... half of this work is definitely yours, and the other is due to you (but it is mine!). For my sisters and brothers I've been watching you the last 29 years closely. Thank you all for being older than me, providing me a large database of your own different mixed life experiences, giving me the possibility to learn and adapt your wise choices, and to avoid repeating mistakes analogous to those committed by you. My stay in the Netherlands could not have been better unforgettably delightful without the time spent with Basim & Hafsa family, the neverending adventures, the unlimited quality food, and the 48,000 minutes of phone calls!. Hanan, thanks for being the first to accompany me and Lidia to the Netherlands, the first to visit us at the 3 different houses we moved to, and no doubt, the first to attend the defence. Anan, thanks for appreciating time (probably yours), having only well controlled time-optimised remarkably short up-to-the-point communications. For Ashraf, Amal and Nashid, thanks for taking care of many arrangements back home. For my parents-in-law, thanks for all your support and faith. My wife, Lidia, your daily support and encouragements had a valuable contribution to my research. However, your enduring support accompanying me to my conferences, and me accompanying you to yours, have created a set of unforgettable adventures around the world, with Grizzly Bears, Crocodiles, harmless 10 m long snakes but deadly tiny mosquitos (and of course many slugs); diving with great white sharks, whales, and dolphin troupes; the never-ending land with thorny and Tasmanian devils, wild Kangaroos, and sleepy Koalas; the peaceful silence of snow covering the horizon of the arctic, the ghostly fjords, and the dominant trees on the steep canyons... Your crazy trip plans, to be able to see and do as much as possible, but also to give space for appreciating the harmony, the peace, and the wonderful beauty of nature, all in all made the last 3 years .. extraordinary.

God

Praises are due to the *Lord*, source of all knowledge and all wisdom.

About the author

Usama Kadri was born in November 18, 1979, Kfar Saba, Israel. He started to play the Piano when he was 6 years old and made his *Abitur* at the Israel Arts and Science Academy (I.A.S.A) in Jerusalem. Between 1998 and 2002 he studied at the Technion - Israel Institute of Technology, Haifa and obtained a *B.Sc.* degree in Aerospace Engineering. In 2005 he obtained the *M.Sc.* degree at the same faculty under the supervision of Prof. Daniel Weihs. Between 2005 and 2009 he became a research assistant at the Department of Multi-Scale Physics, Faculty of Applied Sciences, Delft University of Technology, The Netherlands.

